Chalk production at Tyra West

In the colloidal perspective

Henrik Jepsen

Supervisor: Erik G. Søgaard

Master Thesis in Chemical Engineering

6th June 2012

Esbjerg Institute of Technology
Aalborg Universitet

The thesis is made by use of LaTeX(Miktex), WinEDT, QTikz, Inkscape and JABRef.
The front page picture shows Tyra West on a sunny day. Used with permission from Maersk Oil and Gas.

Preface

The aim of this master thesis was originally to describe mechanisms and treatment possibilities for a recurrent problem with chalk influxes observed at the Tyra Field in the North Sea. During some initial analyses of the ζ-potential on the chalk particles an unexpected result gave the rise for a thorough investigation to see if this was a pure coincidence or not. This investigation lasted more than three months and was both time consuming and very interesting. For this reason the result of the thesis has become more a thorough study of ionic interactions on chalk in electrolyte solutions similar to a sample taken from the Tyra Field.

This thesis applies to those who think that colloidal science is of interest. Since the thesis is written in collaboration with Maersk Oil and Gas in Esbjerg, my hope is that the result can be helpful in their understanding of some of the mechanisms that can be troublesome in the process of dealing with produced water in the North Sea.

References to sources in the thesis is marked with [ZX, p. Y], where Z can be B for books, I for Internet and A for articles and others, dependent of the origin of the source. X is the number in the literature list, and Y is a further specification , in this example a page number of the source in question. Is the reference placed before a period the reference is for the statement in the present line. If the reference is after the period the reference is for the statement in the preceding paragraph. Where nothing is stated the figures and tables is own material.

I wish to thank

Maersk Oli and Gas for delivering samples of produced water for analysis.
Dankalk A/S for donation of chalk fore experimental purposes.
Bo Jensen Vandbehandling A/S for donation of coagulants and flocculants for my solid removal experiments.
Employees at Maersk Oil and Gas None mentioned, none forgotten, for helping me with fact finding and a lot of other things.

Henrik Jepsen

Title page

Theme:	Master thesis
Title:	Chalk production at Tyra West, In the colloidal perspective
Supervisor:	Erik G. Søgaard
Period:	2nd September 2011 - 6th June 2012
Study:	Chemical Engineering
Number of pages:	122
Number printed:	6

Henrik Jepsen

Synopsis

Dette masterprojekt omhandler problematikken omkring kalk i produktionsstrømmen fra Tyra Feltet i Nordsøen, hvor reservoirformationen er kalkformation. Et litteraturstudie er udført m.h.p. at forklare mekanismen bag nogle voldsomme kalk *slugs*, og der gives en mulig forklaring i trykvariationer under skift fra injektion til produktion af gas.

Enhedsoperationer til fjernelse af små kalkpartikler fra strømmen af produceret vand gennemgåes og diskuteres. Det foreslås at overveje brugen af centrifuger til vandbehandling, idet de, afhængigt af tørstofindholdet i vandet, kan fjerne partikler ned til $0{,}1\mu m$, hvor traditionelle hydrocykloner kan fjerne partikler ned til $10\mu m$.

ζ-potentialet på kalkpartiklerne fastlægges, og det fastslåes at ioniske påvirkninger af produceret vand fra Tyra Feltet har en påvirkning på ζ-potentialet der skifter fortegn på værdien ved hhv. lav og høj pH. Der udføres en række forsøg og analyser, der viser en mulig forklaring på fænomenet ved at betragte ligevægtene og dannelsen af hhv. HCO_3^- ved lav pH og $CaOH^+$ og $MgOH^+$ ved høj pH. Samtidigt foreslås disse ionpar som potentiale bestemmende ioner for $CaCO_3$.

Det undersøges, om det er muligt at danne emulsioner af olie/vand/kalk blandinger og om tilstedeværelsen af små kalkpartikler har en stabiliserende effekt på de dannede emulsioner. Der opnås ikke resultater, der bekræfter en stabiliserende effekt af kalkpartiklerne i oile/vand/kalkpartikel blandingen, men det observeres at kalkpartiklerne

kan trække olie ned i vandfasen. Der foretages mikroskopering af udtagne prøver der viser kalkpartikler fra vandfasen, der er omkranset af olie.

Abstract

This master thesis treats the problematic of chalk particles in the production stream coming from the Tyra Field in the North Sea. The reservoir formation consists of chalk. A litterature survey is accomplished in order to explain the mechanism behind some massive chalk influxes observed, and a possible explanation is found to be pressure variations in the switch form injection to production of gas.

Unit operations used for removal of small chalk particles from the stream of produced water is examined. A proposal for use of centrifuges for water treatment is made, since this technique, dependent on the volume of solids, can remove particles down to $0{,}1\mu m$ whereas normal hydro cyclones have a limit of $10\mu m$.

The ζ-potential of the chalk particles is determined, and an interaction of the ionic species on the ζ-potential is found. A shift in operational sign is seen at low and high values of pH respectively. A series of experiments and analyses gives a possible explanation of this phenomena by watching the equilibrium and formation of HCO_3^- at low pH and $CaOH^+$ and $MgOH^+$ at high pH. These found ionic species are proposed as potential determining ions for chalk.

The possible formation of emulsions of oil/water/chalk solutions and the possible stabilizing effect of these by small chalk particles is examined. The results did not indicate clear evidence that chalk particles stabilize an emulsion of oil/water. The ability of chalk to drag oil from the oil phase to the water phase is observed. By examining samples of chalk taken from the water phase under the microscope, particles are found which are encircled in oil.

Contents

1. Oil and gas production

In 1935 an American company received the right to drill for oil in the Danish subsoil. The lack of results lead to the interpretation that there wasn't any oil reserves worth exploiting in Denmark. In 1959 a huge gas reservoir was found outside the coast of Holland. This gas discovery reopened the interest for the Danish subsoil, and A.P. Møller received the exclusive rights for the Danish subsoil for a 50 year period. Since the oil business was a new field of interest for A.P. Møller, they joined up with the oil companies Shell and Gulf in a consortium named *Dansk Undergrunds Consortium* (DUC). [I13]

The first focus was inquiry drilling onshore, and in 1966 the first offshore inquiry drilling was performed. The first oil was found in 1967. The extent of this first oil discovery was limited, and not until 1971 where the Dan-field was found, an exploitation was profitable. Since 1972 there has been a production of oil and gas from the Danish part of the North Sea from several fields, where the fields are either oil, oil/gas or gas fields. [I13]

There has been a decline in oil production from 2004 and gas production from 2005, see figure 1, which has lead to the conclusion that the oil reserves where near to be depleted. Production forecasts support this conclusion with the present oilfield, but new oil findings can break the curve. As a consequence of the decreasing oil production water is injected in

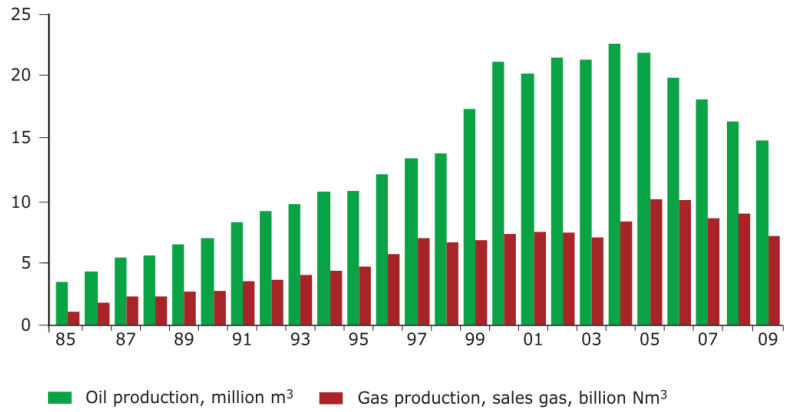

Figure 1: *Produced oil and gas in the Danish part of the North Sea from 1985 - 2009. [A28, p. 27]*

some of the oil fields to maintain reservoir pressure and to "push" more oil to the surface. Along with the water injection an increase in water production is seen, see figure 2 on the next page. This water has to be treated before discharge or re-injection. The demand for water treatment is growing concurrently with the increasing injection volume. With the increasing focus on protecting the marine life the need for pro-environmental solutions is demanded. This focus constantly pushes the oil outlet limits downwards and the need for technology upwards.

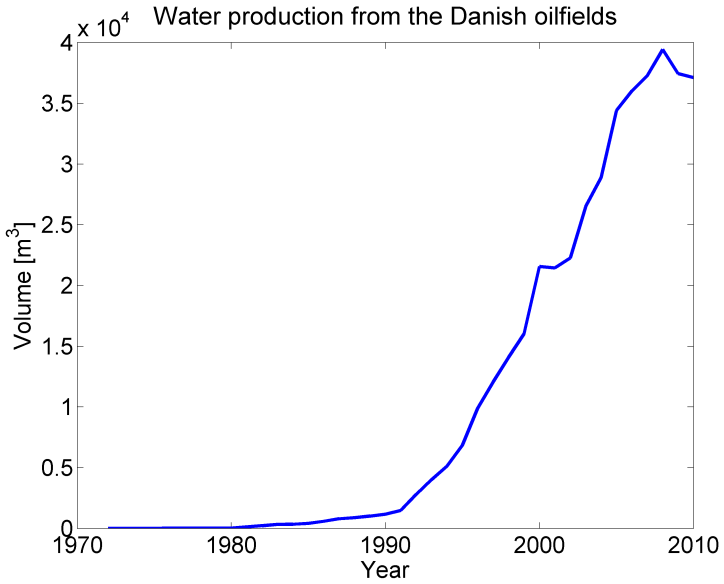

Figure 2: *The volume of produced water is growing along with the need to inject water to maintain the secondary oil recovery. [I14]*

1.1 Tyra Field

One of the fields in the Danish part of the North Sea is the Tyra Field, see figure 3 on the facing page. Tyra Field is mainly a gas producing field and is also used for gas storage (by swing injection). In the start of 2010 the field consists of 22 gas producing wells, 28 oil/gasproducing wells and 18 swing injection wells. The field was discovered in 1968 and put in production in 1986. The reservoir depth is about 2000 meters and the water depth is between 37 and 40 meters. The delineation of the Tyra Field is 177 km^2. The reservoir rock is chalk from the Danian and Upper Cretaceous age. [A28]

Swing Injection

The stream of fluid from a production well consists of a mixture of oil (heavy hydrocarbons), gas (light hydrocarbons) and water (formation water and injection water, if water injection is performed). The production stream is lead from the well to a High Pressure Separator (HP-separator), where the first separation of oil, gas and water is performed, see figure 4 on the next page.

The demand for gas depends on the time of year. The main part of the gas is used for heating purposes, which is why the demand for gas is smaller during summer. Since gas is an inevitable part of the production stream, the gas produced during summertime, has to be stored. A method for gas storage can be usage of existing gas wells. During summertime residual gas is pumped into dedicated gas injection wells where the gas is stored and at the same time is used to keep the well pressure stable. Since the injection gas has been separated from heavier hydrocarbons, the re-injection also helps to *"wash"*

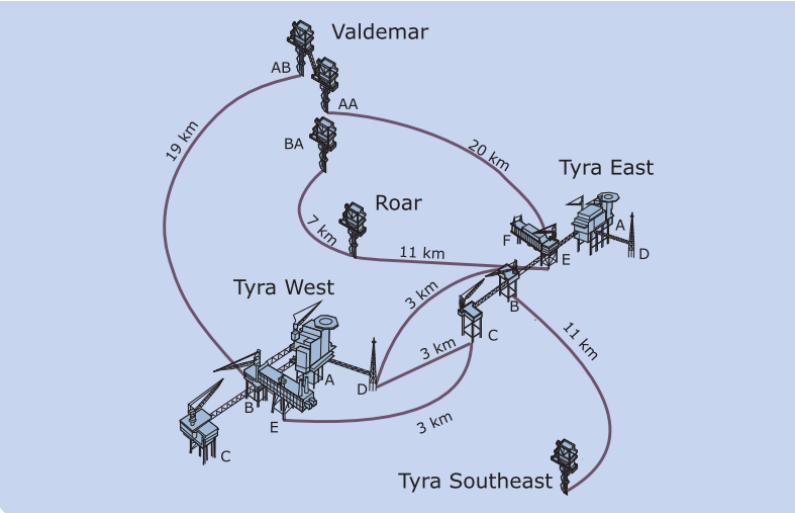

Figure 3: *Overview of the Tyra Field, including the gas connections to Valdemar and Roar field. [A28, p. 142]*

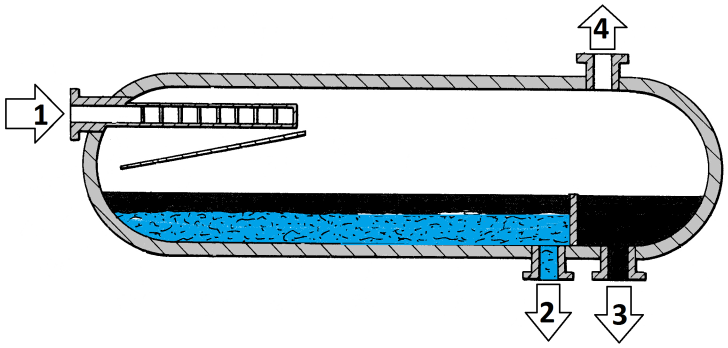

Figure 4: *Projection describing the principle of the Inlet Separator. The production stream enters the separator at point 1. Water and oil separates due to differences in density, and water leaves at point 2 for further water treatment and oil leaves at point 3. The gas stream leaves the separator at point 4.*

heavier hydrocarbons out of the chalk by displacement. The alternative is to reduce the oil production to a level, where the volume of produced gas corresponds to the demand.

1.2 North Sea geology

The North Sea has approximately 2% of the worlds oil resources. In the start of 2011 there were 55 platforms producing oil and gas from 19 existing fields in the Danish part of the North Sea. Maersk Oil and Gas is operating 15 of these fields, DONG operates three fields and Hess has one field.

Source rocks

The hydrocarbons produced in the North Sea origins from organic rich clay deposited on the sea floor during the Jurassic period (206 - 144 mill. years ago). Because of the low content of oxygen at the sea floor the organic material was preserved. As new sedimentation was build up on top of the organic rich clay, the right conditions with high pressure, due to the weight of the deposit, and high temperature (between 100 - 150°C) were created. The conditions supported the conversion of the organic material to oil and gas.

The conversion takes place in two steps

- Diagenesis
- Catagenesis

During Diagenesis a homogeneous substance is created from the organic material. This substance called Kerogen, is the remains of algae and woody plant material. Kerogen is a solid, which is insoluble in organic solvents and has a high molecular weight.

During Catagenesis the long and heavy Kerogen molecules are converted into smaller short chained molecules by cracking.

Whether oil or gas is produced from the Kerogen, depends on the origin of the organic material (simplified explanation). If the organic material comes from plants or wooden material (or generally spoken from dry land), it consists of heavy degradable components like cellulose and lignin. This Kerogen will, during conversion, produce gas. If the Kerogen originates from small single-celled algae from the sea, it will mainly be converted to oil.

Reservoir rocks

During Cretaceous period (144 - 65 mill. years ago) chalk and limestone was deposited on top of the layer of clay, which later, in the North Sea, becomes the reservoir rock of today's oil- and gas production. Chalk in the North Sea is formed from small single-celled plants called Coccolithophores, see figure 5 on the facing page. These plants have shells of $CaCO_3$, which formes the chalk formation, and the shape of the shells increases the porosity of the chalk. In the Tyra East field the porosity is $\approx 25 - 45\%$, see figure 82 on page 107. Porosity is calculated from equation 1

$$\phi = \frac{\text{Void space}}{\text{Total volume}} \times 100\% \tag{1}$$

where ϕ is the porosity [%] and void space and total volume has the unit [m^3].

The ability of the reservoir rock to *send* the hydrocarbons from the pore to the production well is expressed as permeability, see equation 2. In the North Sea the permeability is $\approx 1 - 20$ mD.

$$\kappa = v\frac{\mu \Delta x}{\Delta P} \tag{2}$$

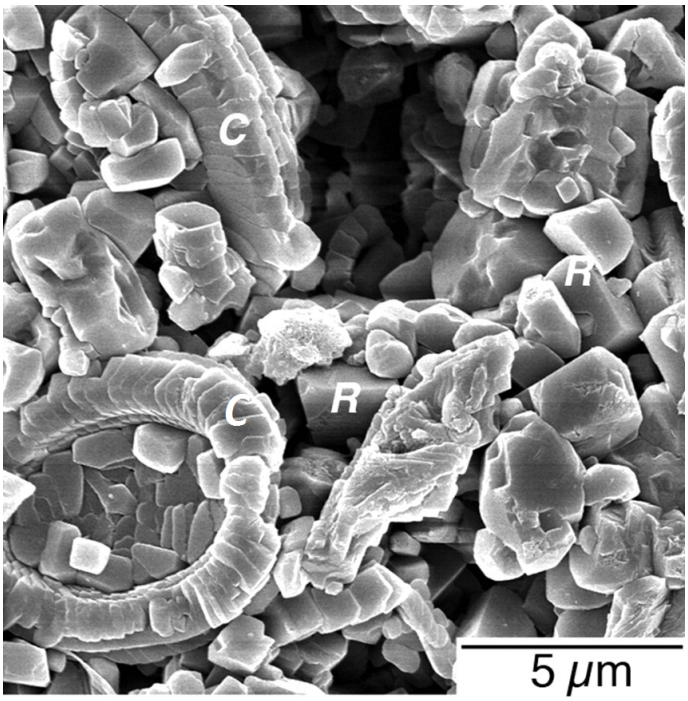

Figure 5: *SEM-picture of North Sea chalk, where* C*-marks shows Coccolithophores and* R*-marks shows calcite particles. [A26]*

where κ is the permeability [m^2], v is the superficial velocity of the fluid through the pores [m/s], μ is the dynamic viscosity of the fluid [Pa s], ΔP is the pressure difference [Pa] and Δx is the thickness of the porous medium. The unit for permeability is also expressed in Darcy (D), where one Darcy equals $9{,}869\,23 \cdot 10^{-13}$ m^2. Chalk formations has normally a low permeability compared to e.g. sandstone formations. In the North Sea the permeability of sandstone is $\approx 100 - 1000$ mD [I16].

Rifting

Geological activity, such as rifting where tectonic plates are moving away from each other, has made the faults and traps which is the source of the oil- and gas production, see figure 6 on the following page. It can be seen that the oil/gas bearing layers are located in different depths throughout the North sea.

1.3 Geological aging

An overview of the Cretaceous era including the formation layers composition can be seen on figure 7 on page 7. The ageing of a formation is important, since the correct interpretation can tell whether the well has reached the correct depth or not, according to the knowledge that the reservoir rock was created during the Cretaceous period.

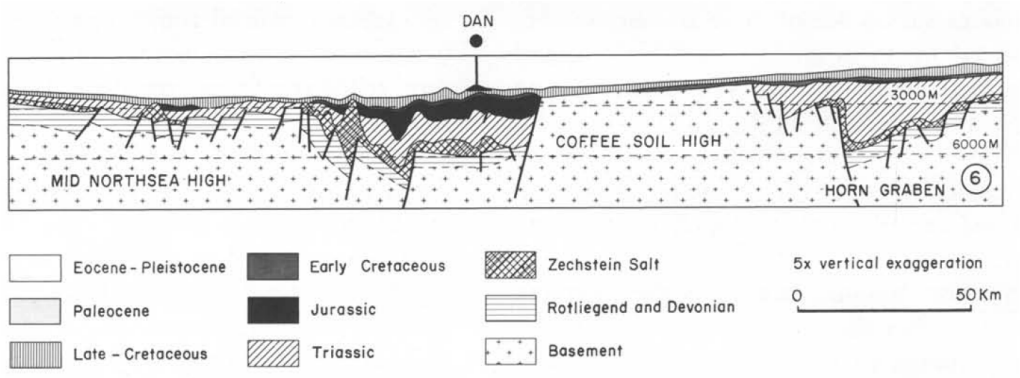

Figure 6: The system of rifting in the North Sea shows the difficulties of finding Oil and Gas. [A45]

1.4 Chalk production

Maersk Oil & Gas has experienced problems with chalk production on Tyra West. The problem has been known since 1998, but in 2008 the problem increased to an extent where 9 wells were producing chalk. Maersk Oil and Gas conducted an investigation, which revealed some correlations of chalk production concerning well locations, the maximum injection Flowing Tubing Head Pressure (FTHP) under operation and pressure changes during swing operations [A42].

No clear correlations could be made between the chalk production and the water production nor chalk production and the minimum production FTHP. Maersk Oil and Gas recommends a cautious procedure concerning pressure settings during swing operations and bean-up operations.

Former research on Chalk Production

In 1980 the Danish Energy Agency (DEA) and the Norwegian Oil Directorate (NPD) invited to a three day seminar on chalk reservoirs, held in Copenhagen. This meeting lead to the establishment of Joint Chalk Research Program (JCR), which should constitute a forum for chalk research. A monograph was published in 1998 by Mark A. Andersen [B1], which describes the problem of chalk production. One of the observations was that similar to oil production from sandstone the flow rates during early stages of pressure reduction should be taken in to account. A sudden initial surge of flow could mobilize solid material from the well causing production of a *toothpaste*-like substance, see figure 8 on page 8.

The reason for the chalk production is described as a chalk instability caused by changes in stress. A numerical study has shown that the effective radial stress exceeded the effective vertical stress. This could lead to instability and chalk production. [B1]

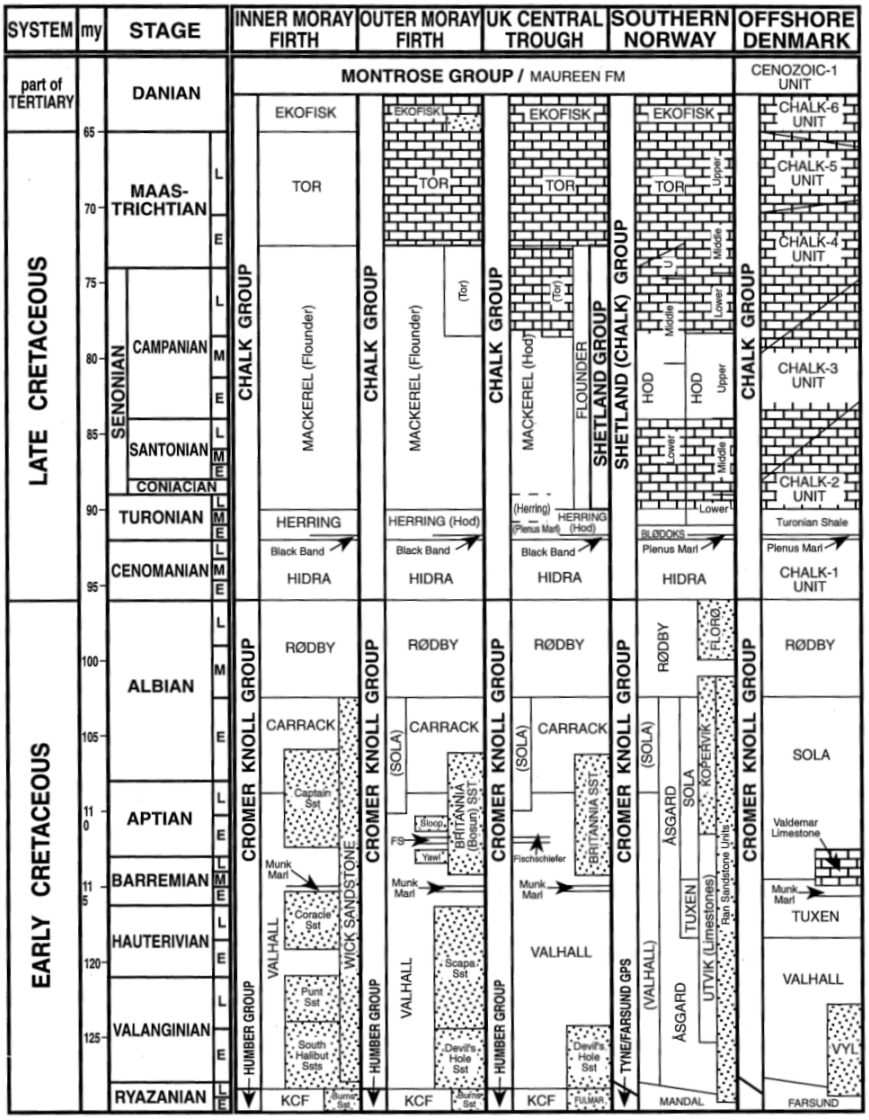

Figure 7: *Age of the oil bearing layers in the North Sea. [B2, p. 297]*

Brief introduction to stresses in generally

Normal stress or average stress τ_{avg} can be expressed as

$$\tau_{avg} = \frac{F_N}{A} \approx \tau \tag{3}$$

where F_N is the normal force acting on an area A.

According to Newtons third law, stating that

> *»To every Action there is always opposed an equal Reaction: or the mutual actions of two bodies upon each other are always equal, and directed contrary parts«*

Figure 8: *Chalk production from well TWC-01 on Tyra West. Photos from Maersk Oil and Gas.*

stress can be explained as

$$\tau = \begin{bmatrix} \tau_{11} & \tau_{12} & \tau_{13} \\ \tau_{21} & \tau_{22} & \tau_{23} \\ \tau_{31} & \tau_{32} & \tau_{33} \end{bmatrix} \equiv \begin{bmatrix} \tau_{xx} & \tau_{yx} & \tau_{zx} \\ \tau_{xy} & \tau_{yy} & \tau_{zy} \\ \tau_{xz} & \tau_{yz} & \tau_{zz} \end{bmatrix} \equiv \begin{bmatrix} \tau_{x} & \tau_{yx} & \tau_{zx} \\ \tau_{xy} & \tau_{y} & \tau_{zy} \\ \tau_{xz} & \tau_{yz} & \tau_{z} \end{bmatrix} \tag{4}$$

where τ_x, τ_y and τ_z respectively are the stresses acting perpendicular on the surface and τ_{xy}/τ_{yx}, τ_{xz}/τ_{zx} and τ_{yz}/τ_{zy} respectively are the shear stresses acting on the surface. In equilibrium the shear stresses are equal to 0, as they are opposite of each other and of equal magnitude. Stress can be shown graphically as seen on figure 9, where stress on an infinite small square is shown with the expressions of equation 4.

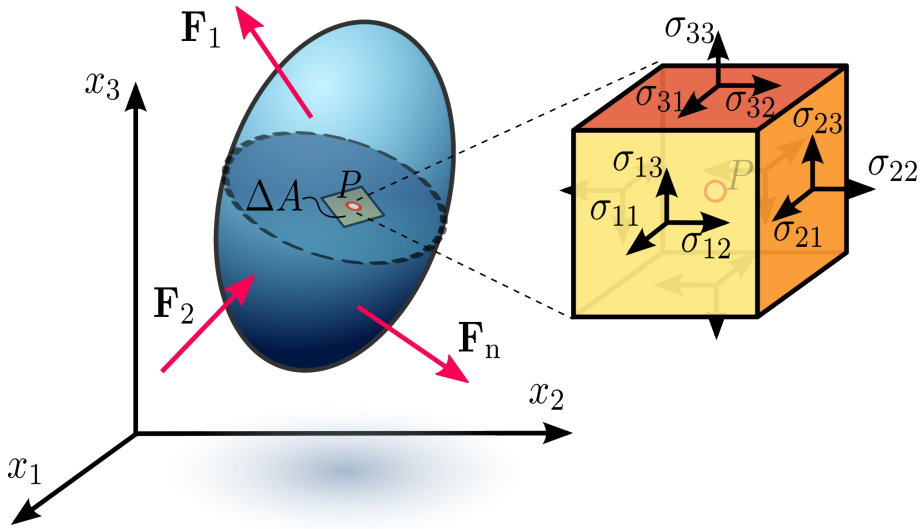

Figure 9: *Graphical example of stress acting on the surface of an infinite small area around a point P. [I21]*

In rock mechanics two additional stress tensors are frequently used. The hydrostatic stress tensor τ_h [N/m^2] describes the pressure performed by the overburden above a point. This

stress tensor is likely to have a volumetric effect on the body affected by the stress.

$$\tau_h = \sum_{i=1}^{n} \rho_i g h_i \tag{5}$$

where ρ is the density of the overhead layer [kg/m^3], g the the gravitational constant [m/s^2] and h the thickness of the overhead layer [m].

The other one is the deviatoric stress tensor τ_D, which distorts the body affected by the stress. The deviatoric stress is described as

$$\tau_D = \begin{bmatrix} \tau_x - \tau_m & \tau_{yx} & \tau_{zx} \\ \tau_{xy} & \tau_y - \tau_m & \tau_{zy} \\ \tau_{xz} & \tau_{yz} & \tau_z - \tau_m \end{bmatrix} \tag{6}$$

where τ_m is the mean stress expressed as

$$\tau_m = \frac{\tau_1 + \tau_2 + \tau_3}{3} \tag{7}$$

and τ_1, τ_2 and τ_3 are the principal stresses where the stres svector is acting normally to the plane affected by the stress, without any shear components.

For simplicity normal stress will be denoted σ and shear stress τ.

In a bore well - here visualized by a hollow cylinder on figure 10 - a hoop stress or circumferential stress acts perpendicular to the radial stress.

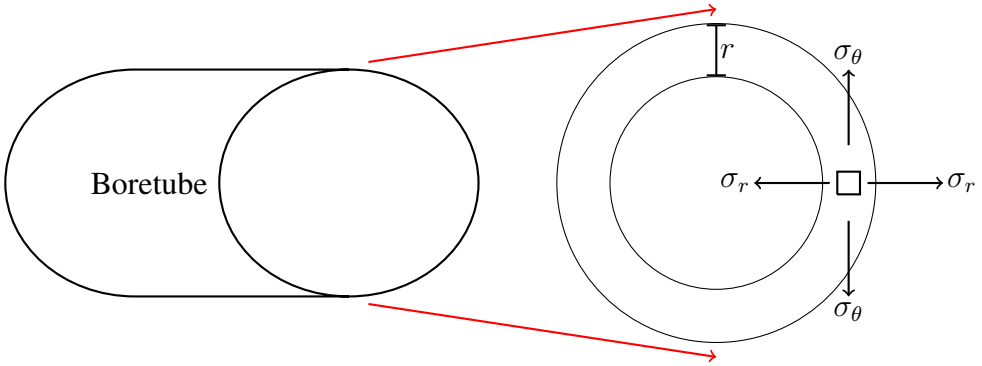

Figure 10: *A tube seen from the end. The wall thickness or the area affected by increased stress because of the well is r, the radial stress is σ_r and the hoop stress is σ_θ.*

An overview of the stress distribution in and near a well is seen on figure 11 on the following page. It can be seen that the hoop stress is largest near the wall whereas the radial stress is smallest near the wall. σ_θ and σ_r decreases and increases respectively asymptotic as the distance from the well bore increases.

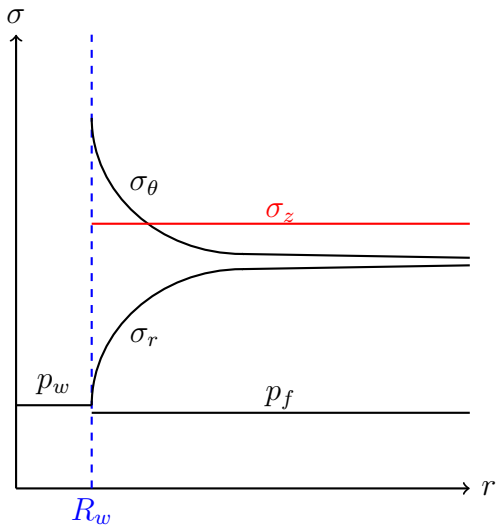

Figure 11: *Stress as a function of distance from the well bore. The hoop stress σ_θ is large near the well bore and decreases asymptotic to the radial stress σ_r. p_f is the formation pressure, p_w the well pressure, σ_z is the axial stress and R_w is the well bore wall. [B7]*

Strain

Strain is the change in length per unit length of a material affected by a stress. The effect of stress on a material depends on the magnitude of the stress and the structure of the material. Strain is divided into normal strain (ϵ)

$$\epsilon = \frac{\delta z}{z_0} \tag{8}$$

and shear strain (δ)

$$\delta = \frac{\delta h}{z_0} \tag{9}$$

Figure 12 shows the change of an object affected by strain.

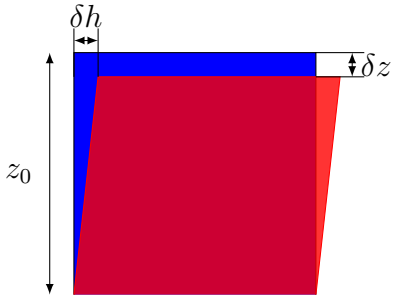

Figure 12: *Effects of normal strain ϵ and shear strain δ.*

When a materiel is exposed to stress, the structure of the materiel is a contributing factor with regards to the fracture of the material. In chalk where atoms are distributed in a crystal

lattice, the construction allows the atoms to move within the limit of the ionic bond length, thereby allowing the chalk structure to bend or stretch. Figure 13 shows the stages during increased stress.

In the first stage of elastic deformation, the ionic bonds are stretched without displacement of the atoms. This allows the structure to recover from the stress without deformation. If the stress is large enough to exceed the elastic deformation area, plastic deformation occurs. Single atoms are moved within the crystal lattice, preventing the complete recovery. Deformation is taking place. If the stress is exceeding the yield strength of the material, the material will fracture. Since chalk is a porous and natural material, the structure will have vacancies and failures which changes the yield strength.

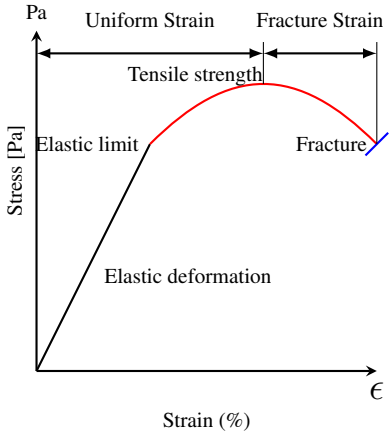

Figure 13: *During increased stress, the material will undergo an elastic deformation from which the material can fully recover. As soon as the elastic limit is crossed, the material will be in the area of plastic deformation (red line). The material structure will change and eventually break (blue line).*

Pore elasticity

In order to describe forces acting on a porous media like chalk, the mechanical properties of the chalk has to be determined. This can be done by the bulk modulus K. This quantity describes the change in volume by a certain uniform pressure applied. It is defined as

$$K = -V\frac{\Delta P}{\Delta V} \tag{10}$$

The larger the value for K, the better is the resistance against pressure caused volume change. Values for K is given for both solids and fluids. The inverse K, $1/K$, is called the compressibility.

The fluid inside the pores of the chalk has to be taken into account. To describe the deformation of the fluid relative to that of the solid, a strain parameter $\bar{A}$ for the fluid part

has to be defined. $\bar{A}$ is defined as

$$\bar{A} = -\theta \left(\frac{\Delta V_p}{V_p} + \frac{p_f}{K_f} \right) \tag{11}$$

which divides the fluid volume into two parts. The change of pore volume and the compression/decompression of the fluid caused by change in pore pressure p_f. $\bar{A} > 0$ if fluid is leaving the pore volume and $\bar{A} = 0$ for a undrained material, e.g. a confined pore.

The chalk formations in the North Sea are affected by the removal of hydrocarbons. The value of $\bar{A}$ will get positive if drainage of the formation takes place. If the pores are drained, the pressure of the overburden will cause the formation to subside. This subsidence can be a driving force in *pushing* hydrocarbons to a wellbore. Subsidence will also cause the sea floor to sink, which is a disadvantage when building offshore installations. A counter measure for the subsidence is to replace the oil with injected water to maintain pore pressure.

2. Litterature survey

In order to get an overview of the research done in chalk production in the past, a litterature survey has been performed. The starting point of the survey is the Monograph "Petroleum Research in North Sea Chalk" written by Mark A. Andersen [B1]. This monograph gathers the threads of the initial research based on experiences and problems concerning oil and gas exploration in chalk reservoirs and is a thorough introduction to experiences gathered until publication. To avoid an iteration of the information only a short summary of the information from this book limited to chalk production issues is given here.

2.1 Chalk formation

Since the discovery of the Ekofisk field in 1969, a large number of oilfields has been build in the North Sea. As these fields have begun to be depleted, a number of challenges has turned up. Since oil exploration in chalk is a relative narrow discipline, solutions for these challenges had to be solved case by case, and the research in this field is performed by a limited group of scientists.

Subsidence

The first production of oil from the chalk formations was performed by the higher pressure in the chalk due to the overburden from the above positioned layers. The oil and gas came out of the chalk more or less by itself. A drop in production because of depletion was beginning to show up in the early 80's, and a plan for water injection in order to rise the formation pressure again was initiated in 1984. As a consequence of the production of oil and gas from the porous chalk layer, subsidence has occurred in several fields. The most famous subsidence incident is the Ekofisk subsidence from 1984. Because of a subsidence rate of $\approx$ 30 cm/yr in the mid- and late 1980s, an increase in height of the platform had to be initiated. In 1987 the Ekofisk platform was raised by 6 meters as a compensation for the lowering seabed.

Compaction

The reason for the subsidence is found to be compaction of the chalk layers. This compaction occurs, partly as a consequence of the lowering pore pressure and partly as a consequence of the water injection, see section 2.1 on page 16. The compaction is related to the highly porous structure of the chalk, hence the mechanical strength of the chalk is low. Figure 14 on the following page shows the correlation between compaction as a function of stress for a chalk sample with 46% porosity. As it is seen the compaction is near 12% with the vertical stress of $\approx$ 35 MPa. A positive side effect of compaction is the hydrocarbons being produced of the compacting layer because the porosity decreases and the hydrocarbons are pushed out of the formation.

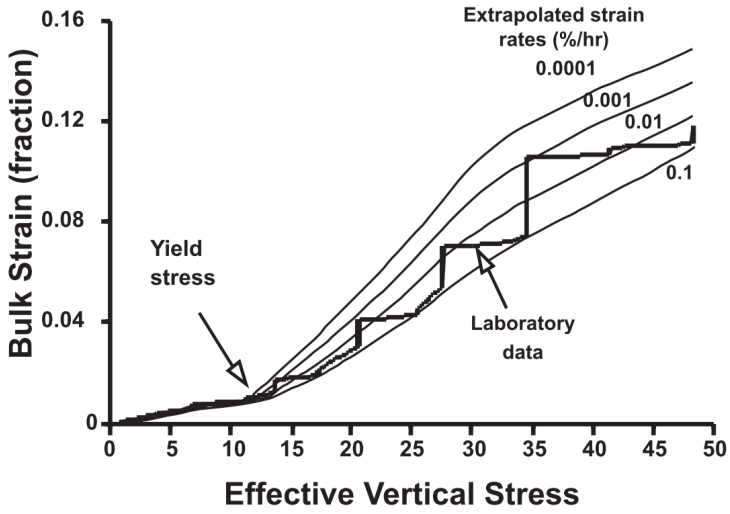

Figure 14: *Compaction as a function of stress for a chalk sample with 46% porosity. [B1, p. 138]*

Compaction is deformation of the rock exceeding the elastic deformation area. The deformation is therefore irreversible. The compaction is a function of the mean effective stress τ'_m defined as

$$\tau'_m = \tau_m - \alpha p_f \tag{12}$$

where τ_m is described in equation 3 on page 7, α is a constant called Biots constant and p_f is the fluid pore pressure. Biots constant is defined as

$$\begin{aligned} \alpha &= \theta \frac{\Delta V_p / V_p}{\Delta V_{tot} / V_{tot}} \\ &= \frac{\Delta V_p}{\Delta V_{tot}} \\ &= 1 - \frac{K_{fr}}{K_s} \end{aligned} \tag{13}$$

where K_{fr} is defined as

$$K_{fr} = K_s \left(1 - \frac{\theta}{\theta_c}\right)$$

and describes the change in pore volume relative to the change in total volume at constant pore pressure. A physical explanation of equation 12 is, that the solid carries the part τ'_m of the total stress τ_m and the rest is carried by αp_f. K_{fr} is the elastic moduli of the framework inside the chalk and K_s is the elastic moduli of the solid. $K_{fr} < K_s$ which induce that $\theta < \alpha \leq 1$. θ_c is the critical porosity.

From equation 12 it can be seen that depletion of a chalk formation will decrease the value of p_f which is the counteracting force inside the chalk formation on the overburden. As a consequence of that, compaction is inevitable without replacing the produced hydrocarbons.

Porosity

In the North Sea porosity is not uniform throughout the entire oil containing area. Different areas has chalk layers of different ages and the depths of the layers also differ. In the Danish part the chalk is mainly Maastrichtian-Danian chalk. The porosity in five fields from the Danish Part of the North Sea is shown in table 1.

Table 1: *Porosity and age of five fields from the Danish part of the North Sea. [A30][A29][A22]*

Field	Age	Porosity	Permeability
Skjold	Danian-Tutorion, Mainly Maastrichtian	35 - 40%	< 1 mD
Kraka	Danian	24 - 32%	1 - 3 mD
Valdemar	Aptian and Barremian	20 - 48%	0,1 - 4 mD
Tyra	Danian and Maastrichtian	> 40%	5 - 20 mD
Dan	Maastrichtian	20 - 35%	avg. 1,75 mD

Drawdown

The stability of chalk formations rely on conditions like formation pressure, porosity and compaction among others. When a well is drilled in the chalk, the support to the surroundings is removed together with the drill cuttings. A casing of concrete or steel can reestablish the support.

In oil production terms *drawdown* is often used instead of well pressure. Drawdown p_d is defined as

$$p_d = p_{fo} - p_w \tag{14}$$

where p_{fo} is the average formation or pore pressure and p_w is the well or flowing bottom hole pressure. p_{fo} alters slowly with depletion, whereas p_w can change rapidly. Rapid variations in drawdown will trigger variations in stresses in the well vicinity, which could induce failure or worse in the well. p_d^c is the critical drawdown where p_w is reduced so much that solids from the formation is pushed into the wellbore. p_d^c is defined as

$$p_d^c = p_{fo} - p_{w,min} \tag{15}$$

During swing operations, where the same well is used for either injection or production of gas, variations in drawdown can happen. According to information from Maersk Oil and Gas, injection FTHP is ca. 3000 psi whereas the average reservoir pressure is 2300 psi in 2008. Observations indicate that chalk producing wells has been exposed to rapid variations in FTHP of 2000-2400 psi. These rapid variations will, accordingly to equation 14, induce stresses in the well vicinity. p_d^c could have been reached and exceeded. [A42]

Water weakening effect

The consequence of injecting seawater in wells to enhance oil production and maintain reservoir pressure has been investigated. It has been shown that chalk layers exposed to seawater injection has been modified. The chalk surface react with ions present in the injection water, which lead to precipitations of solids on the chalk surface. Furthermore enhanced compaction of the chalk layer exposed to seawater injection was noticed. This compaction has, however, a positive effect, as it is used as a drive mechanism for hydrocarbons. The two main purposes of water injection is to

1. keep the reservoir pressure above the bubble point of the hydrocarbons and
2. displace the oil.

During production below the bubble point pressure of the hydrocarbons, lighter fractions of hydrocarbons will go from liquid to a gas phase. A gas can create channeling, which could lead to loss of reservoir energy and a drop in production. The displacement of oil by water is a normal secondary recovery method, which has been used for many years. [A32]

Dolomitization

Experiments has shown that the interaction from Mg^{2+} and the chalk surface depends on the temperature. In a brine solution containing 0,013 M Ca^{2+} (natural concentration in seawater), Mg^{2+} and SCN^- as tracer, the concentration of Ca^{2+} and Mg^{2+} was kept constant until a temperature of approx. 70°C while flooding the brine solution through a chalk core. At increasing temperatures the concentration of Ca^{2+} increased while the concentration of Mg^{2+} decreased, indicating that the substitution shown in equation 16 took place.

$$CaCO_3 + Mg^{2+} \leftrightharpoons CaMg(CO_3)_2 + Ca^{2+} \tag{16}$$

Since the normal concentration of Mg^{2+} in seawater is about 4 times higher, the process of dolomitization can be expected to be even higher. The fact that Ca^{2+} is bigger than Mg^{2+} also indicates structural changes in the chalk during dolomitization which could be a partly explanation of the water weakening effect. [A44]

Since no water is injected in the Tyra Field, the water weakening effect cannot be an explanation for the massive chalk influxes during swing procedures.

Solids production

Solids production is a known problem in many oil wells. The explanation for this phenomena is well described for sand particles. For a single sand grain to be pushed out of the packed sand structure, the force F_r is needed, where

$$F_r = \pi \left(\frac{d_g}{2}\right)^2 [4S_0 + \mu(2\sigma'_z + 2\sigma'_\theta) + T_0] \tag{17}$$

d_g is the diameter of the sand grain, μ is the coefficient of internal friction, T_0 and S_0 is the tension strength and cohesion respectively and σ'_z and σ'_θ is the effective axial and tangential (hoop) stresses respectively. The solids production can occur as

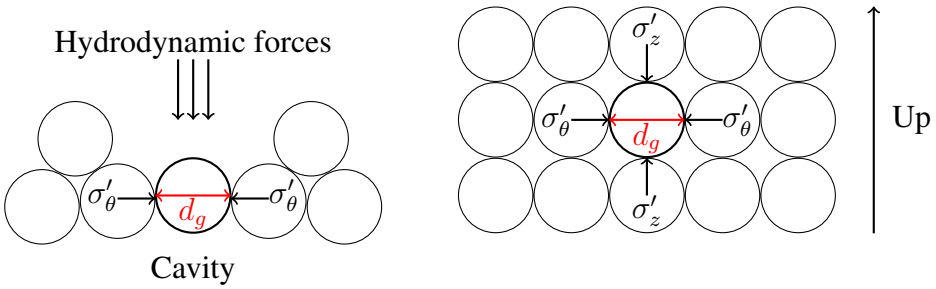

Figure 15: *Hydrodynamic forces acting on a single sand grain seen from above and the shear forces acting on the sand grain seen from the cavity.*

background production, where a small quantity of sand particles are produced along with the hydrocarbon production. The quantity of sand particles is small enough to be removed in the normal produced water treatment devices e.g. hydro cyclones etc. Solids production can also occur as slugs where the volume of solid particles can be so massive that the well bore chokes.

Accordingly to Fjaer et al [B7] the research and investigation on chalk production is limited. The known cause of chalk production is mentioned as sudden changes in well conditions, e.g. closure or opening of the fluid flow. In Tyra Field, estimated 1400 m^3 of solids was produced during the first five years of production as background production [A36]. With 24 producing wells in that period, the normal background production of chalk per well is estimated to $\approx 2{,}643 \cdot 10^{-7}$ $m^3 s^{-1}$. Chalk slugs has been observed during swing operations on several wells [A42].

Chalk extrusion

The late Professor Rasmus Risnes from Rogaland University Centre in Norway has performed several investigations on North Sea Chalk. In 1989 he investigated the capability of solid drained chalk samples to be fluidized under loading and extruded. The result of this laboratory study showed that chalk could be fluidized and extruded as soon as the stress performed on the chalk sample, created a critical stressed zone around the outlet of the test cell. At the same time the stress should be sufficient enough to put the underlying chalk in the plastic deformation area in order to feed the extrusion. [A38]

As seen on figure 16 on the following page results of experiments performed on chalk from Tyra field showed a correlation between the stress applied on the chalk cores and the extrusion of "toothpaste" like chalk. The result showed that plastic deformation developed at $\approx$ 10 MPa. Chalk extrusion occurred at $\approx$ 20 MPa for the TWB-08 sample, figure 16a on the next page, and $\approx$ 40 MPa for the TWC-02 sample, figure 16b on the following page.

The differences in results between the different core samples was explained as TWC-02 chalk being more affected by strain hardening as the TWB-08 sample.

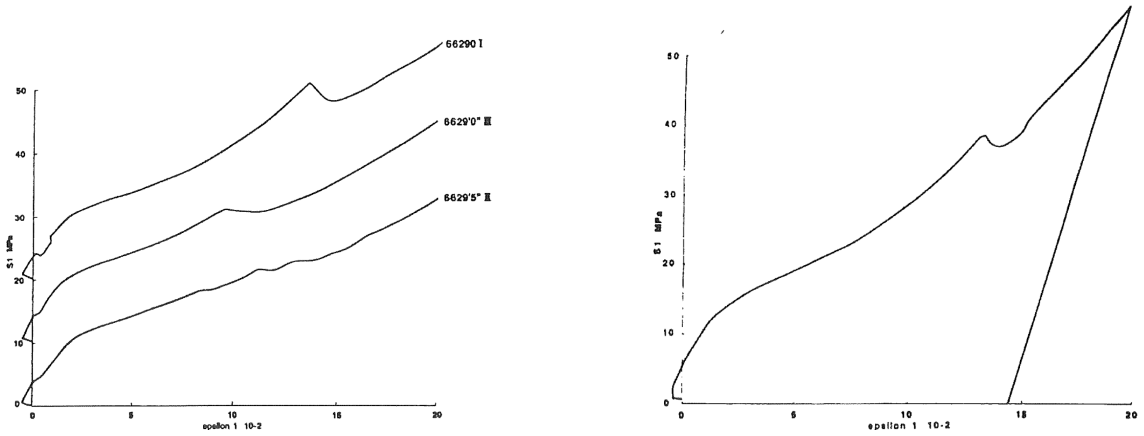

(a) Samples from TWB-08 *(b) Samples from TWC-02*

Figure 16: *Experiments which resulted in chalk extrusion performed on samples from the Tyra field. The y-axis represents stress in MPa and the x-axis the strain. [A38]*

2.2 Discussion

If a small amount of solids is produced over time, the support from the casing can be lost because of cavities created as a result of the solids production. Since the permeability of the chalk formations in the North Sea is very low, rapid variations in drawdown, e.g. due to change from injection of gas to production of gas (swing procedures) can lead to an increase in solids production.

In the porous structure of the Tyra Field the formation fluid is helping to maintain an equilibrium between the pressure from the overburden and the pressure in the well bore. This equilibrium could be disturbed by swing procedures where the injection pressure of 3000 psi is changed to a production pressure of 2300 psi [A42]. The surroundings near the well casing will loose the stabilising pressure from the fluid in the well bore until the formation pressure has pushed the formation fluid back into the well bore and reestablished the equilibrium conditions. During that period only the chalk structure itself will be the bearing structure, see figure 17 on the next page. [A37]

2.3 Conclusion

Laboratory studies performed at the end of the eighties and in the start of the nineties has shown that chalk from the North Sea can be fluidized and can create a *toothpaste*-like substance. The explanation could be that the pressure variations occurring during swing operations can create an increase of stress on the chalk structure near the well bore which finally leads to extrusion of chalk and creation of chalk slugs in the well.

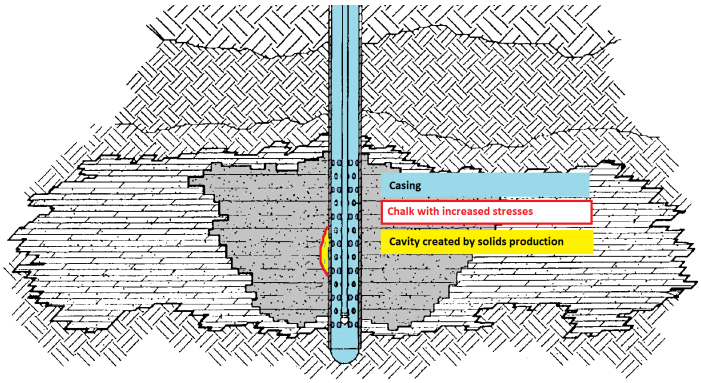

Figure 17: *Principle sketch of cavities in the vicinity of the well casing. Processing of [I18]*

The result indicates that the problem is not the swing procedure itself but the pressure and stress conditions around the well bore. Lowering the pressure to produce oil and gas in low pressure mode to gain benefit of the compaction drive mechanism, could lead to more chalk extrusions and new challenges in the production in the North Sea.

3. Solids removal

3.1 Particle size

Maersk Oil and Gas has ordered a study on particle size from a sample of the produced chalk, taken on 10 march 2010 from TWC-01. This study was performed by GEUS. The result of the particle size distribution, shown in percentage of clay, silt and sand can be seen in table 2. The distribution is given accordingly to the Krumbein phi scale, where

$$D = D_0 \times 2^{-\phi} \tag{18}$$

D is the diameter of the particle [mm], D_0 is 1 mm used for consistency of units and ϕ is the size on the Krumbein phi scale. The Krumbein phi scale is a modification of the Wentworth grade scale, see figure 83 on page 108. As it is seen, 14,12 - 32,84% of the solids are smaller than 2 μm. These particles is estimated to be the biggest challenge when considering removing the solids. The small size is below the minimum particle size for conventional water treatment like hydrocylones [B5, p. 201]. The size distribution was

Table 2: *Particle size distribution in percentage of clay, silt and sand performed by GEUS. Size is given according to Wentworth Grade Scale. [A35]*

Sample		28398,1	28398,2	28399,1	28399,2	28457,1	28457,2
Clay (<2μm)	%	14,12	19,40	18,33	18,84	32,84	32,23
Silt (2-63 μm)	%	73,89	76,21	51,46	60,42	67,16	67,77
Sand (>63 μm)	%	11,99	4,38	30,20	20,74	0,00	0,00

made by the use of Laser Scattering Technique.

3.2 Conventional unit operations

There are different possibilities for treating production streams and streams of produced water on a offshore oil/gas installation. In this thesis a series of unit operations will be mentioned with a comment on pros and cons. These series are not a exhaustive list of all possible methods. Many problems are solved with special solutions tailored to a specific task. The following is therefore a weighted estimate of useable methods. Some of the methods are used in areas where the hydrocarbon production is done in sand layers instead of chalk layers. These methods are still listed, since the unit operation concerns solids removal. The focus is on the massive chalk influx observed at the Tyra Field during swing operations, and not the normal background solids production. Many filtration processes will not be mentioned since the massive chalk influx is assumed to be way above the field of application of these.

3.3 In-hole solutions

Countermeasures to solids production done in-hole in well bores are risky since the accessibility, as a consequence of the placement deep below the platform, is limited. Clocking of well bores would give rise to comprehensive repair/makeover of that particular well.

Gravel packing

In soft formations that could cave into the well, a Gravel Pack completion can be performed. By this procedure the cavity is packed with well sorted, coarse sand. The sand acts as a highly permeable and porous filter which is stabilizing the well formation and catching the produced solids. Open Hole Gravel Packing can be used for both vertical and horizontal wells. In the North Sea, Gravel Packing completion has been used in Valhall Field and other fields. Problems related to stress variations of the well surroundings has lead to solids production that could not be treated with gravel packing. These problems are identified as early and late problems, meaning that a newly established well can cause solids production due to the disturbances in the surroundings by the well bore (early). Late problems are identified as depletion of the well. [A27]

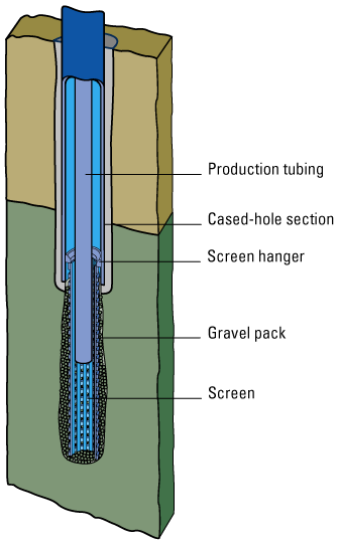

Figure 18: *Simple schematics of an Open Hole Gravel Pack. [I19]*

Since the Tyra Field is an old production field (depletion could be a contributing factor), gravel packing does not seem to be the optimal solution for the solids production problem.

3.4 Top-side solutions

Often top-sides solutions are desirable because of the easy accessibility to equipment for maintenance purposes. The problem with top-side solutions are the limited space available

on an oil/gas installation offshore and the fitting of the equipment into the already existing system of equipment and pipes.

Sand filter

Filtration technologies are widely used for solids removal with a broad range of solutions. The problem with filtration in a process where large volumes of particles can occur is clocking of the filter. Clocking either stops the stream or leads to opening of a bypass valve to prevent shutdown. Since the chalk particles are meant to carry small amounts of oil along with them, this is not a suitable solution. Self cleaning filters, controlled by the exceeding pressure drop as a filter cake is building up, can be an alternative.

Centrifugal separation

A widely used technique is centrifugal sedimentation. The use of centrifugal sedimentation is based on the difference in density of a solid in a liquid or to liquid phases. If a particle with the mass m_p [kg] is rotating at an angular velocity ω [s^{-1}] at the radius r [m] from the axis of rotation, the particle is exposed to a centrifugal force F_c of

$$F_c = (m_p - m_l)r\omega^2 \tag{19}$$

where m_l is the mass of the fluid that the particle displaces.

The term $r\omega^2/g$, where g is the gravity constant, is used to express the separation power of the process. The term is often denoted $\frac{G}{g}$. With ω given as r/min and D as the diameter of the centrifuge bowl, a relative plain expression for the separation power is given by

$$\frac{G}{g} = 0,000559\omega^2 D \tag{20}$$

The heavier part/liquid will move radially outwards and the lighter part radially inwards when exposed to centrifugal forces.

The force F_s acting opposite the sedimentation is given by Stokes law, where

$$F_s = 3\pi\mu d v_s \tag{21}$$

μ is the dynamic viscosity of the fluid, d is the diameter of the particle and v_s is the velocity of the particle. It is assumed that the particle is small, and does not move too fast.

In separation processes using centrifugal sedimentation, the Sigma concept is used for calculations of the theoretical performance. The Sigma concept is based on the relations between the cut size x_{50}, the total volumetric feed stream Q and the centrifuge size index denoted Σ. Σ is a calculated equivalent area of a settling tank, which in theory is capable of doing the same amount of work in a unit gravitational field.

x_{50} is represented by the terminal settling velocity v_g as

$$v_g = \frac{\Delta\rho d^2\omega^2 r}{18\mu} \tag{22}$$

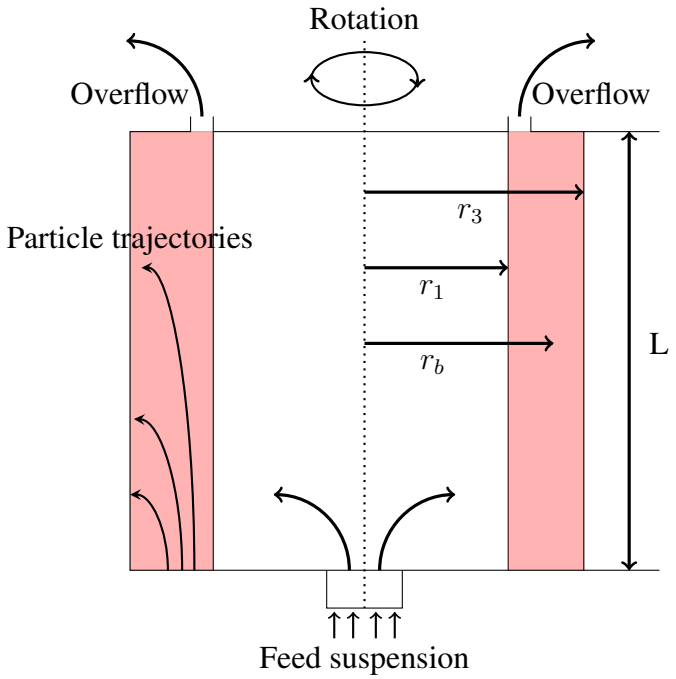

Figure 19: *Schematic illustration of a tubular centrifuge*

or explained with x_{50}

$$\begin{aligned} v_g &= \frac{x_{50}^2 \rho g}{18\mu} \\ &= x_{50}^2 K \frac{g}{\omega^2} \end{aligned}$$

where K is the sedimentation constant defined as

$$K = \frac{\Delta\rho\omega^2}{18\mu}$$

The distance x a particle can move in the fluid is explained by

$$x = v_g t_T = \frac{\Delta\rho d^2 \omega^2 r}{18\mu} \cdot \frac{V}{Q} \tag{23}$$

t_T is the residence time defined as the volume of liquid V [m^3] divided by the flow Q [m^3 s^{-1}]. By substituting x with $\frac{x}{2}$ in equation 23, which is the ideal situation where half of the particles with the diameter d will be removed from the suspension, the flow Q can be isolated as

$$Q = \frac{\Delta\rho d^2}{9\mu} \cdot \frac{V\omega^2 r}{x} \tag{24}$$

The first part of the right-hand side equation is explaining the physical factors of the fluid and the second part is explaining the centrifuge parameters. By rearranging equation 24,

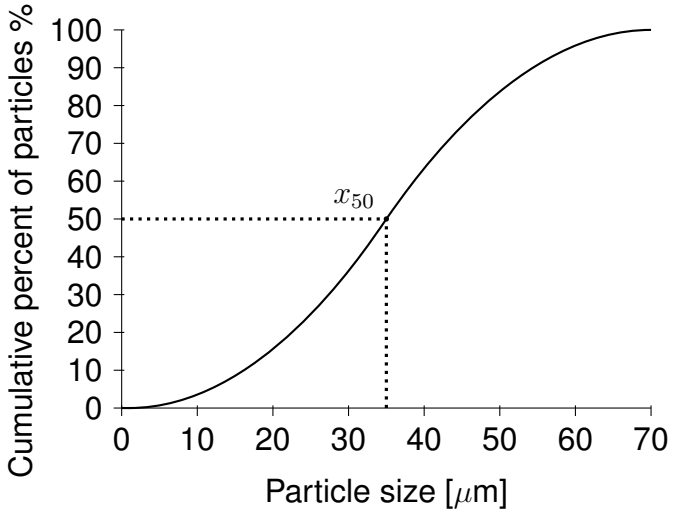

Figure 20: *The cutsize x_{50} shown in a plot of the cumulative percent of particles as a function of particle size.*

and isolate d, the critical diameter d_c can be found as

$$d_c = \left(\frac{9\mu Q}{\Delta\rho} \cdot \frac{x}{V\omega^2 r} \right)^{\frac{1}{2}} \tag{25}$$

which is the diameter of the particles of which the half will be removed.

In figure 19 on the preceding page a schematic illustration of a Tubular centrifuge is shown. The distance r_1 is the radius of the liquid surface determined by the overflow outlets. r_3 is the distance from the center of rotation to the wall of the tube. r_b is the distance from the center of rotation to a particle at the end of t_T. If $r_b < r_3$ the particle will leave with the fluid and if $r_b = r_3$ the particle will be deposited on the wall, and thereby removed from the fluid.

The cut size x_{50}, which is the removal of 50% of the solids from the fluid can be calculated as

$$x_{50}^2 = \left(\frac{Q}{2\pi LK} \right) \left[\ln \left(\frac{2r_3^2}{r_3^2 + r_1^2} \right) \right] \left(\frac{1}{r_3^2 - r_1^2} \right) \tag{26}$$

By rewriting equation 26 and substituting x_{50} with $\frac{v_g}{K\frac{g}{\omega^2}}$, Q can be isolated as

$$\begin{aligned} Q &= \frac{x_{50}^2\, 2\pi LK}{\left(\ln \left[\frac{2r_3^2}{r_3^2 + r_1^2} \right] \right) \left(\frac{1}{r_3^2 - r_1^2} \right)} \\ &\Updownarrow \\ &= 2v_g \left(\frac{\omega^2}{g} \right) \pi L \left(\frac{r_3^2 - r_1^2}{\ln \left(\frac{2r_3^2}{r_3^2 + r_1^2} \right)} \right) \end{aligned}$$

or

$$Q = 2v_g\Sigma \tag{27}$$

where

$$\Sigma = \left(\frac{\omega^2}{g}\right)\pi L\left(\frac{r_3^2 - r_1^2}{\ln\left(\frac{2r_3^2}{r_3^2+r_1^2}\right)}\right) \tag{28}$$

In order to make equation 28 more easy to use, an approximation of the denominator based on the series expansion[1] of the logarithmic function

$$\ln y \simeq 2\frac{y-1}{y+1}$$

is taken from the first series of a series expansion. With that approximation the denominator will get

$$\ln\frac{2r_3^2}{r_3^2+r_1^2} \simeq \frac{r_3^2 - r_1^2}{\frac{3}{2}r_3^2 + \frac{1}{2}r_1^2}$$

When substituted into equation 28 the final expression for Σ is

$$\Sigma \simeq \left(\frac{\omega^2}{g}\right)\pi L\left(\frac{3}{2}r_3^2 + \frac{1}{2}r_1^2\right) \tag{29}$$

This approximation is by Ambler claimed to trigger a failure of maximum 4% [A24].

Scale-up between centrifuges can be done with the expression

$$\frac{Q_1}{\Sigma_1} = \frac{Q_2}{\Sigma_2} \tag{30}$$

as long as the type of centrifuges are the same and the cut size x_{50} is to remain constant.

Hydrocyclones

A normal unit operation in water treatment is hydrocyclones, see figure 21 on the following page. Hydrocyclones can be used for liquid/liquid and solid/liquid separation. The separation factor $\frac{G}{g}$ for hydrocyclones is in the range form 100 - 1000 depending on the diameter and operating pressure. Mixtures with low interfacial tension can create foams and emulsion caused by the turbulent flow and the high shear field produced [B6, p. 15-102]. In solid-liquid separation the removal size is $> 10\,\mu$m. Hydrocyclones are used during produced water treatment and well make over, and has successively been used for

[1] $\ln y = 2\left[\frac{y-1}{y+1} + \frac{1}{3}\left(\frac{y-1}{y+1}\right)^3 + \frac{1}{5}\left(\frac{y-1}{y+1}\right)^5 \cdots \frac{1}{n}\left(\frac{y-1}{y+1}\right)^n\right]$

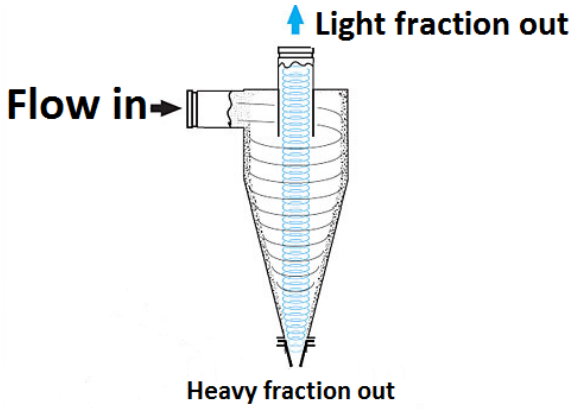

Figure 21: *The principle of the hydrocyclone is to use centrifugal forces in order to separate a heavy fraction from a lighter fraction, e.g. solids (heavy fraction) from water (lighter fraction).*

removing the chalk influxes as seen on figure 8 on page 8 in some occasions but the limit for efficiency for the hydrocyclones has been reached [A42].

The centrifugal force generated in a hydrocyclone is mainly from the feed stream pressure. The limit of the size of a hydrocyclone depends on the creation of a centrifugal force large enough to generate the needed separation factor. The need for better performance is often fulfilled by putting hydrocyclones in parallel.

To calculate the estimated particle size x that can be separated from the feed stream with the help of a hydrocyclone, the following expression can be used

$$x_{98} = \frac{0,0094 D^{1,18} \exp^{6,3c}}{Q^{0,45}(\rho_s - \rho_l)^{0,5}} \tag{31}$$

where D is the internal diameter of the hydrocyclone, c is the solids concentration, x_{98} is the particle size at 98% efficiency, Q the volumetric flow rate and ρ_p and ρ_l is the particle density and liquid density respectively.

Pros Cheap, no moving parts, low technology.
Cons Limited in size, low separation factor, can create foam/emulsion.

Since hydrocyclones are used in the normal treatment of produced water for solids removal, this technology has showed its effectiveness. When it comes to special cases like the chalk production during swing operations, this technology has proven to be near the limits or beyond of the field of application. Therefore hydrocyclones are not recommended as the treatment for chalk production.

Centrifuges

An alternative for hydrocyclones and the possibility of gaining an increased separation factor comes with the use of centrifuges. The difference from hydrocyclones is that the

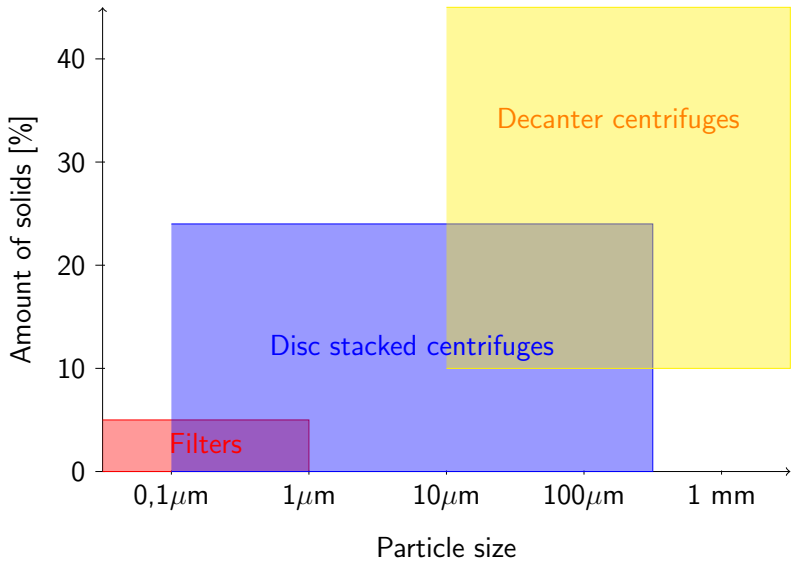

Figure 22: *Determination of solid-liquid separation method depended on particle size and the amount of solids.*

centrifuge creates the centrifugal force by rotation. The rotating motion is created with the help of an engine for which reason the separation factor depends on the momentum and size of the engine in use. In figure 22 three different types of solid-liquid separation is shown. Two by the use of centrifuges and one with the use of filtration. It is seen that quite large solid fractions can be separated from the liquid with the help of centrifuges. Filtration can remove all particles, but the range in which filtration is applicable is limited and a large volume of solids will cause clocking of the filter.

Decanter centrifuges

The Decanter centrifuge is a separation process for both solid/liquid, liquid/liquid and liquid/solid/liquid separation. The key principle in the technique is a horizontal separation chamber, where the inlet feed stream is separated by the help of a rotating conveyor. Both the chamber and the conveyor is rotating at different speed. The method enables a coarse removal of solids down to a grain size of approximately 10μm. The operating pressure is up to 150 psig and the temperature range is from -87°C - 260°C. The amount of solids in the feed stream and the calculated power consumption of typical scroll conveyors can be seen from table 3 on the next page.

The maximum volumetric flow is calculated as

$$\frac{Q}{V_{gd}} = \left(\frac{\pi\omega^2 L}{g}\right)\left(\frac{r_p^2 - r_b^2}{\ln(1 - \mathrm{Rec}_d[1 - (r_p/r_b)^2])}\right) = \Sigma_{Rec_d} \tag{32}$$

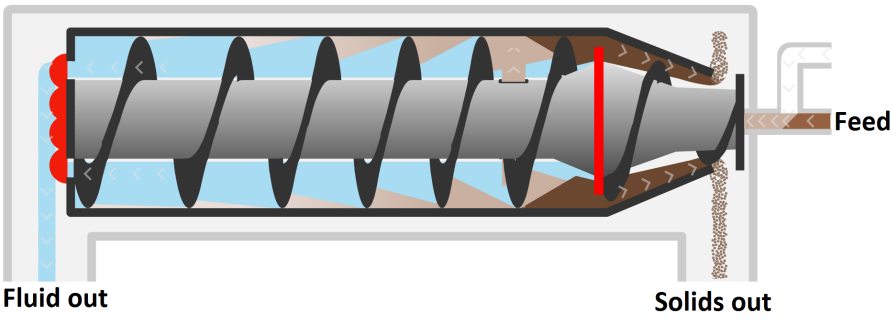

Figure 23: *Principle of separation in the Decanter Centrifuge. The feed stream enters the separator and is separated by the help of centrifugal forces. Solids are removed from the separator by a rotating conveyor which makes it possible to treat feed streams with a high solids concentration. [I10]*

where V_{gd} is the settling rate under $1g$, r_b and r_p are the bowl and pool surface radii respectively and Rec_d is given as

$$\text{Rec}_d = \frac{r_3^2 - r^2}{r_3^2 - r_1^2}$$

Rec_d is the *grade efficiency* which describes the recovery of particles with the size d that are uniformly distributed across the annular pool. If Rec_d is set to 50% the equation to use is explained earlier, see equation 28 on page 25.

Table 3: *Specifications and performance characteristics of typical scroll conveyor. [B6, p. 18-121]*

Bowl diameter	Speed	Separation factor	Throughput, up to		Motor size
mm	r/min	G/g	Liquid L/s	Solids tons/h	kW
152,4	8000	5500	1,26	0,25	4
355,6	4000	3180	4,73	1,50	15
457,2	3500	3130	6,30	3,00	37
609,6	3000	3070	15,75	12,00	93
762,0	2700	3105	22,05	15,00	149
914,4	2250	2590	37,80	25,00	224
1117,6	1600	1600	44,10	25,00	298
1371,6	1000	770	47,25	60,00	187

The use of a decanter centrifuge is a possibility as long as the expected volume of solids is large. The efficiency is the same as the conventional hydro cyclone with a removal of particles $\geq 10\,\mu m$. The volume of solids can be up to 45 w/%.

Pros Can handle large volumes of solids, self cleaning.

Cons Moving parts, expensive, high technology.

Decanter centrifuges will not increase the solids removal from the produced water but increase the resistance of the water treatment system against chalk influxes.

Disc-stack centrifuges

The Disc-stack centrifuge is an effective separation method which is capable of separating solid/liquid, liquid/liquid and liquid/solid/liquid feed streams. Two-phase equipment is commonly known as clarifiers and three-phase equipment as separators. The Disc-Stack centrifuge can be used with internal pressure up to 150 psig or higher and with feed temperature up to 315°C. The disc centrifuges comes in three different categories.

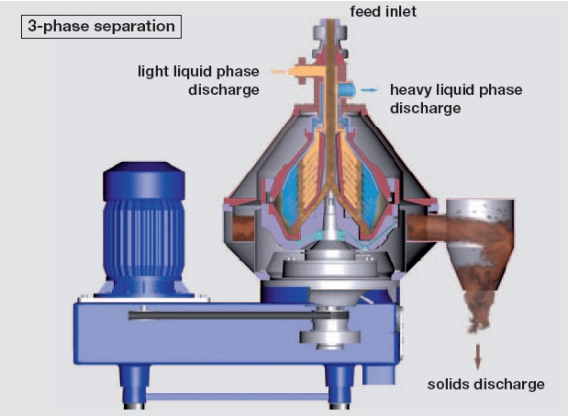

Figure 24: *A 3-phase Disc-Stack centrifuge. [I15]*

Manual Discharge Disc Stack Centrifuge where manual removal of solids has to be performed.

Self-cleaning Disc Centrifuges Solids are discharged automatically on a timed cycle.

Disc Nozzle Centrifuges A continuously discharge of solids along with some of the liquid phase.

During an underbalanced drill campaign in the North Sea, DONG Energy used the Disc Stacked Centrifuge to clean injection fluid from fine chalk drill cuttings. After some adjustments to prevent clocking of outlet nozzles the method seemed successful [I17].

For a disc-stacked centrifuge the equation for Σ is

$$\Sigma = \frac{2\pi\omega^2(N-1)(r_o^3 - r_i^3)}{3g\tan\theta} \tag{33}$$

where N is the number of discs in the stack, r_o and r_i are the outer and inner radii of the disc stack and θ the conical half-angle of the disc stack.

Pros Removes smaller particles, self cleaning possible.
Cons Moving parts, expensive, high technology.

The use of Disc-Stack centrifuges can increase the solids separation significantly based on the theoretical knowledge. The technology has been used in the offshore industry to remove chalk cuttings, and can probably be used to remove solids from produced water also. The particles passing through the system will be $\lesssim 0,1\mu m$ which is a big improvement.

3.5 Chemicals addition

A conventional treatment is the addition of chemicals to the system. Flocculants and coagulants increases the particle size of solid particles and can thereby increases the efficiency of the solids removal. Demulsifiers are countermeasures against the formation of emulsions and foams and many types of this chemical is used as a normal treatment.

Flocculants

By adding flocculants to a suspension, individual particles can form aggregates. This process is used to treat many different types of waste water to improve settling and filtration. Flocculants can possess different surface charges and be of either natural or synthetic origin. The size of the flocculant molecule has influence of the aggregation of the particles. Large shear forces can break an aggregate into smaller parts whereby the effect of the flocculant is reduced. There are many considerations to take into account in order to find the right flocculant to a specific need. This attempt to discuss flocculants will be bounded by the specific conditions found in the water treatment facilities on an oil/gas platform, where elevated temperatures, high pressure conditions and lack of space are the dominating conditions. A brief introduction to the different types of flocculants will still be given in order to understand the process of flocculation.

Bridging flocculants

A method for creating aggregation of particles is to combine the particles by small bridges of polymer chains, see figure 25 on the next page, where polymer particles create particle/polymer bridges or polymer/polymer bridges. A prerequisite for bridging flocculants to work is the presence of sites on the solid surface where the polymer can anchor.

Adsorbing flocculants

Particles in a suspension will, because of their surface charge either repel or attract each other. Identical particles will have the same surface charge and therefore repel each other. Adsorbing flocculants can adsorb on the surface of these particles and neutralize the surface charge of the particle. By neutralizing the surface charge the repulsive forces decreases and the van der Walls attractive forces can promote the aggregation of the particles. This aggregation can be either reversible or irreversible.

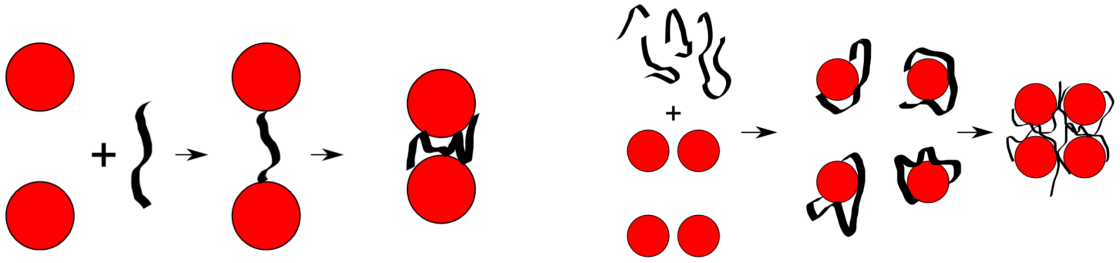

(a) Bridging by polymer flocculants where the polymer attaches to the particles and draws them together.

(b) Bridging by polymer flocculants where the polymer attaches several times to the particle. The polymer later creates bridges to other attached polymers.

***Figure 25:** Two theories of bridging interactions by polymer flocculants*

In order to get particle aggregation, the surrounding conditions of the aggregate has to be taken into account.

Different types of flocculants are available.

- Anionic
- Cationic
- Nonionic

Like the name indicates, the charge of the flocculant determines the category to which it belongs. The anionic flocculant will have a net negative charge whereas the cationic flocculant will have a net positive charge. The charge determines which particles will be affected by the presence of the flocculant and how the flocculant itself acts in a suspension.

Natural flocculants

In the category *natural flocculant* belongs starch, gums, glues and alginates

Synthetic polymeric flocculants

A widely used synthetic flocculant is Polyacrylamid, see figure 26 on the following page.

Coagulants

The difference between coagulation and flocculation is that coagulation is based on the formation of aggregates due to unstable conditions among the colloidal particles (ζ-potential is $\pm$ 30 mV). The collision of these unstable colloidal particles can induce aggregation where Van der Walls forces will keep the particles together in agglomerates.

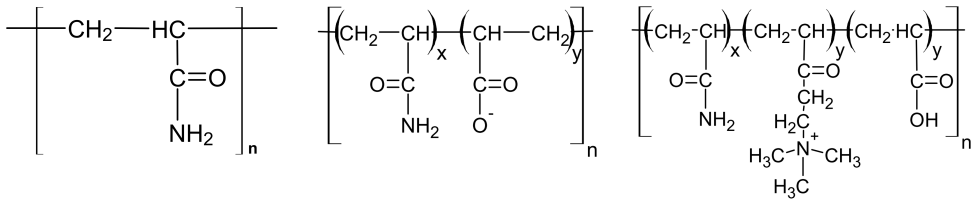

(a) The nonionic Polyacrylamide *(b) The anionic Polyacrylamide* *(c) The cationic Polyacrylamide*

Figure 26: *The nonionic, anionic and cationic Polyacrylamide flocculant*

Demulsifier

The addition of demulsifiers to the production stream of oil/water can break emulsions by

- coagulation of oil droplets, or
- coalescence of water droplets

Demulsifiers are a necessary chemical to add to improve separation of oil/water. The harsh conditions with high temperature and large volume flows of the oil/water mix in twisting pipe segments create the perfect conditions for foam and emulsions.

3.6 Best available technology (BAT)

The review of the unit operations in this thesis is done on a theoretical basis only. Theory and reality can be two different entities and the practical experiences with water treatment cannot be taken into account yet.

Based on the chosen methods the best separation will be provided by the use of centrifugal separation. The separation will be done on the topside which makes it easy to perform maintenance on the equipment. Decanter centrifuges do not increase the separation in cut size but can handle large solid influxes. Disc-Stack centrifuges on the other hand push the cut size upwards and removes many of the particles in the background particle production.

The choice of unit operation must be based on the problems created by the solids compared to the costs of treatment. Centrifugal separation is an expensive but efficient technology. A possibility could be the use of Disk-Stack centrifuges as a supplement (polishing step) in the water treatment placed after the initial treatment of the hydrocyclones. This setup will prevent the massive influxes to choke the centrifuge. By the use of the three phase unit the discharge water could increase in quality and thereby be of benefit to both the environment and the oil company.

4. Produced water and chalk classification

In order to identify possible influences on a unit operation handling the solids production in the produced water (PW) treatment, some analytical work is done on the PW. The PW used in this thesis is recovered from TWC-01 on the 10th of March 2010. Since PW is troublesome to get when ever needed, the experiments for this thesis will be performed in a homemade electrolyte solution (called artificial produced water (APW)) based on the constituents found during analysis of PW. To be able to add chalk particles to PW, Dankalk A/S in Løgstør in northern Jutland has delivered 9 kg chalk which will be used for the manufacturing of APW with chalk particles.

4.1 PW composition

To map ionic interactions in PW, different analyses of the ionic species in the water have been performed. These analyses will help calculating equilibrium conditions and solubilities of present salts.

Chloride

The chloride concentration was first found with a Merck Spectroquant Cl^- 5-125 mg/L analysis. A sample was diluted 1:250 and measured. A double determination was done. The result of the analysis showed a chloride concentration of 65 mg/L for both diluted samples. The actual chloride concentration follows to be 16,25 g/L which equals a molar concentration of 0,46 mol/L. A second analysis was made on IC, showing a slightly lower concentration of 14,71 g/L.

Former analyses of produced water recovered from the Dan Field has revealed a Cl^- concentration of 32,09 g/L [A31]. This indicates large differences of ionic compositions between the production fields.

Analysis of present ions

An analysis has been performed in order to show the concentrations of various ions in the produced water. The result of this analysis can be seen in table 4 on the next page. The concentration of Na is lower than expected since formation water normally has a high value for salinity. With the value for Na the molar concentration is 0,38 mol/L which equals a salinity of ≈ 22 ‰.

Conductivity

Conductivity measurement at 21,7°C gave the value of 38,83 mS. In the literature a conversion from conductivity to TDS and vice versa is done by multiplying a conversion factor to the result [A41]. To convert the measured conductivity to TDS, the conductivity

Table 4: *The analysis of the produced water gave this composition of the PW.*

Analysis from ICP, IC and alkalinity			
Species	[mg/L]	[mol/L]	Mol fraction
K^+	196,40	$5{,}02 \cdot 10^{-3}$	$6{,}08 \cdot 10^{-3}$
Mg^{2+}	83,45	$3{,}43 \cdot 10^{-3}$	$4{,}15 \cdot 10^{-3}$
Ca^{2+}	146,70	$3{,}66 \cdot 10^{-3}$	$4{,}43 \cdot 10^{-3}$
Na^+	8693,00	$3{,}78 \cdot 10^{-1}$	$4{,}57 \cdot 10^{-1}$
Cl^-	14 706,50	$4{,}15 \cdot 10^{-1}$	$5{,}02 \cdot 10^{-1}$
HCO_3^-	1305,00	$2{,}14 \cdot 10^{-2}$	$2{,}59 \cdot 10^{-2}$
SO_4^{2-}	7,05	$7{,}34 \cdot 10^{-5}$	$8{,}88 \cdot 10^{-5}$
Total	-	$8{,}27 \cdot 10^{-1}$	1,00
TDS	25 138,10	-	-

is multiplied with 0,67. This gives a proposal for TDS of 26016,1 mg/L. In table 4 the measured TDS is 25138,1 mg/L. The calculated result is within 5% of the measured result (discrepancy is $\approx 3,5\%$). In this thesis the conversion form conductivity to TDS is considered precisely enough with the conversion factor of 0,67.

4.2 Solubility of $CaCO_3$

The solubility of $CaCO_3$ depends on the various ions present in the PW and their individual concentration. The normal equilibrium reaction at 25°C is among other

$$CaCO_{3(s)} \leftrightharpoons [Ca^{2+}][CO_3^{2-}] \qquad K_1 = 4{,}8 \cdot 10^{-9} \tag{34}$$

Along with the equilibrium described in equation 34, other coupled CO_3^{2-} equilibrium reactions take place.

$$[H^+][CO_3^{2-}] \leftrightharpoons [HCO_3^-] \qquad K_2 = 10^{-10,3} \tag{35}$$
$$[H^+][HCO_3^-] \leftrightharpoons [H_2CO_3] \qquad K_3 = 10^{-6,3} \tag{36}$$
$$H_2O \leftrightharpoons [H^+][OH^-] \qquad K_w = 10^{-14} \tag{37}$$

As Mg^{2+} and K^+ is present in the produced water, the interaction of these ions with CO_3^{2-} has to be calculated as well.

$$MgCO_{3(s)} \leftrightharpoons [Mg^{2+}][CO_3^{2-}] \qquad K_4 = 1{,}0 \cdot 10^{-5} \tag{38}$$
$$K_2CO_{3(s)} \leftrightharpoons [K^+]^2[CO_3^{2-}] \qquad K_5 = 1{,}1 \cdot 10^{-1} \tag{39}$$

These equilibriums has to be calculated simultaneously with the wanted reaction in order to follow the path of CO_3^{2-}. Since TWC-01 is a swing producer, injection of gas is taking place. The composition of the gas is seen in table 5 on the facing page. CO_2 is a fraction

Table 5: *The composition of the lift gas used for injection/storage in TWC-01. [A25]*

	Mole Fractions	Vapour Phase
Nitrogen	0,0032	0,0032
CO_2	0,0016	0,0016
H_2S	0,0000	0,0000
Methane	0,9104	0,9104
Ethane	0,0522	0,0522
Propane	0,0195	0,0195
i-Butane	0,0036	0,0036
n-Butane	0,0057	0,0057
i-Pentane	0,0018	0,0018
n-Pentane	0,0013	0,0013
n-Hexane	0,0007	0,0007
Te1*	0,0001	0,0001
Total	1,0000	1,0000

of the gas, which leads to two equilibriums involving CO_2 and $CaCO_3$.

$$\mathrm{H_2O + CO_2 \leftrightharpoons [H_2CO_3]} \qquad \mathrm{K_6 = 1{,}7 \cdot 10^{-3}} \tag{40}$$

$$\mathrm{CaCO_{3(s)} + H_2O + CO_2 \leftrightharpoons [Ca^{2-}] + 2[HCO_3^-]} \qquad \mathrm{K_7 = \text{not found}} \tag{41}$$

There are apparently eight coupled CO_3^{2-}-equilibriums found which takes place in the PW.

Solubility has to be considered with respect to the concentrations of the ions present in the electrolyte. The activity coefficient γ of each reaction must be incorporated. γ is a value for the non ideality of the electrolyte solution, where $\gamma \to 1$ for the ionic strength $\mu \to 0$, an ideal electrolyte solution. The solubility product of $CaCO_3$, K_{sp}, is defined as

$$K_{sp} = [\mathrm{Ca^{2+}}][\mathrm{CO_3^{2-}}] \tag{42}$$

This expression does not take the effect of ionic interactions into account. The individual concentrations therefore has to be substituted by the activity A as

$$A_{\mathrm{Ca^{2+}}} = [\mathrm{Ca^{2+}}]\gamma_{\mathrm{Ca^{2+}}} \quad \text{and} \quad A_{\mathrm{CO_3^{2-}}} = [\mathrm{CO_3^{2-}}]\gamma_{\mathrm{CO_3^{2-}}} \tag{43}$$

which changes equation 42 to

$$K_{sp} = A_{\mathrm{Ca^{2+}}}\, A_{\mathrm{CO_3^{2-}}} = [\mathrm{Ca^{2+}}]\gamma_{\mathrm{Ca^{2+}}}[\mathrm{CO_3^{2-}}]\gamma_{\mathrm{CO_3^{2-}}} \tag{44}$$

To be able to calculate γ, the value of μ has to be calculated.

μ in the PW is calculated with the found ionic concentrations from table 4 on the facing page and equation 45 as

$$\begin{aligned} \mu &= \frac{1}{2}(c_1 z_1^2 + c_2 z_2^2 + \dots) \\ &= 0,42\mathrm{M} \end{aligned} \tag{45}$$

The extended Debye-Hückel equation, see equation 46, is valid for $\mu < 0,1$M and is defined as

$$\log \gamma_i = \frac{-Az_i^2\sqrt{I}}{1 + Ba_0\sqrt{I}} + bI \tag{46}$$

where z_i^2 is the valency of the ion, I is the ionic strength of the electrolyte solution, a_0 is the size of the ion, b is a constant related to the specific ion and

$$A = 1{,}82 \cdot 10^6 \, (\epsilon T)^{-3/2}$$

and

$$B = 50,3(\epsilon T)^{-1/2})$$

ϵ is the dielectric constant of water and T the temperature in K. Since μ is 0,42M, this equation is not applicable for calculation of the activity coefficient.

A processing of equation 46, called the Davies equation, see equation 47, is found valid for $\mu < 0,5$M [B3]. The Davies equation does not have the ion size included in the equation, and will give activities based only on the valency of the ions.

$$\log \gamma_i = -Az_i^2 \left(\frac{\sqrt{I}}{1 + \sqrt{I}} - 0,3I \right) \tag{47}$$

In table 6 the calculated activities for the PW are shown, based on equation 46 and equation 47 and the found concentrations of ions present from table 4 on page 34. As seen the Debye-Hückel equation has different values for γ for each ion, whereas the Davies Equation only distinguishes between the valency of the ions. The result of the activity calculations are given for a temperature of 25°C. In the Tyra Field the temperature is ≈ 65°C.

Table 6: *Values of γ based on the Debye-Hückel equation and the Davies equation on ions present in the PW from Tyra Field at 25°C.*

Ion	mol/L	z	Debye-Hückel	Davies
K^+	5,02 $\cdot 10^{-3}$	1	0,628	0,735
Mg^{2+}	3,43 $\cdot 10^{-3}$	2	0,325	0,292
Ca^{2+}	3,66 $\cdot 10^{-3}$	2	0,263	0,292
Na^+	3,78 $\cdot 10^{-1}$	1	0,663	0,735
Cl^-	4,15 $\cdot 10^{-1}$	-1	0,628	0,735
HCO_3^-	2,14 $\cdot 10^{-2}$	-1	0,663	0,735
SO_4^{2-}	7,34 $\cdot 10^{-5}$	-2	0,193	0,292

It can be seen that equilibrium calculations in high ionic strength electrolyte solutions will have an element of uncertainty attached to the results.

Charge balance

In every electrolyte solution the net charge of ions will be zero if equilibrium is established. A charge balance can be made to see which ionic concentrations should be present in the electrolyte.

The charge balance in the system is

$$2[\mathrm{CA}^{2+}] + [\mathrm{H}^{+}] + 2[\mathrm{Mg}^{2+}] + [\mathrm{K}^{+}] + [\mathrm{Na}^{+}] = 2[\mathrm{CO}_3^{2-}] + [\mathrm{HCO}_3^{-}] + [\mathrm{OH}^{-}] + [\mathrm{Cl}^{-}] + 2[\mathrm{SO}_4^{2-}] \quad (48)$$

4.3 Chalk from Dankalk A/S

For the APW chalk from Dankalk A/S is used as the chalk constituent. The chalk has been treated with hydrocyclones to remove sand and rubble. The composition of the chalk is shown in table 7, and the analysis is conducted by Dankalk A/S on the Oxford LAB-X 3000 using X-ray fluorosence.

***Table 7:** XRF-analysis of chalk from Dankalk A/S.*

Species	%
$CaCO_3$	96,20
SiO_2	1,25
Al_2O_3	0,17
$MgCO_3$	0,54
Total CO_3	96,74

4.4 Electrophoresis

In order to determine the ζ-potential of the dispersed $CaCO_3$ particles in the PW, several electrophoretic analyses has been performed. The principles in this analysis is measurement of the electrophoretic mobility u_e of the particles while exposed to an electric potential. This electrophoretic mobility can be used in the Smoluchowski equation as

$$u_e = \frac{\zeta \epsilon}{\eta} \quad (49)$$

where ϵ is the permittivity of the electrolyte, η is the viscosity of the electrolyte and ζ is the ζ-potential of the colloid particles in the electrolyte.

The measurement of the produced water gave the result seen in table 8 on the following page at a pH of 7,43.

This average value of -20,81 mV shows that the $CaCO_3$ particles are in the unstable area of $\pm$30 mV. Furthermore, the value of -20,81 mV was not expected. Compared to S.K.

Table 8: *Measurement of the ζ-potential of $CaCO_3$ particles in the produced water samples from Tyra West.*

Measurement	1	2	3	4	5	Average	Std. dev.
ζ-potential [mV]	-20,45	-20,71	-20,90	-21,02	-20,99	-20,81	$\pm$ 0,21

Mishra [A34] reporting the ζ-potential for $CaCO_3$ as being between -10 and 10 mV at the same pH, depending on the ions present in the water, the value is somewhat lower.

4.5 Composition of APW

For future laboratory work APW is used. The composition can be seen in table 9. The composition is based on the analysis of the produced water taken from the Tyra Field (TWC-01) received from Maersk Oil and Gas, see table 4 on page 34.

Table 9: *Composition of the artificial produced water with the added weight in bold face.*

Species (†Cl)	M	Conc	**Add**	Added†	Added Cl^-	TDS
	[g/mol]	[mol/L]	**[g/L]**	[mg/L]	[g/L]	[g/L]
KCl	74,55	$5{,}02 \cdot 10^{-3}$	0,37	196,27	0,18	0,37
NaCl	58,44	$3{,}78 \cdot 10^{-1}$	22,09	8690,13	13,40	22,09
$CaCl_2$	110,98	$3{,}66 \cdot 10^{-3}$	0,41	146,69	0,26	0,41
$MgCl_2$ $6H_2O$	203,30	$3{,}43 \cdot 10^{-3}$	0,70	83,37	0,24	0,33
Total Cl^-	-	$3{,}97 \cdot 10^{-1}$	-	-	14,08	-
TDS	-	-	-	-	-	23,20

5. Chemical removal of chalk

In order to investigate on the chalk particles and their interaction with different types of flocculants and coagulants, a series of experiments and analyses have been conducted. The following chapters will describe the experiments and their results together with an overall conclusion of the experimental part.

5.1 Flocculants and coagulants

Bo Jensen Vandbehandling A/S has willingly contributed with two types of flocculants and two types of coagulants, see table 10 and figure 27. To see which of the chemicals

Table 10: *Flocculants and coagulants contributed by Bo Jensen Vandbehandling A/S.*

	Type	Polymer	Formula	Active site
BoFloc 10-35	Flocculant	X	Unknown	Anionic
BoFloc RA 20-03	Flocculant	X	Unknown	Cationic
BoFer	Coagulant	-	$FeCl_3$	-
BoPac 18	Coagulant	-	$Al(OH)_{1,2}Cl_{1,8}$	-

Figure 27: *Chemicals provided by Bo Jensen Vandbehandling A/S.*

from table 10 has the greatest effect on removing chalk particles, an experiment was created, using design of experiments. To measure the effect of the chemicals, two response variables was chosen.

- Turbidity
- Mean particle size

Turbidity

A measurement of the turbidity of water is a normal procedure in waste water control. Since small chalk particles is dispersed in water, the turbidity will be high in non treated water and will decrease by adding an additive which can precipitate the chalk particles. In the experiment the Turbidity measurement instrument from AquaLytic was used, see figure 28. The instrument has a limitation of 10 mL samples, which is the maximum volume in the enclosed vial. The instrument has an IR-source, which emits a specific intensity of light

Figure 28: *Instrument used for turbidity measurements manufactured by AquaLytic*

that is scattered by the particles present in the water. A detector measures the intensity of the scattered light at an angle of 90° and calculates a Nephelometric Turbidity Unit (NTU), which is an expression of the turbidity.

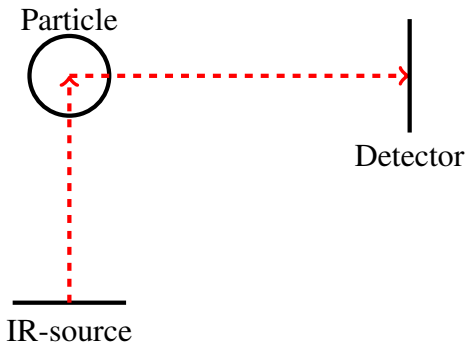

Figure 29: *Only the light scattered in an angle of 90° from the particle is used for measurement.*

Laser scattering technique

The change in particle size as a consequence of adding flocculants and/or coagulants is measured with the help of dynamic laser scattering. The instrument can be seen on figure 30.

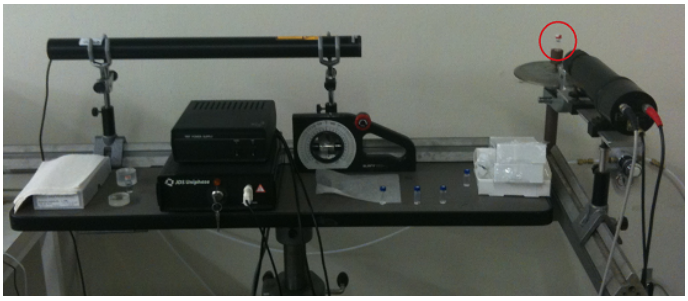

Figure 30: *Arrangement of the instrument used for particle size measurement. The small vial with the sample is seen inside the red circle.*

The method is called photon correlation spectroscopy and relies on the measurement of the movement of particles caused by diffusion. When a photon of light is scattered from a particle, an exchange of energy between the photon and the particle takes place where the photon either gains or loses energy to the particle. This results in a shift in energy of the photon and thereby a shift in frequency ω of the scattered light. Since the light source is a monochromatic laser, the frequency of the light ω_0 is known. The shape of the spectrum $I(\omega)$ from the particle will normally follow a Lorentzian shape as

$$I(\omega) \propto \frac{DQ^2}{(\omega - \omega_0)^2 + (DQ^2)^2} \tag{50}$$

D [cm^2 s^{-1}] is the diffusion coefficient defined by Stokes-Einstein equation and Q is the scattering vector. D is defined as

$$D = \frac{kT}{6\pi\eta R} \tag{51}$$

k is the Boltzmann constant [m^2 kg s^{-2} K^{-1}], T the temperature [K], η the solvent viscosity [Pa s] and R is the hydrated radius of the particle [m].

The scattering vector Q is given as

$$Q = \frac{4\pi \sin\theta/2}{\lambda} \tag{52}$$

θ is the angle between the transmitted light and the scattered light and λ is the wavelength of the light. Q is a normal vector to the scattered light.

5.2 Preparation of chalk containing water

A electrolyte solution of APW and chalk particles was made by mixing 0,5 L of APW with 0,3 g of fine chalk powder. The chalk powder was made from the chalk described in

section 4.3 on page 37 where a chunk of that particular chalk was dried for three days at 110°C to remove water and moisture. A small piece of the dried chalk was crushed in a mortar to get as fine particles as possible, see figure 31.

Figure 31: *Chalk was crushed in a mortar to get small and fine chalk particles.*

The solution of APW and chalk powder was treated with a 750 Watt Ultrasonic Processor from Sonics Materials, Inc, see figure 32.

(a) *750 Watt Ultrasonic Processor used for the dispersion of chalk particles in APW.*

(b) *APW with chalk particles before dispersion*

(c) *APW with chalk particles after dispersion*

Figure 32: *Procedure for dispersion of chalk particles in APW*

5.3 Experimental plan

As mentioned in section 5.1 on page 40, the maximum volume of sample in the turbidity instrument is 10 mL. As a consequence the experiment was performed in the vial with a volume constraint of 10 mL.

The experimental plan was made as a mixture design plan since the volume constraint of 10 mL was present. The plan was created as a simplex centroid plan which demands 31 runs. One replicate run and augment design was chosen leading to additional 6 runs. The replicate run was randomly chosen and the augment design was made to create additional points used to check the statistical model created in the analysis. All in all 37 runs had to be made. The order of runs was randomized to respond to external factors having an effect on the results. The components where

1. Water
2. BoFloc 10-35
3. BoFloc RA 20-03
4. BoPac 18
5. BoFer

Simplex centroid

The simplex centroid plan is a mixture design plan which tests interaction of different components of specific blends. On figure 33a on the following page a three component simplex centroid mixture design is shown. The numbers refer to different blends of the mixture with the numbers 1,2 and 3 representing the pure components. 4,6 and 10 show an equal amount of two components, e.g. 10 being a mixture of 50% BoFer and 50% BoPac 18 with no water included. 7,8 and 9 is a blend of all three components in varying amounts and 5 represent the centroid, which is the blend with equal amount of each component. For a four component system a graphical representation creates a tetrahedron as seen on figure 33b on the next page. A five component simplex centroid system cannot be represented graphically.

The full experimental plan can be seen in table 15 on page 51.

5.4 Preparation of components

The four components from Bo Jensen Vandbehandling A/S had to be prepared in order to be used for the experiment.

The two coagulants were diluted 1:500 to compensate for the small vial, in which the precipitation should take place. The dilution factor was arbitrary chosen.

The two flocculants were prepared as instructed by Bo Jensen Vandbehandling A/S as seen in table 11 on the next page.

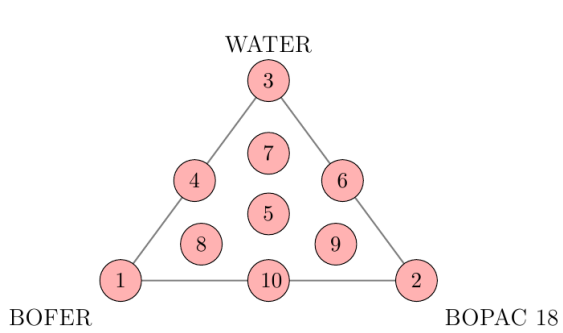

(a) Simplex centroid for a three component system of water, BoFer and BoPac 18.

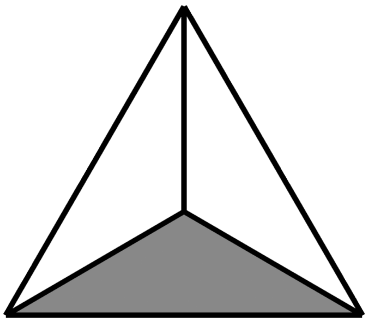

(b) Simplex centroid for a four component system, with a triangle for every combination of the four components.

Figure 33: *Graphical presentation of the three and four component simplex centroid system.*

Table 11: *Mix proportions of the two flocculants from Bo Jensen Vandbehandling A/S.*

Component	Water	Polymer
BoFloc RA 20-03	0,5 L	1,2 mL
BoFloc 10-35	0,5 L	1,65 mL

The mixing of the flocculant and water had to be done under heavy stirring. For this a turbine impeller was used as seen on figure 34. The flocculants were also diluted 1:500 for a equal comparison with the diluted coagulant.

Figure 34: *Mixing of the polymer flocculants was done with a turbine impeller.*

The final experimental setup can be seen on figure 35.

Figure 35: *Setup of the Simplex Centroid mixture design with components diluted 1:500 and the 10 mL vial.*

The experiment was performed by measuring out 9 mL of chalk water in the 10 mL vial with a glass pipette. For each run a combination of components adding up to 1 mL were added the vial as seen in table 15 on page 51. The turbidity was measured and a small sample for particle size determination was taken from the 10 mL vial and transferred to a 1,5 mL vial for a photon correlation spectroscopy measurement. Each measurement of particle size was done over a 30 second period in which the instrument software calculated a mean particle size. Before taking the 9 mL sample of chalk water, the remaining chalk water was treated with ultra sonic vibrations for homogenization of the chalk dispersion for 10 seconds.

5.5 Statistical results

The result of the experiment is divided in two statistical analysis. One for turbidity as a response factor and one for the mean particle size measurement.

Turbidity

The overall statistical result is seen in table 12 on the next page. A calculation is performed for a linear model, a quadratic model and a special cubic model. It is shown that the best model to describe the variability of the turbidity measurements is the linear model. It has a P-value of 0,0000 and shows a significant relationship between adding components to the chalk water and the change in turbidity on the 95,0% confidence level. The model created explains 88,91% of the variability of the measurements and the standard deviation is $\pm$54,4649 NTU.

Table 12: *The overall result is for three different models. Linear, quadratic and special cubic respectively.*

Estimated Full Model Effects for Turbidity (NTU)

Source	*Sum of Squares*	*Df*	*Mean Square*	*F-Ratio*	*P-Value*
Mean	1,36387E7	1	1,36387E7		
Linear	761297,	4	190324,	64,16	0,0000
Quadratic	42070,7	10	4207,07	1,75	0,1313
Special Cubic	13949,5	10	1394,95	0,43	0,9046
Error	38905,4	12	3242,12		
Total	1,44949E7	37			

Full Model Results

Model	*SE*	*R-Squared*	*Adj. R-Squared*
Linear	54,4649	88,91	87,53
Quadratic	49,0152	93,83	89,90
Special Cubic	56,9396	95,46	86,37

To check the validity of the statistical calculation the measurement points should follow a normal probability plot, be statistical independent and comply with the demand for variance homogeneity. Since the weren't any repeated measurements, the variance homogeneity can not be checked. A closer look at figure 36 does not give any clear indication of outliers, and

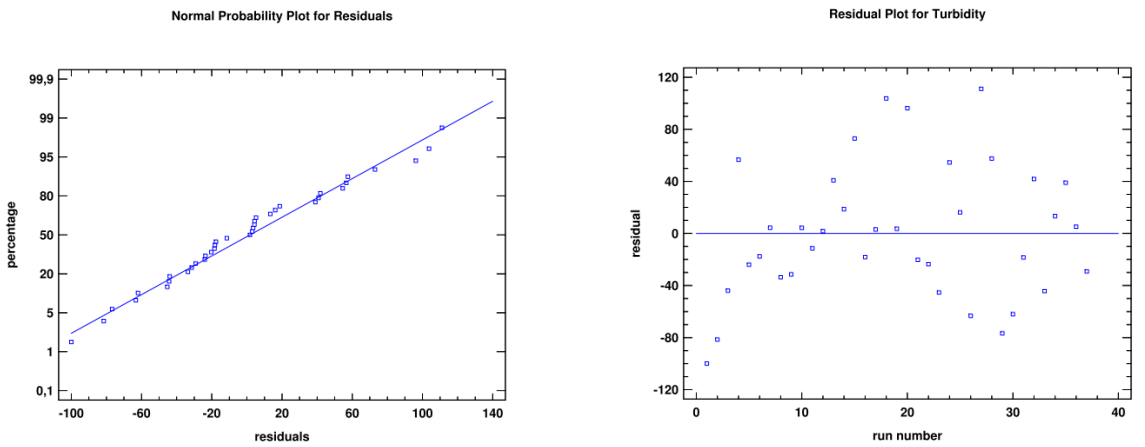

(a) *The normal probability plot shows a location of the residuals near the fitted line, which indicates a normal probability distribution of the residuals.*

(b) *The residuals does not indicate any dependency and is placed randomly around the mean residual, which indicates statistical independency of the residuals.*

Figure 36: *The control for independency and normal probability of the residuals does not give any reason to reject the statistical result of the turbidity experiment.*

it is therefore assumed that no outliers a present. The residuals are following the normal probability plot and are statistically independent. Further interpretation of the analysis can be done.

A trace plot, seen in figure 37 on the next page, shows the effect on turbidity for all five components in the same plot. It can be seen that decreasing of turbidity is accomplished

by adding the two coagulants BoFer and BoPac 18. The pseudo component mentioned on the x-axis is the volume of the single component compared to the 1 mL total component volume added for each run. The trace plot shows the reference point at 0,2, which is the point with equal volume of the five components. The steepness of the lines through this reference point makes the different components effect on turbidity comparable.

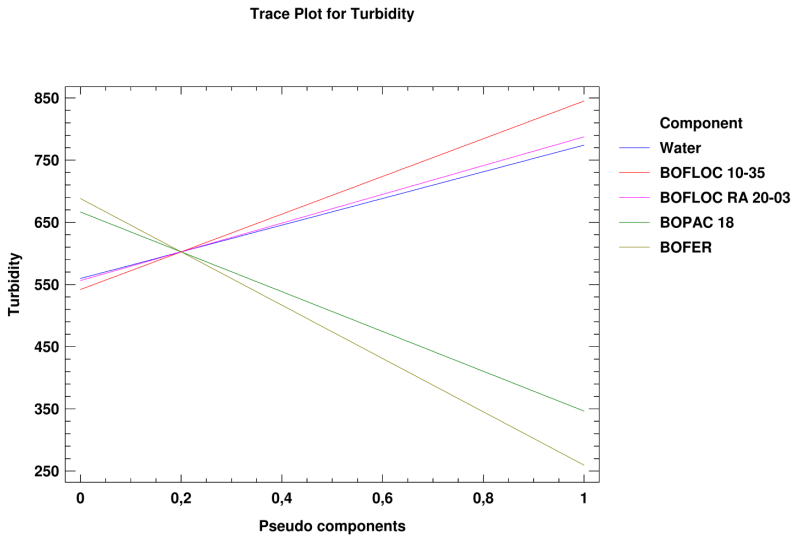

Figure 37: *The trace plot shows a steap angle on the effect of lowering turbidity by adding BoPac 18 and BoFer to the suspension. The flocculants shows an increasing effect on turbidity together with water.*

The optimization response, seen in table 13, shows the component composition for the lowest resulting turbidity. As seen, the only component that has to be added the suspension is BoFer.

Table 13: *The optimal decreasing of turbidity is accomplished by adding only BoFer to the suspension.*

Optimize Response
Goal: minimize Turbidity

Optimum value = 259,448

Factor	*Low*	*High*	*Optimum*
Water	0,0	1,0	0,0
BOFLOC 10-35	0,0	1,0	0,0
BOFLOC RA 20-03	0,0	1,0	0,0
BOPAC 18	0,0	1,0	0,0
BOFER	0,0	1,0	1,0

The conclusion of the experiment using turbidity as response factor, is that BoFer gives the lowest turbidity followed by BoPac 18. Non of the flocculants nor water gave any statistically measurable decrease in turbidity.

Mean Particle size

The result of the mean particle size measurement was analyzed concurrent the analysis for turbidity. The overall result of the measurement can be seen in table 14. It can be

Table 14: *The overall result of the statistical analysis of the particle measurement is not as profound as the analysis for turbidity.*

Estimated Full Model Effects for Mean particle size (nm)

Source	*Sum of Squares*	*Df*	*Mean Square*	*F-Ratio*	*P-Value*
Mean	5,40653E7	1	5,40653E7		
Linear	6,99417E6	4	1,74854E6	6,52	0,0006
Quadratic	1,52849E6	10	152849,	0,48	0,8872
Special Cubic	1,71857E6	10	171857,	0,39	0,9289
Error	5,3299E6	12	444159,		
Total	6,96364E7	37			

Full Model Results

Model	*SE*	*R-Squared*	*Adj. R-Squared*
Linear	517,716	44,92	38,03
Quadratic	566,026	54,73	25,93
Special Cubic	666,452	65,77	0,00

seen that the best model to describe the change in particle size by adding different blends of the components is the linear model. The P-value is 0,0006 which makes the change statistically significant on the 95% confidence level. The F-ratio is 6,51 and quite low compared to the F-ratio of the turbidity analyses of 64,16. The F-ratio is a number which describes the ratio between the variance caused by the experimental treatment and the variance caused by the experimental error. A smaller F-ratio indicates a larger influence of experimental errors.

The correlation coefficient is 44,92 which means that the model can explain 44,92% of the variability in the measurements.

The normal probability plot and the residuals vs run order, see figure 38 on the facing page, indicate that the measurements are not valid for statistical analysis. The measurements are not following a normal distribution fitted line nor showing statistical independency.

The trace plot indicates that the change in particle size is caused by adding the two coagulants BoFer and BoPac 18, with the largest particles created with the help of BoPac 18.

Experimental error

The experimental error is large and the reason for this error is likely the fact, that the particles are coagulating while the measurement is being made. This makes the particles gain size and weight, which again makes the particles move in the fluid. This movement is interfering with the principles in the laser scattering technique where the diffusion constant D is used to calculate the particle size, see section 5.1 on page 41.

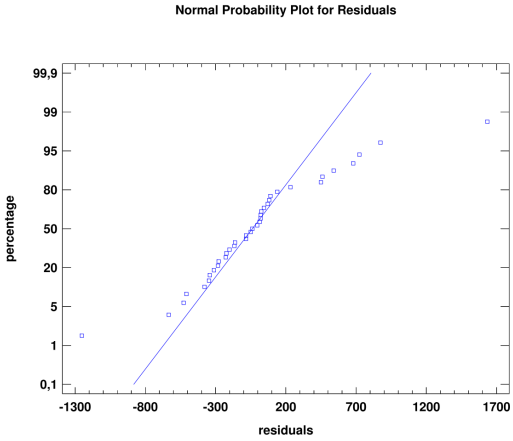

(a) The normal probability plot of the particle size measurement shows a bad fit to the fitted normal probability line.

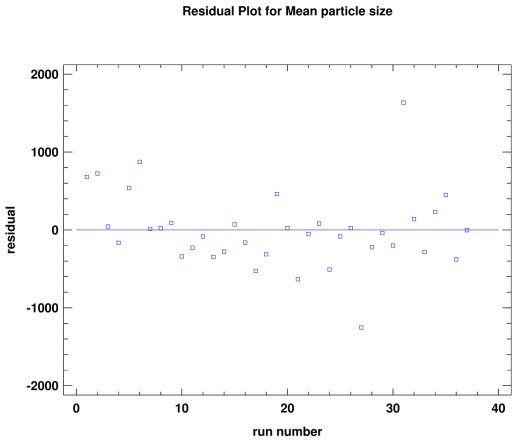

(b) The statistically independence

Figure 38: *The test for normal distribution and statistical independency is not clear and satisfactory.*

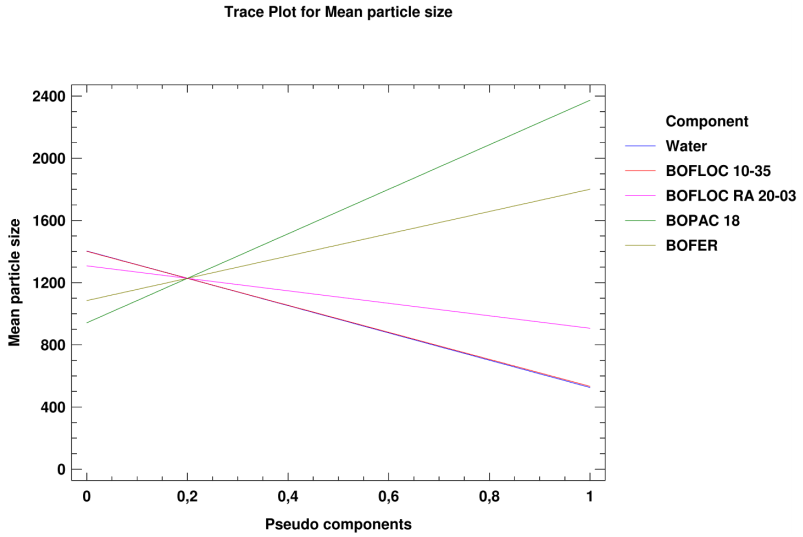

Figure 39: *The trace plot for the particle measurement shows the largest particles by adding the two coagulants BoFer and BoPac 18 to the suspension.*

For a particle to be exposed to Brownian motion, it has to be small enough to be sensitive to collisions with small molecules like water molecules and other ionic species present in the fluid. At the same time there has to be a situation, where the particle has a terminal velocity v_t=0. The term v_t is derived from the terms

$$F_b = \frac{m\rho g}{\rho_p} \qquad F_g = mg \qquad F_D = C_D \frac{v^2}{2} \rho A \tag{53}$$

F_b is the buoyant force of the particle, F_g is force of gravity acting on the particle and F_D id the drag force of the particle. m is the mass of the particle, ρ is the density of the liquid, g is the gravitational constant, ρ_P is the particle density, C_D is the drag coefficient of the particle, v is the velocity and A is the area of the particle.

The resulting force on the particle can be explained by

$$m\frac{dv}{dt} = F_g - F_b - F_D \tag{54}$$

$$= mg - \frac{m\rho g}{\rho_p} - C_D\frac{v^2}{2}\rho A \tag{55}$$

where $m\frac{dv}{dt}$ is the acceleration of the particle. Setting the acceleration term $m\frac{dv}{dt}$ = 0 and isolating the velocity v gives the expression

$$v = \sqrt{\frac{2g(\rho_p - \rho)m}{A\rho_p C_D \rho}} \tag{56}$$

Since the term m will increase faster than the terms A and C_D, the velocity will increase with coagulating particles. It is therefore not only the Brownian motion which is affecting the movement of the particle. Also the hydrated radius of the particle is affected, which directly interferes with the calculation of the diffusion constant seen in equation 51 on page 41.

An obvious failure contribution could originate from the concentration of the particles in the suspension. If the concentration of particles is too large the risk of multiple scattering occurs. The method of photon correlated spectroscopy is sensitive to multiple scattering.

Conclusion

The experiments with coagulants and their results show that coagulation with BoFer and BoPac can be used to remove fine chalk particles in water with high ionic strength. The flocculants used in the experiment showed no effect on turbidity and is therefore considered ineffective for removing fine chalk particles.

Table 15: *Experimental plan for the Simplex Centroid mixture design experiment and the results of the turbidity and particle size measurements.*

Component	1	2	3	4	5	Turbidity	Mean particle size
Run	mL	mL	mL	mL	mL	NTU	nm
1	0,10	0,10	0,10	0,10	0,60	331	2194
2	0,25	0,25	0,25	0,00	0,25	585	1665
3	0,00	0,00	0,50	0,50	0,00	523	1683
4	0,00	0,00	0,00	1,00	0,00	403	2207
5	0,33	0,00	0,00	0,33	0,33	436	2107
6	0,00	0,33	0,00	0,33	0,33	466	2442
7	0,50	0,50	0,00	0,00	0,00	814	543
8	0,00	0,33	0,33	0,33	0,00	626	1291
9	0,00	0,00	0,33	0,33	0,33	433	1784
10	0,00	0,50	0,00	0,50	0,00	600	1112
11	0,00	0,00	1,00	0,00	0,00	776	679
12	0,33	0,33	0,33	0,00	0,00	804	571
13	0,33	0,33	0,00	0,00	0,33	667	606
14	0,50	0,00	0,00	0,50	0,00	579	1171
15	0,00	1,00	0,00	0,00	0,00	918	604
16	0,33	0,33	0,00	0,33	0,00	637	982
17	0,10	0,10	0,60	0,10	0,10	698	540
18	0,00	0,50	0,50	0,00	0,00	920	408
19	0,00	0,00	0,50	0,00	0,50	527	1814
20	0,50	0,00	0,50	0,00	0,00	877	737
21	0,25	0,25	0,00	0,25	0,25	536	674
22	0,00	0,25	0,25	0,25	0,25	536	1353
23	0,60	0,10	0,10	0,10	0,10	643	959
24	0,00	0,00	0,00	0,00	1,00	314	1293
25	0,25	0,00	0,25	0,25	0,25	558	1318
26	0,00	0,50	0,00	0,00	0,50	489	1192
27	0,00	0,00	0,00	0,50	0,50	414	835
28	0,20	0,20	0,20	0,20	0,20	660	1005
29	0,10	0,60	0,10	0,10	0,10	647	842
30	0,33	0,00	0,33	0,33	0,00	574	1068
31	0,10	0,10	0,10	0,60	0,10	456	3435
32	1,00	0,00	0,00	0,00	0,00	816	665
33	0,25	0,25	0,25	0,25	0,00	644	801
34	0,00	0,33	0,33	0,00	0,33	644	1313
35	0,33	0,00	0,33	0,00	0,33	646	1527
36	0,50	0,00	0,00	0,00	0,50	522	784
37	1,00	0,00	0,00	0,00	0,00	745	522

6. ζ-potential analysis

Results of ζ-potential measurements are often used to explain coagulation of suspended solids. A measurement of chalk particles in produced water, as seen in table 8 on page 38, shows an average ζ-potential of -20,81 mV at a pH of 7,43. That value for the ζ-potential indicates an unstable state for the $CaCO_3$ particles, as the stable state is normally given as ± 30 mV for colloidal particles. This instability can contribute to coagulation of the $CaCO_3$.

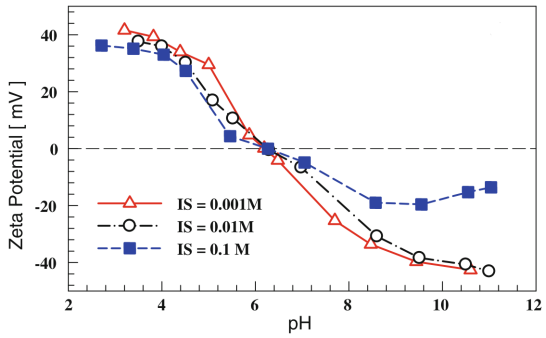

Figure 40: *ζ-potential on TiO_2 as a function of pH at different ionic strengths. [A40]*

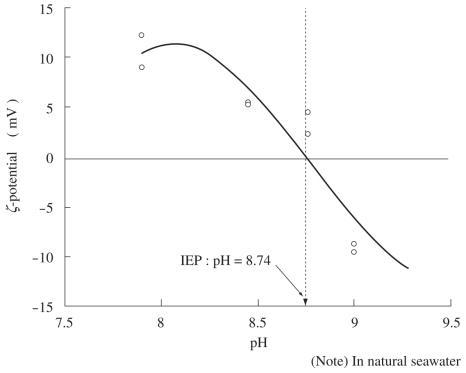

Figure 41: *ζ-potential on $CaCO_3$ as a function of pH measured in natural seawater. The IEP is given at a pH of 8,74. [A23]*

The value of -20,81 mV is lower than expected. According to Akamine et al[A23], the value of the ζ-potential should be positive at a pH of 7,43, see figure 41. Therefore a series of ζ-potential measurements on $CaCO_3$ is prepared which should show the behavior of the ζ-potential on $CaCO_3$ in the electrolyte similar to APW described in table 9 on page 38.

Many solid particles suspended in water will gain a ζ-potential which would be similar to figure 40, where a high pH will induce a negative ζ-potential and vice versa. The change in ζ-potential is caused by the concentration of the potential determining species H^+ and OH^-. At low pH the increased concentration of H^+, or more accurate H_3O^+ will push more positive charged H_3O^+ into the diffuse double layer. TiO_2 in a lattice structure can gain a proton creating $TiOOH^+$ at low pH inducing the positive ζ-potential. At high pH the increased concentration of OH^- will rip protons of the lattice to form H_2O, leaving TiO_2^- back inducing the negative ζ-potential. The net charge will change, which is the change in the ζ-potential. Figure 42 on the next page shows the principle of the double layer surrounding the negatively charged particle and at what distance from the particle surface (the slipping plan) the ζ-potential is measured.

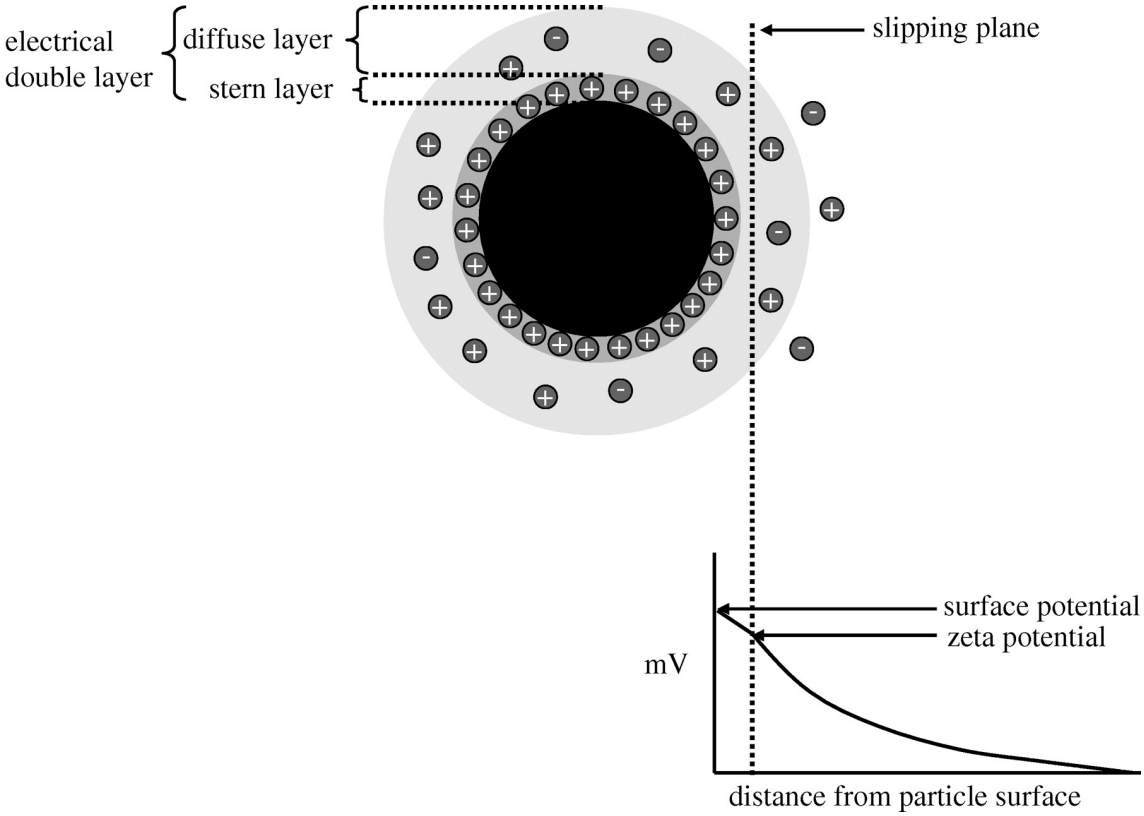

Figure 42: *The principles of the diffuse double layer surrounding a particle suspended in water which makes it possible to measure the ζ-potential. [I11]*

Since $CaCO_3$ acts as a buffer at low pH, a pH of 7 is found as the lowest pH which is possible to reach. Attempts to reach lower pH values by addition of acid dissolves the $CaCO_3$.

6.1 $CaCO_3$ samples

The different analysis of the ζ-potential is done on $CaCO_3$ of various origins, which are

Dankalk Chalk from the northern part of Jutland, described in section 4.3 on page 37.
Analytical grade $CaCO_3$, ACS reagent from Agros Organics.
Precipitated $CaCO_3$ $CaCO_3$, precipitated by mixing of equal mols of $CaCl_2$ dehydrated from Fluka and Na_2CO_3 analytical grade from Merck. The precipitated $CaCO_3$ was washed in deionized water and dried.
Tyra Field Chalk samples collected from TWC-01 on the 10th March 2010.

Benchmark experiment

The first part of the the experiments were done mainly on the $CaCO_3$ provided by Dankalk. As a benchmark experiment, the first experiment should show the influence of the ionic

species present in the APW on the ζ-potential. An analysis was conducted with 0,5 L of APW and 0,5 L dionized water in two beakers. 0,25 g $CaCO_3$ was added to each beaker and the $CaCO_3$ was dispersed after the method explained in section 5.2 on page 41. For both beakers the pH was adjusted by adding 0,01 M HCl or 0,01 M NaOH. The result of these analysis can be seen in table 16 and on figure 43 on the next page.

Table 16: *First measurement on $CaCO_3$ particles from Dankalk in APW and deionized water at varying pH.*

APW							
pH	7,01	7,43	8,68	8,90	9,41	9,77	10,98
ζ-potentiale	−17,45	−14,54	−2,63	−4,79	−9,53	−0,30	23,90
	−16,45	−14,60	−5,13	−3,84	−7,48	−6,18	23,51
	−14,51	−14,73	−12,88	−5,37	−8,24	−9,35	11,68
Average	−16,14	−14,62	−6,88	−4,67	−8,42	−5,28	19,70
Deionized water							
pH	8,46	8,86	9,03	9,24	9,54	-	-
ζ-potentiale	−6,76	−4,56	−7,24	−9,58	−12,52	-	-
	−9,03	−6,31	−5,69	−8,01	−11,19	-	-
	−5,22	−4,57	−7,28	−9,02	−11,18	-	-
Average	−7,00	−5,15	−6,74	−8,87	−11,63	-	-

It can be seen that an increase in pH induced a shift of the ζ-potential measured in APW in the positive direction while the ζ-potential measured in the deionized water increased in the negative direction, following a similar tendency as described by Akamine et al[A23]. This result indicated an ionic influence in the APW that reversed the change in ζ-potential as a function of pH.

This effect of the ionic species was interesting and an attempt to clarify this effect was taken.

The first attempt was done in reproducing the results in order to see if potential failures in the instrument or similar caused the result. To remove possible failures in the mixing of the APW, a new batch of APW was made. A 0,5 L beaker with APW and a 0,5 L beaker with deionized water was added 0,25 g $CaCO_3$ each. In APW the pH was 5,84 before adding the $CaCO_3$ and 8,93 after. In the deionized water the pH was 5,45 before adding the $CaCO_3$ and 9,98 after. The differences in pH shows an ionic influence caused by the decrease of the activity coefficient of H^+ due to the ionic strength of APW.

To see indications of the instrument inducing the behavior of the ζ-potential, a measurement was performed on TiO_2 (P25 Degussa) particles in deionized water. The purpose was to see if the results could relate to figure 40 on page 52. 0,1 g TiO_2 was added 0,5 L

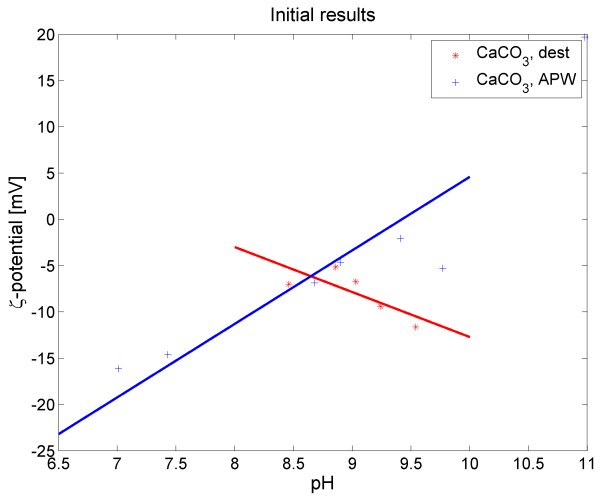

Figure 43: *Result of the first measurement of the ζ-potential of $CaCO_3$ immersed in APW and deionized water.*

deionized water and dispersed. pH was adjusted with 0,1 M HCl and 0,1 M NaOH. As seen on figure 44, the analysis with TiO_2 gave results which did not indicate instrumental interference of the measurement. The deviation of the ζ-potential values could most likely origin from the conditions under which the analysis was performed e.g. differences in ionic strength and the specific ions present in the electrolyte. Both experiments with $CaCo_3$ in deionized water and APW where similar to the initial result. The reverse behavior was thereby reproducible.

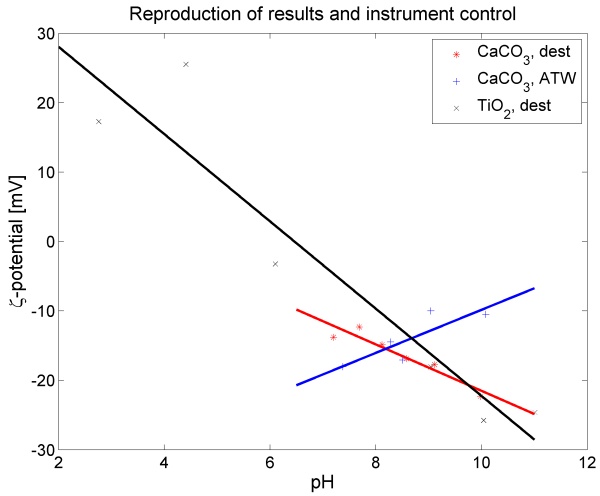

Figure 44: *Reproduction of the result from the initial analysis. It is seen that the same reverse tendency of the ζ-potential is present. To test the instrument a measurement on TiO_2 has been performed, which gave results similar to those shown in figure 40 on page 52.*

Table 17: *Attempt to reproduce the results of the the ζ-potential measurements of $CaCO_3$ immersed in APW and deionized water respectively.*

APW						
pH	7,38	8,28	8,51	9,04	10,08	-
ζ-potentiale	−17,04	−16,51	−15,93	−10,75	−13,92	-
	−18,60	−13,41	−18,42	−11,57	−8,34	-
	−18,46	−13,50	−16,89	−7,61	−9,22	-
Average	−18,03	−14,47	−17,08	−9,98	−10,49	-
Deionized water						
pH	7,20	7,69	8,12	8,58	9,11	9,98
ζ-potentiale	−14,84	−11,70	−16,28	−15,72	−16,84	−19,11
	−14,36	−12,80	−14,41	−17,95	−19,35	−22,00
	−12,20	−12,45	−13,92	−16,95	−17,02	−25,84
Average	−13,80	−12,32	−14,87	−16,87	−17,74	−22,32
TiO_2						
pH	2,76	4,41	6,10	9,04	10,04	11,01
ζ-potentiale	18,14	24,45	−0,82	−20,53	−26,23	−25,22
	15,83	26,21	−4,91	−16,19	−25,41	−24,19
	17,80	25,89	−3,98	−17,42	−25,71	−24,45
Average	17,26	25,52	−3,24	−18,05	−25,78	−24,62

6.2 Ion response DOE

To find a correlation between present ionic species in APW and the ζ-potential, an experimental design was created. A surface response design was chosen with five independent variables on level low and high. These variables were the concentration of the four cations Mg^{2+}, Ca^{2+}, Na^{+} and K^{+} and the pH. The values of the independent variables can be seen in table 18 on the facing page. The low and high level for pH was 7,5 and 10,5 respectively. The values in the table are the actual measured values. A total of 16 runs were created.

To gain some more information, and with the knowledge of the differences in pH caused by the ionic strength, additional 16 runs were added. The extra runs were the measurement on the $CaCO_3$ with the natural pH gained by equilibrium adding $CaCO_3$ in the electrolyte. Thereby a total of 32 runs were available with a minimum of extra work. The violation of the principle of randomization of the samples was accepted.

The result of the measurements can be seen in table 19 on page 58. These results were processed in StatGraphics to gain some statistical knowledge of the measurements.

Table 18: *Experimental plan for the Ion response experiment. The upper part of the table is the values after adding $CaCO_3$ with the natural pH. The lower part is the adjusted values after adding HCl or NaOH.*

Run	Mg^{2+}	Ca^{2+}	K^+	Na^+	pH
	[mg/L]	[mg/L]	[mg/L]	[mg/L]	
1	0	146,69	0	8690,13	8,85
2	83,37	0	0	8690,13	9,69
3	83,37	146,69	0	8690,13	8,81
4	83,37	0	196,27	0	9,64
5	0	0	196,27	0	9,50
6	83,37	146,69	196,27	0	8,50
7	0	0	196,27	8690,13	9,62
8	83,37	0	0	0	9,60
9	0	146,69	0	0	8,37
10	83,37	146,69	196,27	8690,13	8,73
11	0	0	0	0	9,71
12	0	0	0	8690,13	9,55
13	83,37	0	196,27	8690,13	9,48
14	0	146,69	196,27	8690,13	8,68
15	83,37	146,69	0	0	8,43
16	0	146,69	196,27	0	8,55
Run	Mg^{2+}	Ca^{2+}	K^+	Na^+	pH
	[mg/L]	[mg/L]	[mg/L]	[mg/L]	
1	0	146,69	0	8690,13	10,47
2	83,37	0	0	8690,13	10,55
3	83,37	146,69	0	8690,13	7,71
4	83,37	0	196,27	0	10,62
5	0	0	196,27	0	7,45
6	83,37	146,69	196,27	0	7,35
7	0	0	196,27	8690,13	10,70
8	83,37	0	0	0	7,51
9	0	146,69	0	0	7,48
10	83,37	146,69	196,27	8690,13	10,61
11	0	0	0	0	10,64
12	0	0	0	8690,13	7,35
13	83,37	0	196,27	8690,13	7,44
14	0	146,69	196,27	8690,13	7,67
15	83,37	146,69	0	0	10,65
16	0	146,69	196,27	0	10,60

Table 19: *Results of the measurements for the Ion response design analysis. The upper part is the measurements before adjusting the pH. Two outliers were identified and removed from the analysis (numbers in bold face).*

Sample	ζ-potentiale $CaCO_3$			Average	Conductivity [mS/cm]			Average	pH
1	−12,97	−11,73	−14,52	−13,07	34,32	35,04	35,56	34,97	8,85
2	−11,13	−13,10	−10,79	−11,67	34,18	35,01	35,56	34,92	9,69
3	−9,68	−10,34	−10,67	−10,23	34,83	35,70	36,51	35,68	8,81
4	−4,89	−0,74	−5,52	−3,72	1,42	1,43	1,44	1,43	9,64
5	−17,66	−18,41	−19,03	−18,37	0,70	0,71	0,71	0,71	9,50
6	−5,26	−6,15	−4,56	−5,32	2,11	2,13	2,15	2,13	8,50
7	−14,70	−13,10	−12,25	−13,35	33,63	34,68	35,22	34,51	9,62
8	−7,57	−5,05	−7,42	−6,68	0,80	0,80	0,80	0,80	9,60
9	−3,79	−3,32	−3,95	−3,69	0,78	0,79	0,79	0,79	8,37
0	−9,63	−11,74	−10,67	−10,68	35,14	35,97	36,79	35,97	8,73
11	−11,52	−11,93	−10,45	−11,30	0,04	0,04	0,04	0,04	9,71
12	−14,78	−17,28	−16,62	−16,23	33,50	34,47	35,30	34,42	9,55
13	−11,78	−10,40	−16,11	−12,76	35,97	36,45	36,76	36,39	9,48
14	−9,71	−13,72	−15,17	−12,87	34,32	35,30	36,00	35,20	8,68
15	−3,58	−4,97	−4,83	−4,46	1,49	1,51	1,53	1,51	8,43
16	−6,66	−7,01	−6,57	−6,75	1,42	1,44	1,45	1,44	8,55
Sample	ζ-potentiale adjusted pH			Average	Conductivity [mS/cm]			Average	pH
1	−10,22	−10,24	−7,25	−9,24	33,98	34,79	35,28	34,68	10,47
2	−8,27	−4,12	−7,33	−6,57	34,12	34,86	35,60	34,86	10,55
3	−15,39	−16,38	−19,25	−17,01	34,36	35,24	35,79	35,13	7,71
4	14,01	14,71	15,50	**14,74**	1,49	1,50	1,51	1,50	10,62
5	−11,27	−10,96	−10,12	−10,78	0,87	0,88	0,90	0,88	7,45
6	−7,76	−9,06	−6,70	−7,84	2,29	2,31	2,31	2,30	7,35
7	−12,95	−14,94	−15,61	−14,50	35,72	36,12	36,39	36,08	10,70
8	−7,50	−9,17	−7,11	−7,93	0,98	0,99	1,00	0,99	7,51
9	−6,57	−7,56	−6,32	−6,82	0,90	0,92	0,92	0,91	7,48
0	1,47	4,91	4,83	3,74	34,77	35,53	36,16	35,49	10,61
11	−15,01	−13,69	−10,86	−13,19	0,11	0,11	0,11	0,11	10,64
12	−19,90	−22,93	−28,27	−23,70	31,99	32,73	33,67	32,80	7,35
13	−17,74	−16,89	−21,41	−18,68	33,64	34,43	35,00	34,36	7,44
14	−20,15	−19,30	−16,04	−18,50	35,30	36,03	36,27	35,87	7,67
15	25,10	28,68	28,14	**27,31**	1,55	1,57	1,57	1,56	10,65
16	9,75	6,56	6,09	7,47	1,47	1,49	1,50	1,48	10,60

Statistical result

The result of the StatGraphics processing gave the result in table 20. It is seen that all independent variables except potassium is statistically significant. The interesting result is the result of calcium and magnesium which indicates a strong influence on the ζ-potential with a P-Value of 0,0002 and 0,0077 respectively. pH and sodium do also show an influence on the ζ-potential but that is expected since the concentration of sodium is 103 and 110 times the concentration of calcium and magnesium respectively. Previous research has shown that Mg^{2+} and Ca^{2+} acts as potential determining ions towards $CaCO_3$, but the measurements performed did not include variations in pH and can therefore not explain the effect seen in pH altering [A32] [A43] [A44] [A39]. Adjusting pH will push the equilibrium

$$CaCO_{3(s)} \rightleftharpoons Ca^{2+} + CO_3^{2-} \underset{-H^+}{\overset{+H^+}{\rightleftharpoons}} Ca^{2+} + HCO_3^-$$

which directly interferes with the concentration of calcium.

Table 20: *Result of the statistical processing of the Ion response experiment.*

Analysis of Variance for Zeta-potential

Source	*Sum of Squares*	*Df*	*Mean Square*	*F-Ratio*	*P-Value*
A:Mg2+	128.477	1	128.477	8.45	0.0077
B:Ca2+	299.97	1	299.97	19.72	0.0002
C:K+	5.61449	1	5.61449	0.37	0.5492
D:Na+	358.466	1	358.466	23.56	0.0001
E:pH	356.381	1	356.381	23.43	0.0001
Total error	365.086	24	15.2119		
Total (corr.)	1243.91	29			

R-squared = 70.6502 percent
R-squared (adjusted for d.f.) = 64.5357 percent
Standard Error of Est. = 3.90025
Mean absolute error = 2.67761
Durbin-Watson statistic = 2.47944 (P=0.9140)
Lag 1 residual autocorrelation = -0.243353

Two measurements were identified as potential outliers and removed from the analysis which gave a total of 30 measurements for the analysis. The analysis can explain 70,65% of the variability in the measurements which reveals an influence of some experimental errors or some unidentified influences.

To see if the analysis is statistically valid, the residuals vs run order and the normal probability plot is inspected, see figure 45 on the next page and figure 46 on the following page. There is no indication of statistically dependency in the residuals and they follow more or less the normal probability curve. Inspection of the Pareto chart for the ζ-potential shows an unexpected effect, see figure 47 on page 61. The length of the bars is a visual indication of the P-value mentioned earlier, but the color indicates a positive or negative effect on the ζ-potential at the high level. Sodium at high concentration increases the ζ-potential in the negative direction. A possible explanation could be that the high concentration of sodium ions in the electrolyte will compress the diffuse double layer so that the negative surface charges will interfere with the measurement. That explanation

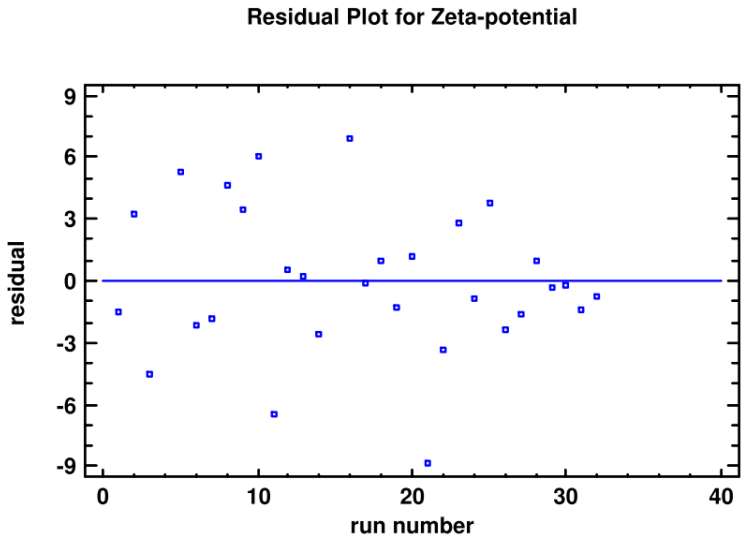

Figure 45: *Plot of the residuals as a function of runs did not show any dependency issues.*

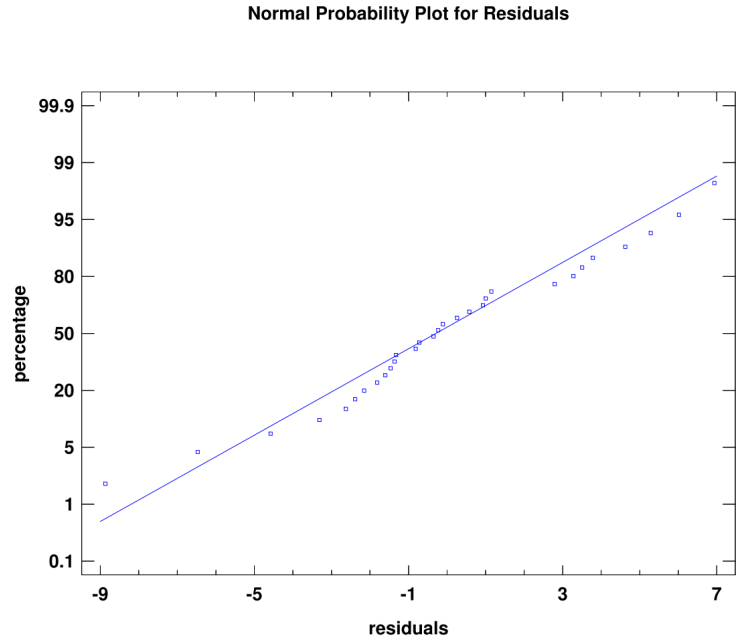

Figure 46: *The residuals follow the normal probability line.*

seems unrealistic, since the negatively charged $CaCO_3$ particle will be surrounded by positively charged sodium ions that are present in a large number.

Another explanation could be the amount of Cl^- ions added. Since the cations are all affiliated with Cl^-, the largest contribution of that anion comes from sodium. On the other hand the concentration of Cl^- from the divalent anions contributes with twice the amount of anions per cation. If Cl^- is the hidden contributor of the effect from sodium this effect should also be visible with calcium and magnesium. The main effects plot, shown on

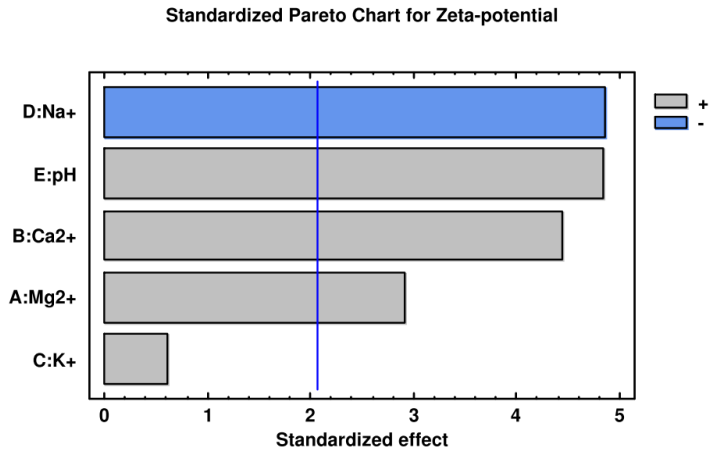

Figure 47: The Pareto chart gives a graphical interpretation of the significant contribution. 0,05 P-value is given as the blue line.

figure 48 shows the effect on the ζ-potential from the independent variables at low and high level. The effect is shown as steepness of the lines, indicating the results discussed earlier. The effect of pH is the opposite of the normal behavior seen on figure 41 on page 52. The main effect plot indicates a positive increase in ζ-potential as the concentration of H^+ decreases. That observation is the same as seen on the previous experiments and does not reveal any new knowledge helping to find a possible explanation.

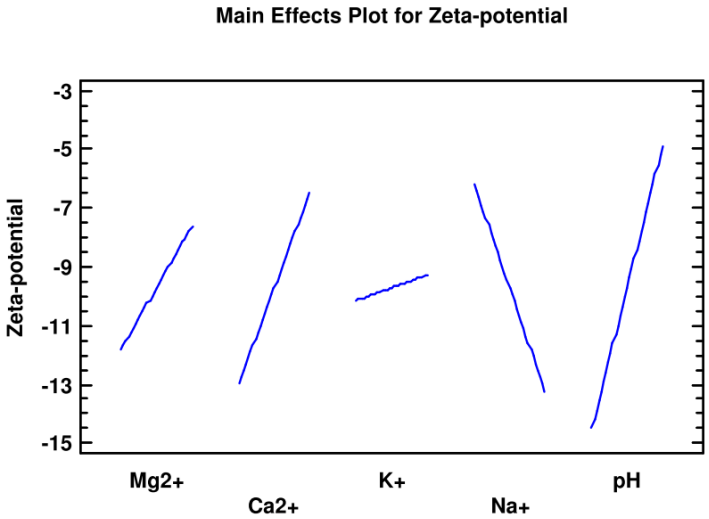

Figure 48: Main effects from the ionic species on the ζ-potential.

Conclusion of the ion response experiment

The experiment does not reveal new knowledge concerning the reverse behavior of the ζ-potential. The results show that previous result are reproducible and indicates a strong

affinity of Ca^{2+} and Mg^{2+} towards $CaCO_3$. The reversed results of the ζ-potential is not explained by the analysis.

6.3 Fixed Cl^-

The molar concentration of Cl^-, added via NaCl, is added via either magnesium, calcium or potassium salts. The total concentration of Cl^- in APW is given in table 9 on page 38 as $3{,}97 \cdot 10^{-1}$ M. By swapping the concentration of NaCl with the other three species in APW and recalculate the weight of the salt to be added to contribute with the same amount of Cl^-, the possible effect of the cation with the fixed $[Cl^-]$ could be revealed one by one. The calculations of the amount of the salts are seen in table 21.

Table 21: *Recalculation of the salts in order to get the same concentration of Cl^- as in APW.*

Molar concentration [mol/L]			
	KCl	$MgCl_2$	$CaCl_2$
KCl	$3{,}78 \cdot 10^{-1}$	$5{,}02 \cdot 10^{-3}$	$5{,}02 \cdot 10^{-3}$
NaCl	$5{,}02 \cdot 10^{-3}$	$3{,}43 \cdot 10^{-3}$	$3{,}66 \cdot 10^{-3}$
$CaCL_2$	$7{,}32 \cdot 10^{-3}$	$7{,}32 \cdot 10^{-3}$	$3{,}82 \cdot 10^{-1}$
$MgCl_2$	$6{,}86 \cdot 10^{-3}$	$3{,}81 \cdot 10^{-1}$	$6{,}86 \cdot 10^{-3}$
Total Cl^-	$3{,}97 \cdot 10^{-1}$	$3{,}97 \cdot 10^{-1}$	$3{,}97 \cdot 10^{-1}$
Weight of salt [g]			
KCl	28,18	0,37	0,37
NaCl	0,29	0,20	0,21
$CaCl_2$	0,41	0,41	21,18
$MgCl_2$	0,70	38,77	0,70

It can be seen from figure 49 on the facing page that $MgCl_2$ induces a shift in the ζ-potential in the positive direction. $CaCl_2$ is also acting differently. Whereas $MgCl_2$ is inducing a shift of approximately 20 mV in the positive direction at varying pH, compared to the monovalent KCl and NaCl, $CaCl_2$ is acting completely different. The change in ζ-potential can be explained in a satisfactory manner with a linear regression for KCl, NaCl and $MgCl_2$. $CaCl_2$ can only be explained with a polynomial regression. The reason for this behavior is not explainable with the current experiment and could rely on an instrument failure or similar.

6.4 Effect of the ionic strength

An experiment is prepared which could show some information of the ionic strengths influence on the ζ-potential of $CaCO_3$ by the ions in APW. The result of the response surface experiment gave the idea that ionic strength could influence the ζ-potential. To find a similarity, four different concentrations of each salt, see table 23 on page 64, used

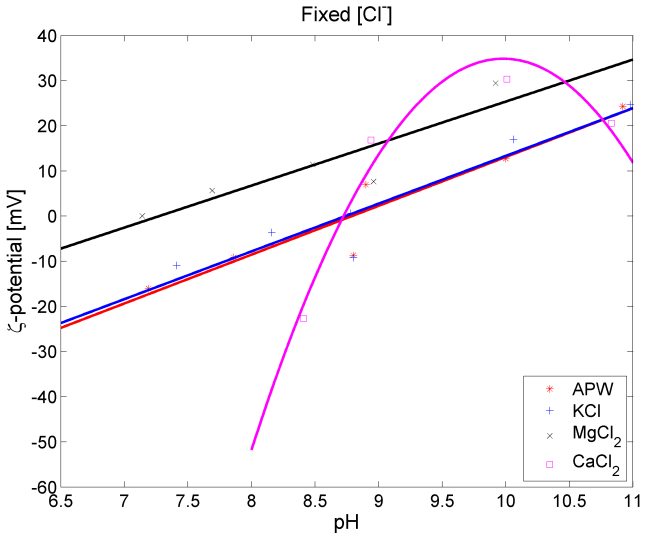

Figure 49: *The ζ-potential as a function of pH with contributions of Cl^- coming from the different salts.*

for APW was created. The concentration of each salt gives comparable ionic strengths and could give some useful information of the influence on that. The electrolyte solution seen in table 23 on the following page is diluted to get four different ionic strengths of 0,4 , 0,2 , 0,1 and 0,05 M for each salt. As seen in in figure 50 and in table 25 on page 65 the

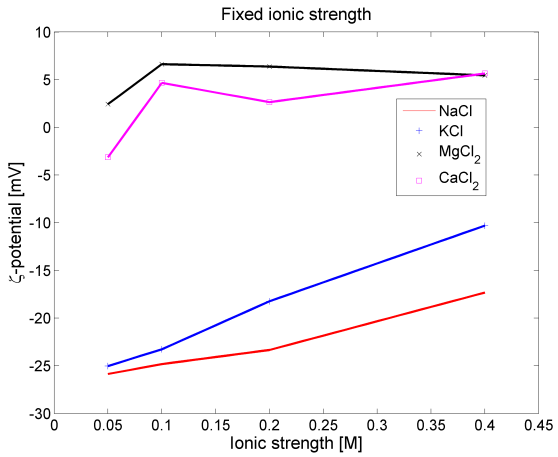

Figure 50: *The ζ-potential as a function of the ionic strength shows that Ca^{2+} and Mg^{2+} has a large influence on the results of the $CaCO_3$ measurements.*

Table 24: *Ionic radii of the cations present in APW. [B8]*

Ion	Ionic radii $[1 \cdot 10^{-12}$ m]
Na^+	116
K^+	152
Mg^{2+}	86
Ca^{2+}	114

mono valent and the divalent cations are producing similar results respectively. There is a remarkable difference of the impact the mono valent an divalent cations conducts on the ζ-potential of $CaCO_3$. The possible explanation is the size of the hydrated cations. With

Table 22: *Result of the experiment where the Cl^- contributing from NaCl was swapped with the concentration of the other ions.*

		ζ-potential			
	pH	1	2	3	Average
High KCl	8,80	−5,07	−12,95	−9,50	−9,17
	10,98	16,58	35,52	22,03	24,71
	10,06	21,08	12,20	17,63	16,97
	8,78	5,44	−6,33	2,71	0,61
	8,16	−4,02	−5,69	−1,14	−3,62
	7,41	−14,83	−10,45	−7,48	−10,92
High $MgCl_2$	8,48	14,61	10,43	9,30	11,45
	9,92	30,01	28,68	29,61	29,43
	8,96	7,22	1,79	13,92	7,64
	7,69	2,41	4,55	9,94	5,63
	7,14	−0,08	0,00	0,10	0,01
High $CaCl_2$	8,41	−7,56	−46,53	−13,93	−22,67
	10,83	5,61	31,91	24,12	20,55
	10,01	24,12	12,70	54,20	30,34
	8,94	20,72	12,71	17,11	16,85
Normal	8,80	−10,80	−9,66	−5,63	−8,70
	10,92	28,33	21,58	22,97	24,29
	10,00	11,78	12,31	14,13	12,74
	8,90	6,52	9,57	4,77	6,95
	7,86	−8,05	−12,17	−7,22	−9,15
	7,19	−16,15	−17,23	−14,81	−16,06

Table 23: *The calculated weight of each salt in order to get the ionic strength of 0,40 M.*

	Added [g/L]	Mol/L c_i	Cation z_i	Anion z_i	$I = 0,5 \times \sum c_i\, z_i^2$
KCl	29,82	0,40	1	−1	0,40
NaCl	23,38	0,40	1	−1	0,40
$CaCl_2$	14,79	0,13	2	−1	0,40
$MgCl_2$	27,10	0,13	2	−1	0,40

a higher charge the hydrated radii of the ion will decrease, see table 24 on the previous page. The size of Mg^{2+} is the smallest of the cations and would therefore be less physical hindered in getting close to the $CaCO_3$ surface. That explanation does not fit with the hydrated radii of Ca^{2+}, since the size is more or less the same as for Na^+. The explanation for Ca^{2+} could be that $CaCO_3$ is having a greater affinity for Ca^{2+} than for Na^+.

Table 25: *The result of the analysis of the effect of the ionic strength created by the different ionic species in APW towards the ζ-potential. The pH of the solutions are not adjusted.*

Salt	Ionic strength	ζ-potentiale [mV]				Conductivity [mS/cm]				pH
		1	2	3	Average	1	2	3	Average	
$CaCl_2$	0,05	−1,08	–4,55	−3,75	−3,13	6,053	6,167	6,225	6,148	7,83
	0,10	3,03	6,11	4,88	4,67	11,439	11,733	12,010	11,727	8,04
	0,20	1,92	3,49	2,54	2,65	21,278	21,900	22,334	21,837	8,25
	0,40	5,34	7,12	4,49	5,65	39,399	40,220	40,749	40,123	8,45
$MgCl_2$	0,05	2,89	1,57	2,86	2,44	6,233	6,348	6,425	6,335	8,89
	0,10	8,91	5,19	5,80	6,63	11,810	12,140	12,371	12,107	8,87
	0,20	5,79	7,03	6,33	6,38	21,676	22,438	22,978	22,364	8,78
	0,40	1,69	6,18	8,52	5,46	39,597	40,445	40,999	40,347	8,55
KCl	0,05	−25,45	−24,58	−25,07	−25,03	6,323	6,429	6,489	6,414	9,45
	0,10	−21,64	−24,06	−24,12	−23,27	12,059	12,396	12,690	12,382	9,63
	0,20	−14,81	−19,83	−20,06	−18,23	23,064	23,642	24,067	23,591	9,66
	0,40	−12,33	−10,15	−8,41	−10,30	44,372	45,039	45,631	45,014	9,68
NaCl	0,05	−25,61	−26,71	−25,27	−25,86	5,297	5,365	5,405	5,356	9,46
	0,10	−23,38	−26,05	−25,02	−24,82	9,972	10,232	10,413	10,206	9,59
	0,20	−21,01	−23,37	−25,64	−23,34	19,357	19,889	20,384	19,877	9,62
	0,40	−21,11	−15,35	−15,49	−17,32	35,853	36,732	37,300	36,628	9,58

6.5 XRD-analysis

The results from the ζ-potential measurements could be influenced by differences in the crystal structure of the chalk samples. Since Dankalk is used for the experiments, and the analysis of the $CaCO_3$ made by Dankalk shows presence of small pollutants, see table 7 on page 37, an analysis of the $CaCO_3$ could reveal some information. To see an indication of possible differences in the chalk structure, a XRD-analysis has been performed with the four different chalk samples mentioned in section 6.1 on page 53.

If two beams with the same wavelength hits an atom in a crystal lattice and the reflecting beams are in phase the result will be a peak on the chromatogram. If the angle of the ingoing beam results in the two outgoing beams being out of phase, no peak will be present. By performing a scan in a wide range of ingoing angles, the resulting peaks at the various

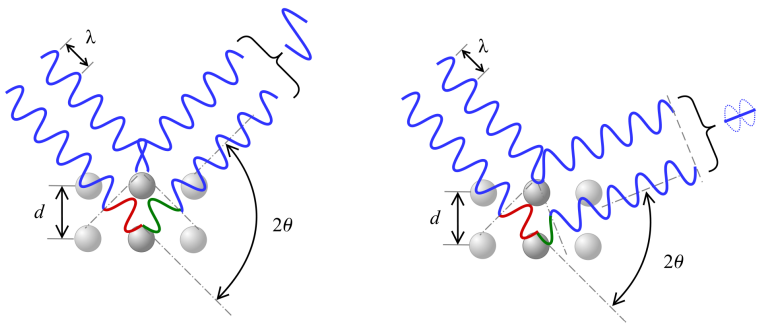

Figure 51: *Example of the x-ray beams diffraction from the crystal lattice with constructive phase shift (left) and destructive phase shift (right) interference.*

angles can tell the structure of the lattice as seen in figure 51. The peak intensity and the value of 2θ in a chromatogram is a fingerprint of a specific substance. According to Braggs law constructive interference is given when the path distance of the of the beam is given as

$$2d \sin\theta = n\lambda \tag{57}$$

n is an integer and λ is the wavelength of the x-ray beam.

Setting description

The analysis has been performed with a Co anode, see table 26 on the next page, and the scan is performed in the region from 5 - 75 $^\circ$ 2θ.

XRD result

The result of the analysis is seen in figure 52 on the facing page. As seen, the four different chalk samples are more or less of the same type. The XRD-scans did not show any significant differences in the lattice structure, and the identification of the scans all indicated $CaCO_3$ in the form of calcite.

Table 26: *During XRD-analysis the following settings where used.*

Settings for the XRD-analysis	
Diffractometer type	XPERT PRO
Anode material	Co
K-Alpha1 wavelength [nm]	178,897
K-Alpha2 wavelength [nm]	179,285
Ratio K-Alpha2/K-Alpha1	0,500

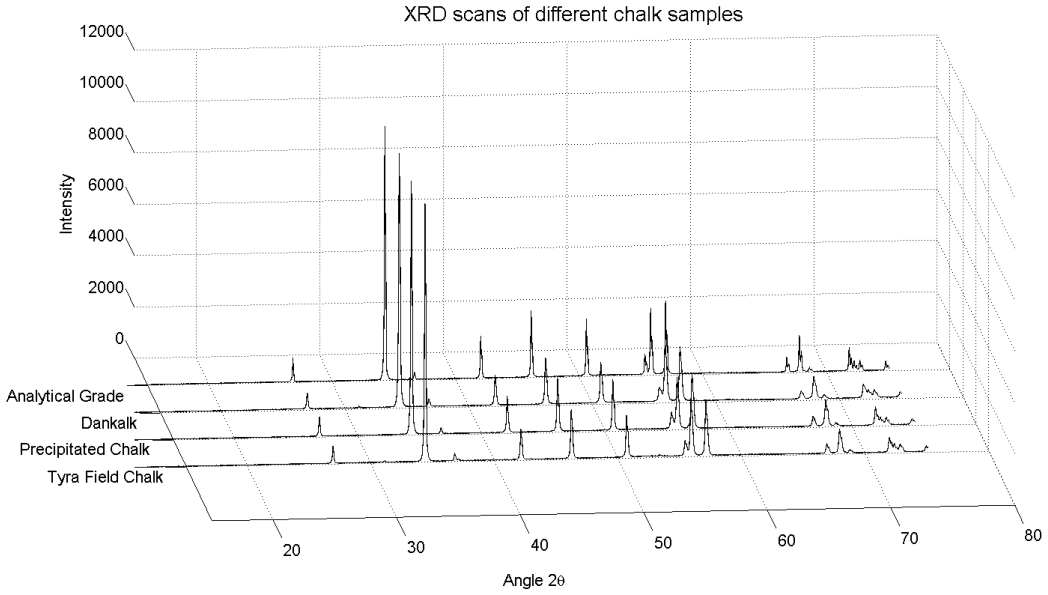

Figure 52: *Comparison of XRD-scans performed on the four different chalk samples, which are used during experiments.*

6.6 HCO_3^- as potential determining ion?

A possible explanation of the reversed behavior of the ζ-potential could be HCO_3^- acting as a potential determining ion (PDI) towards $CaCO_3$. The theory is explained with the increasing concentration of HCO_3^- caused by the increase of $[H^+]$ following

$$\mathrm{CaCO_{3(s)}} \overset{+H_2O}{\rightleftharpoons} \mathrm{Ca^{2+} + CO_3^{2-}} \overset{+H^+}{\rightleftharpoons} \mathrm{Ca^{2+} + HCO_3^-}$$

By adding Na_2CO_3 to a solution of deionized water containing $CaCO_3$, the concentration of CO_3^{2-} should increase which again would form more HCO_3^- and induce a change in pH, following

$$\mathrm{CaCO_{3(s)}} \overset{+H_2O}{\rightleftharpoons} \mathrm{Ca^{2+} + CO_3^{2-}} \overset{+Na_2CO_3}{\rightleftharpoons} \mathrm{Ca^{2+} + 2Na^+ + HCO_3^-} \Rightarrow [\mathrm{H^+}]\downarrow, \mathrm{pH}\uparrow$$

An experiment was prepared with a 0,5 L beaker containing APW and 0,1 g $CaCO_3$ from Dankalk. After dispersion the ζ-potential was measured and the pH was altered by adding

Figure 53: *Phillips Expert XRD used for analysis of the $CaCO_3$ samples.*

1 mL of 0,002 M Na_2CO_3 to the solution. This procedure was repeated several times to see a change, if any, in the ζ-potential indicating that HCO_3^- is a PDI. The result is seen in figure 54 on the next page and table 27.

Table 27: *First experiment with addition of Na_2CO_3 to change the pH and increase the concentration of CO_3^-. Missing values are marked as -.*

pH	ζ-potential			Average
8,86	−13,21	−15,53	−12,60	−13,78
8,96	−13,15	−9,74	−11,16	−11,35
9,00	-	−14,04	−16,07	−15,06
9,01	−9,63	−11,58	−10,48	−10,56
9,04	−10,84	−10,37	−11,87	−11,03
9,08	−9,17	−10,94	−10,87	−10,33
9,11	−9,76	−9,90	−7,81	−9,16
9,12	−6,26	−9,75	−10,49	−8,83
9,16	−7,75	−11,63	−11,84	−10,41
9,18	−11,05	−13,94	−9,34	−11,44
9,22	−8,06	−8,40	−8,98	−8,48
9,27	−5,15	−12,41	−9,16	−8,91
9,33	−9,80	−7,83	-	−8,82
9,34	−10,99	−11,09	−9,33	−10,47

The analysis was repeated once to reproduce the result but this time with a reduced number of measurements and an increased volume of 0,002 M Na_2CO_3 added each time, see figure 54 and table 28.

Table 28: *Second experiment with addition of Na_2CO_3 to change the pH and increase the concentration of CO_3^-.*

pH	ζ-potential			Average	Added 0,002 M Na_2CO_3 [mL]
8,78	−33,68	−36,76	−33,59	−34,68	0,01
8,96	−15,65	−15,11	−17,27	−16,01	9,00
9,13	−11,08	−12,14	−12,95	−12,06	21,00
9,21	−11,72	−10,62	−10,48	−10,94	33,00
9,25	−9,19	−14,75	−8,60	−10,85	45,00
9,31	−9,38	−10,82	−10,97	−10,39	60,00
9,40	−9,23	−11,91	−13,82	−11,65	75,00

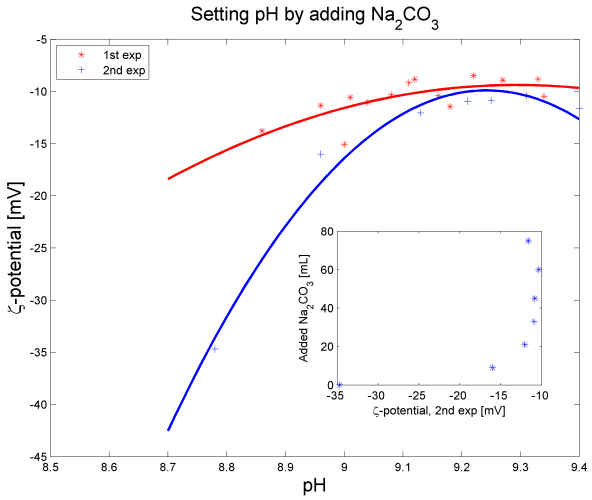

Figure 54: *Plot of the ζ-potential as a function of pH, altered with Na_2CO_3*

It is seen that both analyses show the same tendency, which is an increase in $[CO_3^{2-}]$ changes the pH i the positive direction and altering a change of the ζ-potential in the positive direction. At a pH of approximately 9,3 the change in ζ-potential flatten off.

This result does not indicate that HCO_3^- is causing the reverse effect on the ζ-potential in that specific pH-range, since the ζ-potential is moving towards the positive side together with the increase of HCO_3^- species. The flatten out of the curve is explained with the equilibrium

$$H_2CO_3 \underset{+H^+}{\overset{-H^+}{\rightleftharpoons}} HCO_3^- \underset{+H^+}{\overset{-H^+}{\rightleftharpoons}} CO_3^{2-}$$

where the pH of 9,3 is the turning point where CO_3^{2-} no longer takes up a H^+, but remains as carbonate ions in the solution. It is seen in the figure where the ζ-potential as a function of the added Na_2CO_3 is going asymptotic $\rightarrow \infty$.

6.7 PHREE-PLOT simulation

To see which ion pair species are possible with the added constituents for APW, a simulation is performed in the software PHREE-PLOT, based on the geochemical modelling software PHREEQC, see supplement 9 on page 99 for information concerning the code for the simulation.

The purpose of this simulation is to see which ion pairs are possible with the given ionic concentrations in APW. The result is given as a function of the pH, which makes the plot useful in the investigation of the PDI of $CaCO_3$. For each species there are made two plots. One with the % species distribution and one with the logarithmic concentration of the species. The simulations are performed with the use of the Debye-Hückel equation, see equation 46 on page 36, even though the ionic strength is beyond the limit of that equation. PHREEQC could not perform the simulation using the Davis equation. The Pitzer equation, which is the better alternative, did not have thermodynamic data of all the possible ionic pairs and could not be used either. A small discrepancy is expected from that choice of using the Debye-Hückel equation.

Magnesium

Mg will preferably stay as Mg^{2+} in the range of pH 6 - 8, see figur 55 on the next page. From pH 8 and up Mg^{2+} will establish ion pair with OH^- creating an increasing concentration of $MgOH^+$. From pH 12 and up [$MgOH^+$] is dominating.

Since CO_3^{2-} is present from the dissolved $CaCO_3$, Mg^{2+} will establish ion pairs with CO_3^{2-} creating $MgCO_3$ and $MgHCO_3^+$. The rise in pH induces the formation of $MgOH^+$ from $1 \cdot 10^{-8}$ mol L^{-1} at pH 6 to $1 \cdot 10^{-3}$ mol L^{-1} at pH 12, see figure 56 on the facing page. Since Mg has shown a significant influence on the ζ-potential of $CaCO_3$, see figure 50 on page 63, the rapidly increasing concentration of $MgOH^+$ could be a contributor to the positively growing ζ-potential with the rise in pH. $MgCO_3$ is neutral and is not considered as an influence on $CaCO_3$. [$MgHCO_3^+$] is unaltered in the range of pH 6 - 9 and is decreasing thereafter. $MgHCO_3^+$ is not considered as an influence on $CaCO_3$.

Calcium

Ca is showing a behavior similar to Mg, see figure 57 on page 72. Ca will dominate as Ca^{2+} from pH 6 - 8, whereafter a slight decrease is seen parallel to the increase in formation of $CaOH^+$. In the entire range from pH 6 - 13 as shown on the figure, Ca^{2+} is dominating.

The ion pair formation with the CO_3^{2-} species is shown on figure 58 on page 72. Similar to [$MgOH^+$] the concentration of $CaOH^+$ is increasing with the rise in pH. The effect of Ca^{2+} on the ζ-potential of $CaCO_3$, shown on figure 50 on page 63, combined with the increasing

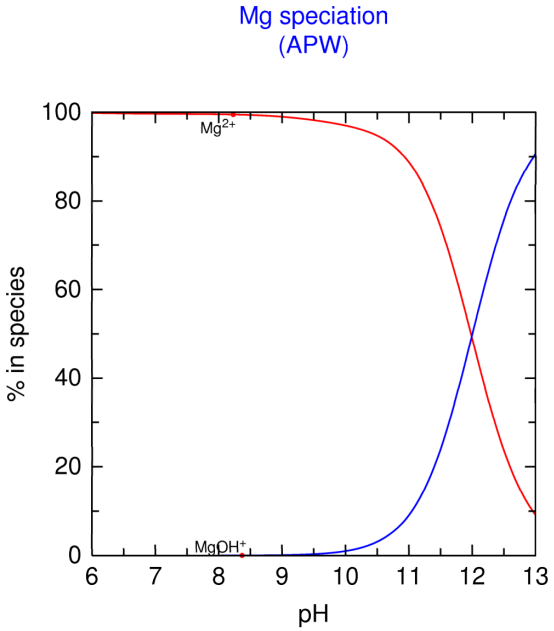

Figure 55: Plot of the % species distribution of magnesium containing ions.

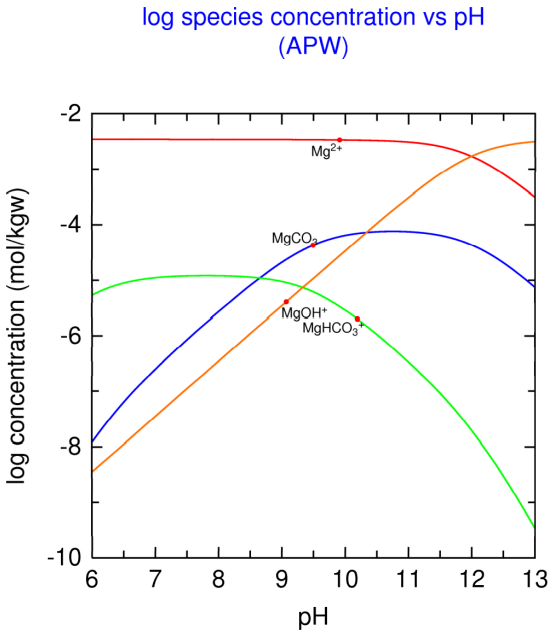

Figure 56: Plot of the logarithmic concentration of the magnesium containing ions.

[$CaOH^+$], shows a possible interaction of the rising ζ-potential which could originate from the increasing [$CaOH^+$]. $CaCO_3$ is neutral and [$CaHCO^+$] is decreasing with the rise in pH.

Potassium

K is not showing any signs of interaction with $CaCO_3$ in any way. Both figures 59 and 60 on the next page does not indicate any possible ion pairs that could influence the ζ-potential of $CaCO_3$.

Sodium

Na is dominating as Na^+ in the entire range of pH from 6 - 13, see figure 61 on page 73. Na^+ is establishing ion pair with CO_3^{2-} species only, see figure 62 on page 73. Since [$NaCO_3^-$] is increasing and flatten out towards pH 10, no possible interaction can be correlated towards the ζ-potential of $CaCO_3$. Na_2CO_3 is neutral and is therefore not considered as a contributor to any change in ζ-potential.

Carbon

C is present in the electrolyte as CO_3^{2-}. Figure 63 on page 73 shows that HCO_3- is dominating at the pH range from 6 - 10. The dominating presence of HCO_3^- is fitting well with the idea that HCO_3^- is a PDI towards $CaCO_3$. At low pH values the ζ-potential is

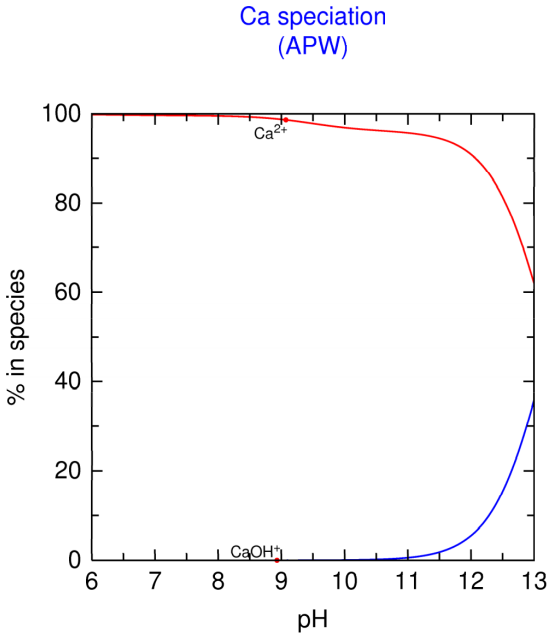

Figure 57: Plot of the % species distribution of calcium containing ions.

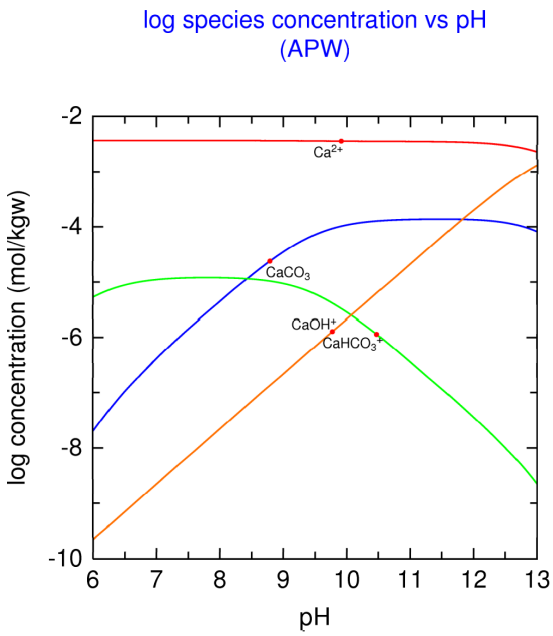

Figure 58: Plot of the logarithmic concentration of the calcium containing ions.

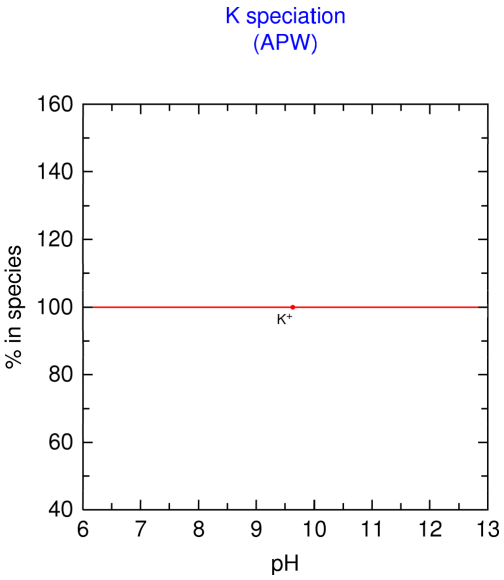

Figure 59: Plot of the % species distribution of potassium containing ions.

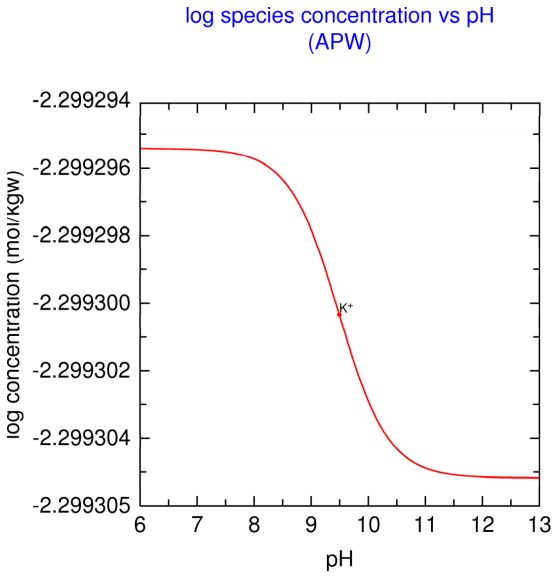

Figure 60: Plot of the logarithmic concentration of the potassium containing ions.

negative and growing positively with rising pH. CO_2 is neutral and its concentration is decreasing with rising pH, see figure 64 on the next page.

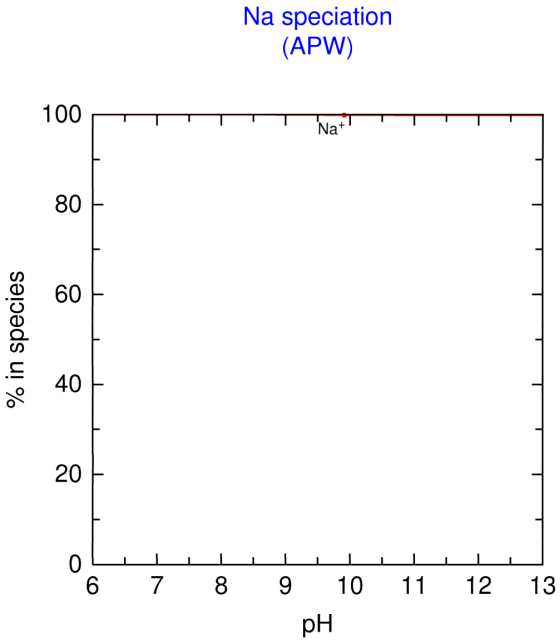

Figure 61: Plot of the % species distribution of sodium containing ions.

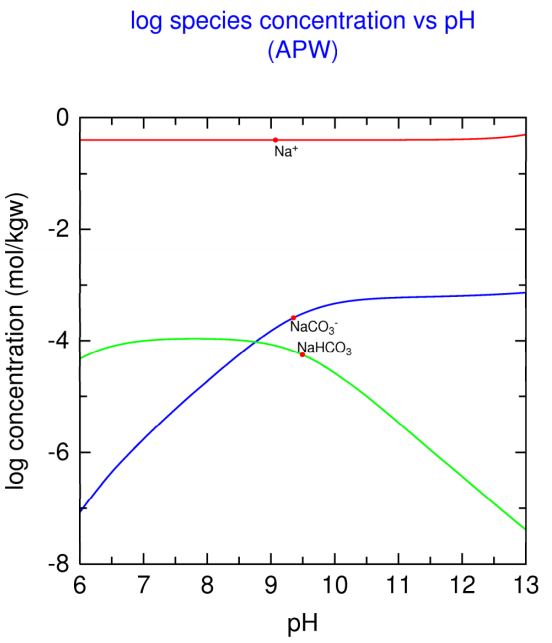

Figure 62: Plot of the logarithmic concentration of the sodium containing ions.

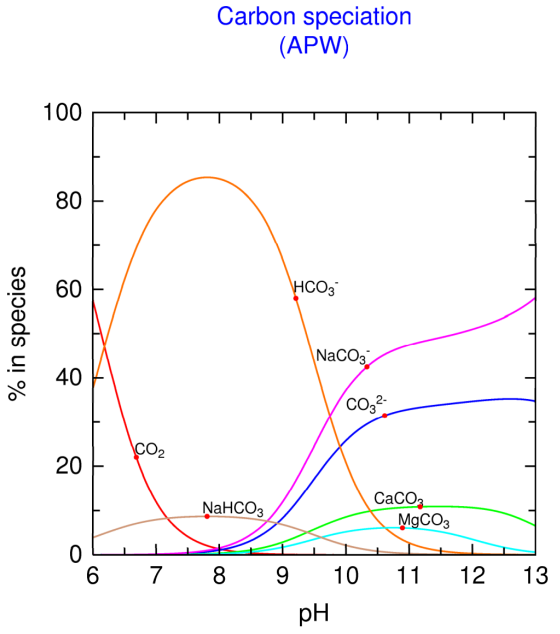

Figure 63: Plot of the % species distribution of carbon containing ions.

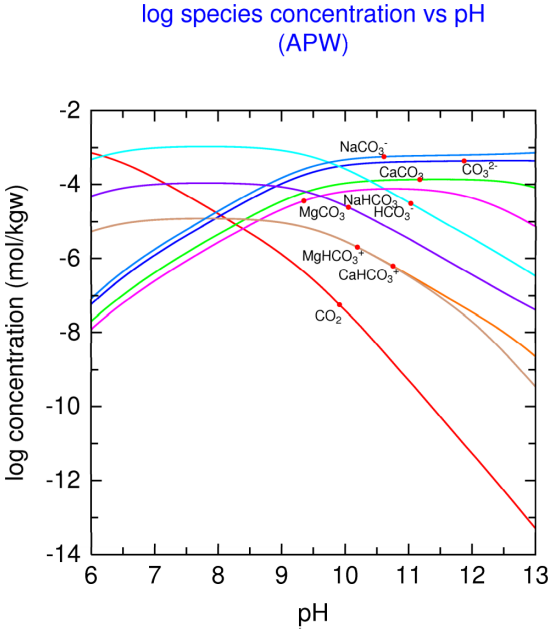

Figure 64: Plot of the logarithmic concentration of the carbon containing ions.

6.8 Verification of HCO_3^- as PDI

To see if the theory concerning HCO_3^- acting as a PDI on $CaCO_3$ is plausible, an experiment is prepared in which $NaHCO_3$ is added to APW consisting $CaCO_3$. By adding $NaHCO_3$

instead of Na_2CO_3, the pH should remain constant, since no H^+ is taken from the solution as it was the case in the experiment discussed in section 6.6 on page 67. A 0,01 M solution of $NaHCO_3$ was prepared. 0,1 g $CaCO_3$ from Dankalk was added and dispersed in a 250 mL beaker containing APW. The ζ-potential was measured and 1 mL of the $NaHCO_3$ solution was added at a time. The result is shown on figure 65 and in table 29 and table 30.

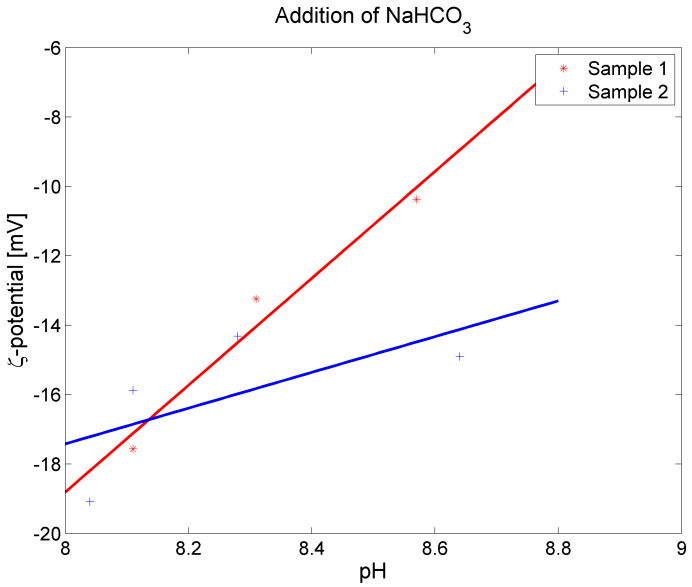

Figure 65: *The result of two measurements with $NaHCO_3$ shows a negative increase in the ζ-potential of $CaCO_3$ when adding HCO_3^- to the solution.*

Table 29: *First analysis of the effect of $NaHCO_3$ addition, sample 1.*

pH	8,57	8,31	8,11
	−9,91	−11,81	−15,37
ζ-potential	−13,35	−16,08	−19,63
	−7,87	−11,84	−17,70
Average	−10,38	−13,24	−17,57

Table 30: *Second analysis of the effect of $NaHCO_3$ addition, sample 2.*

pH	8,64	8,28	8,11	8,04
	−14,37	−14,97	−13,38	−19,42
ζ-potential	−14,96	−10,99	−14,67	−20,26
	−15,38	−16,99	−19,57	−17,56
Average	−14,90	−14,32	−15,87	−19,08

The result consolidates the theory of HCO_3^- as PDI towards $CaCO_3$. The ζ-potential is decreasing by addition of $NaHCO_3$ to the solution. A small decrease in pH is observed possibly because HCO_3 is acting as an acid as

$$NaHCO_3 + H_2O \rightleftharpoons Na^+ + CO_3^{2-} + H_3O^+$$

The change in pH is negligible compared to the previous results where the pH was adjusted with HCl and NaOH, and is therefore not considered as the main contributor to the negatively increasing ζ-potential.

6.9 Electro Spray Ionization-Mass Spectrometry (ESI-MS)

To confirm the presence of the species $MgOH^+$ and $CaOH^+$ at various pH, an anlysis by the help of ESI-MS is conducted. Solutions of deionized water containing $MgCl_2$ and $CaCl_2$ at concentrations of $1 \cdot 10^{-4}$ mol L^{-1} are used. The concentration of the electrolyte is chosen according to the limitations of the ESI-MS instrument to prevent clocking. The analysis is performed in the m/z range from 30 - 400, and the peaks of interest are present at 41,31 m/z and 57,09 m/z for $MgOH^+$ and $CaOH^+$ respectively. The solutions at low pH has not been pH adjusted and consists purely of deionized water and the salts. pH is adjusted with 0,05 M NaOH at high pH. The specific pH-values are shown in table 31 on the next page. The resulting spectrums have been processed in MatLab to remove some noise. A background spectrum of pure deionized water was made and subtracted from the resulting spectrums.

$MgCl_2$

The spectrums of $MgCl_2$ and $CaCl_2$ are shown in figure 67 on page 77. It can be seen that several peaks are present with isotopes of mainly Cl dominating the spectrum. Since the peak of interest is below 150 m/z, only the range from 30 - 150 m/z will be explained.

To understand the spectrum of $MgCl_2$, the isotope abundance of Mg and Cl has to be explained briefly. Figure 66 on the next page shows the peaks of Mg isotopes and the Cl_2-isotope with the relative abundance of the isotope given as intensity. The pattern of the intensity difference and the m/z distribution can be used to find these specific ions in the spectrum. It is shown that Mg has three isotopes at 24, 25 and 26 m/z with the abundance ratio of 78,99%, 10,00% and 11,01% respectively. Cl_2 has two isotopes at 35 and 37 m/z with the abundance ratio of 75,78% and 24,22% respectively.

In figure 67 on page 77 two peaks in Mg high pH are marked. 41,7 m/z is recognized as $MgOH^+$, having a molar weight of (24,305 + 15,9994 + 1,00794 = 41,3132) g/mol. The discrepancy from 41,7 to the calculated molar weight is possibly originated from the calibration of the instrument, which was done in the range from 118 m/z to 2200 m/z. Ions occurring below 118 m/z could have a discrepancy. The peak at 51,7 m/z has been investigated further by MS/MS, see figure 68 on page 77, which is a technique in which the ions of interest are fragmented by He atoms, revealing the composition of the peak. It is

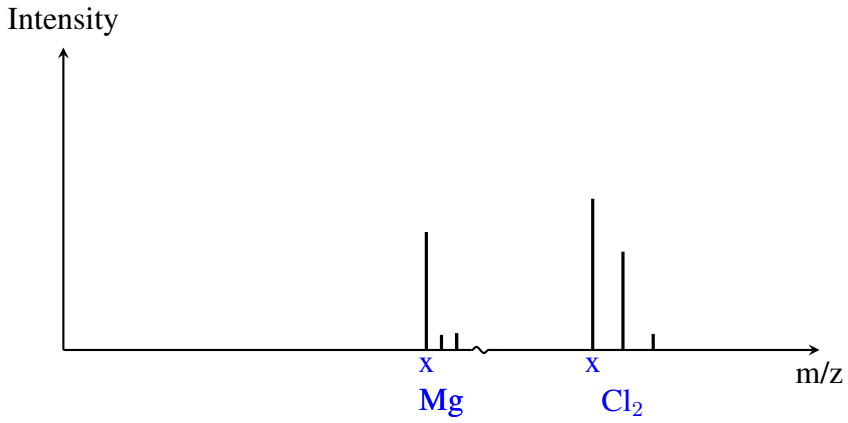

Figure 66: *Mg has three isotopes at 24 (x),25 and 26 m/z. Cl has 24 isotopes in the range of ^{28}Cl to ^{51}Cl. The shown isotope is for Cl_2 consisting of 35 (x), 37 and 39 m/z. The intensity of the peak shows the relative abundance of the specific isotope.*

seen that one of the fragmentation peaks is at 41,7 m/z indicating the presence of $MgOH^+$.

Table 31: *pH of the solutes used for ESI-MS analysis.*

	$MgCl_2$ pH low	$MgCl_2$ pH high	$CaCl_2$ pH low	$CaCl_2$ pH high
pH	5,85	10,31	5,58	10,41

$CaCl_2$

The spectrum of $CaCl_2$ at low pH has a peak at 57,4 m/z, see figure 67 on the facing page, which is identified as $CaOH^+$ with the molar weight of (40,078 + 15,9994 + 1,00894 = 57,0853) g/mol with a small discrepancy. The spectrum for $CaCl_2$ at high pH has a significant peak at 129 m/z. MS/MS on that peak reveals that the peak is the hydrated ion of $CaOH^+$ with four H_2O, $[(CaOH)(H_2O)_4]^+$. The first fragmentation peak is at 111 m/z, indicating the loss of a water molecule. The peak at 57,4 m/z is identified as the $CaOH^+$.

6.10 Coagulation by $FeCl_3$

To measure the effect of the coagulant found in section 5.5 on page 50, an analysis of the change in the ζ-potential as a function of added $FeCl_3$ was conducted. The $FeCl_3$ delivered by Bo Jensen Vandbehandling A/S was diluted 1:1000, to be able to measure the change. Undiluted $FeCl_3$ dissolved the $CaCO_3$ because of the Fe^{3+} acting as a Lewis acid, see equation 58.

$$FeCl_3 \overset{+H_2O}{\rightleftharpoons} Fe^{3+} + 3Cl^- \Rightarrow [Fe(H_2O)_6]^{3+} \Rightarrow [Fe(H_2O)_5OH]^{2+} + H^+ \qquad (58)$$

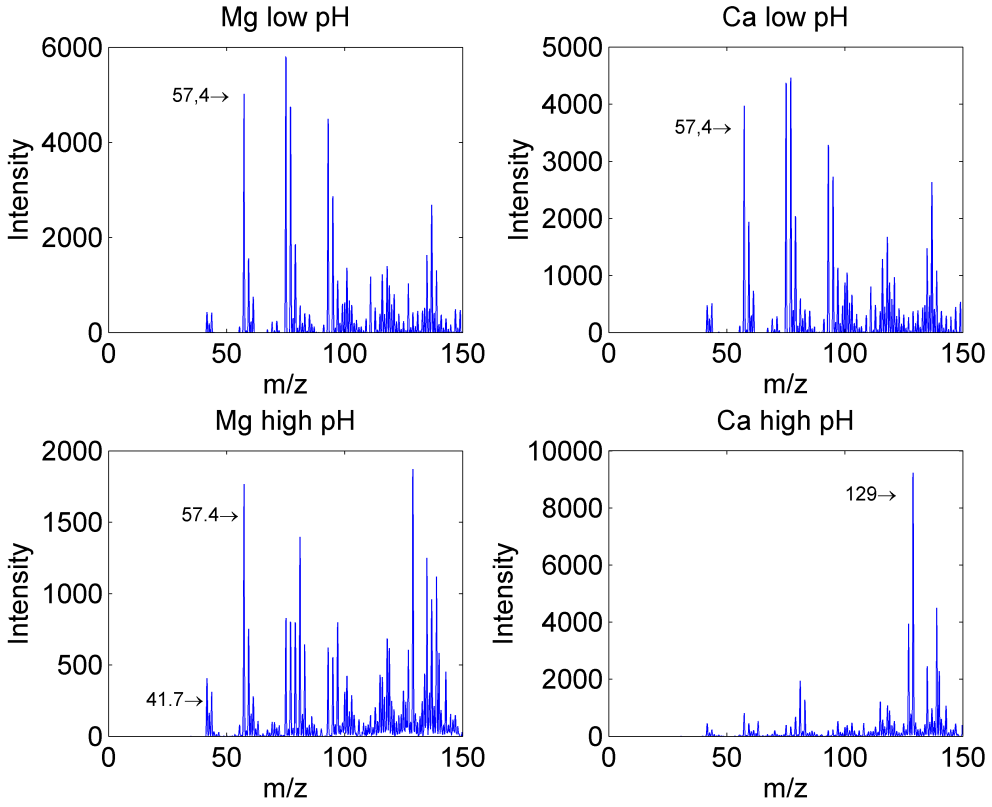

Figure 67: *ESI-MS spectrum of dissolved $MgCl_2$ and $CaCl_2$ at low and high pH.*

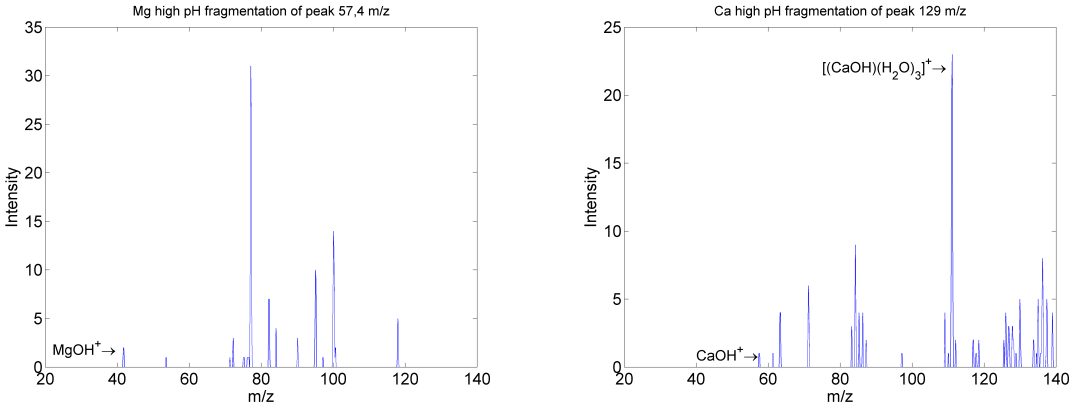

(a) *Fragmented 57,4 m/z peak of $MgCl_2$ high pH.* ***(b)*** *Fragmented 129 m/z peak of $CaCl_2$ high pH.*

Figure 68: *The fragmented peaks of 57,4 and 129 m/z for $MgCl_2$ and $CaCl_2$ respectively indicates the presence of the PDI at high pH, which consolidates the theory of $MgOH^+$ and $CaOH^+$ having an effect of the ζ-potentiale of $CaCO_3$.*

The measurement was conducted with 500 mL APW in which 0,25 g $CaCO_3$ from Dankalk was added and dispersed. The pH of the solution was 8,87 with a ζ-potential of -12,48 mV

at start. After addition of 4 mL diluted $FeCl_3$ the ζ-potential was -0,83 mV which caused the $CaCO_3$ particles to coagulate and settle. Figure 69 indicates a good linear correlation between added $FeCl_3$ and the effect on the ζ-potential.

Table 32: *The effect of adding 1 mL diluted $FeCL_3$ 1:1000 to a 500 mL beaker with APW and $CaCO_3$ is seen as a rapid change of the ζ-potential.*

pH	8,87	8,76	8,73	8,71	8,63
ζ-potential	−10,80	−7,95	−7,61	−4,36	−2,79
	−12,80	−6,84	−4,94	−0,88	0,26
	−13,85	−7,27	−4,35	−4,54	0,04
Average	−12,48	−7,35	−5,63	−3,26	−0,83

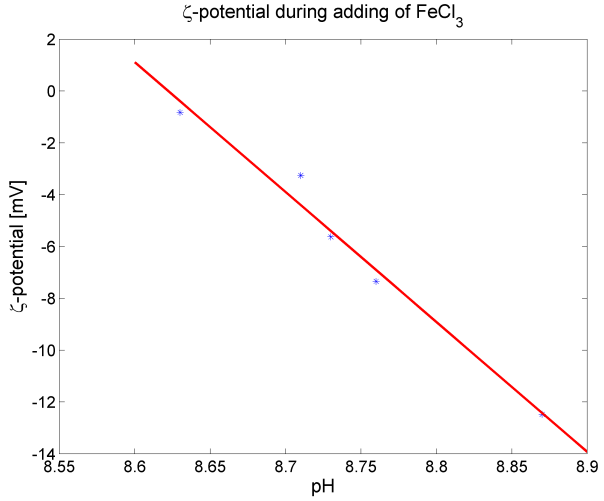

Figure 69: *The ζ-potential going rapidly against zero by adding 1 mL $FeCl_3$ diluted 1:1000 for each measurement. R^2 = 0,9887.*

6.11 Conclusion on the ζ-potential analysis

It has been shown that the ζ-potential does not always follow a normal behavior. In this case the ζ-potential of $CaCO_3$ in APW reversed the sign of the ζ-potential compared to results emerged in deionized water. The reversing effect is most likely caused by the high ionic strength of the electrolyte solution. Several experiments with varying concentrations of the ionic species present in APW has shown a plausible explanation in the presence of HCO_3^- at low pH and $MgOH^+$ and $CaOH^+$ at high pH acting as PDI, pushing the ζ-potential in negative and positive direction respectively. Equilibrium simulations performed in PHREEQC and PHREE-PLOT support that explanation showing ionic species concentrations and distributions which favours the formation of HCO_3^- and little or no formation of $CaOH^+$ and $MgOH^+$ at low pH and vice versa. K, Na and Cl is not

participating in the change of the ζ-potential directly. But Na and Cl is the main contributor to the magnitude of the ionic strength.

ESI-MS analyses of pure solutions of $MgCl_2$ and $CaCl_2$ dissolved in deionized water at low and high pH show the presence of both $MgOH^+$ and $CaOH^+$ at high pH which underlines the theory of the PDI.

$FeCL_3$ has been used for coagulation of $CaCO_3$ in APW. Measurements of the ζ-potential show a good effect on the neutralization of the ζ-potential of $CaCO_3$ by adding $FeCL_3$ and the concomitant coagulation and sedimentation of the $CaCO_3$.

To strengthen the explanation of the reversed ζ-potential effect, an extensive sample series with varying ionic concentrations and pH containing $CaCO_3$ could be manufactured. The ζ-potential measured could be used as a variable together with the known species concentration. A sample of each beaker could be analyzed with Electro Spray Ionization Mass Spectrometry (ESI-MS). The resulting spectrum from the ESI-MS analysis could be precessed in a Principal Component Analysis (PCA) which is a multivariate data analysis tool, capable of showing possible correlations between the concentration of HCO_3^-, $CaOH^+$ and $MgOH^+$ and the ζ-potential respectively. This experiment has not been conducted due to lack of time.

7. Emulsions

Emulsions of oil in water or water in oil is a well known issue, which is treated in many different industries like the food industry (e.g. liquid butter) and the paint industry. In issues regarding water treatment emulsions are often unwanted since the effect of emulsions can be a degraded quality of the treated water. In produced water, treatment emulsions are counteracted with demulsifiers, which are chemicals increasing the rate of phase separation of the dispersed liquid from the matrix. Coalescence of O/W emulsions is also a normal unit operation. In the experiments, which will be performed for this thesis, only oil in water (O/W) emulsions will be processed.

The purpose of the experiments is to investigate the possibility of the transfer of oil into the water phase by the help of small chalk particles. Small oil droplets can adsorb to the surface of the chalk particles and thereby move with the produced water stream instead of the crude stream.

7.1 Theory

The theory of emulsions is based on the fact that two immiscible fluids will have different surface tensions, and the thermodynamically most stable condition is the one where the surface area between the matrix (e.g. water) and the dispersed liquid (e.g. crude) is the smallest one possible. Water and oil are by definition immiscible under normal conditions. The oil phase has a lower density than water and will move upwards and create a top layer of oil. Under the right conditions though oil drops can create a stabilized colloid dispersion, as long as the oil droplets are small enough.

Surface tensions between solids and liquids are measured with contact angle measurements. Specific surface energies γ for various materials are known. By combining the information given in figure 70 on the facing page and Young's equation, se equation 59, the contact angle can give useful information of the behavior of a solid/liquid interaction.

$$\gamma_{ls} + \gamma_{vl} \cos\theta = \gamma_{vs} \tag{59}$$

Kralchevsky et al[A33] has shown theoretically that small particles can create a boundary layer between the two immiscible fluids, see figure 71 on the facing page, which stabilizes the dispersed droplets. Hydrophillic particles ($\theta < 90°$) stabilizes O/W emulsions and hydrophillic particles ($\theta > 90°$) stabilizes W/O emulsions. The vapor phase is replaced by the oil phase, and the contact angle θ is measured in the liquid phase (water phase). An emulsion stabilized by solid particles is called a Pickering emulsion.

Thermodynamically the creation of an emulsion is causing a change in the Gibbs free energy (ΔG) of the system [J]. ΔG of the emulsion can be described as

$$\Delta \mathrm{G} = \Delta \mathrm{H} - \mathrm{T}\Delta \mathrm{S} \tag{60}$$

where ΔH is the change in enthalpy [J], T the temperature [K] and ΔS the change in entropy [J/K]. Since the creation of an emulsion is creating a larger contact area $\Delta \mathrm{A} = \mathrm{n_d} 4\pi \mathrm{r}^2$ [m^2]

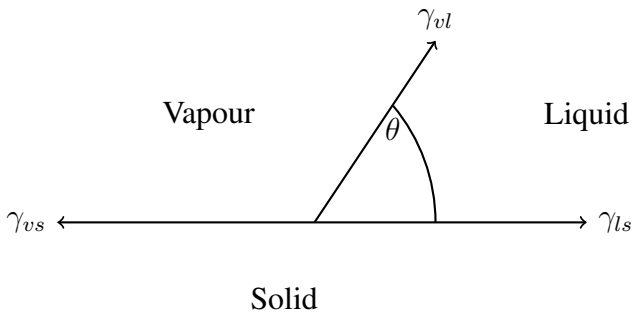

Figure 70: *Example of the balance of forces for a liquid drop on a solid surface in a three phase system.*

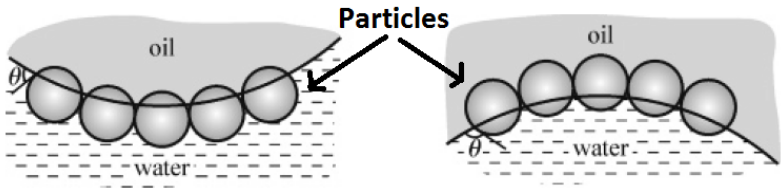

Figure 71: *Particle stabilized emulsions of two immiscible fluids, O/W and W/O respectively. [A33]*

between the two immiscible phases A and B, the interfacial tension γ_{AB} [N/m] between phase A and B will increase. The change in Gibbs free energy can be rewritten as

$$\Delta \mathrm{G}_{\mathrm{Dispersion}} = \gamma_{\mathrm{AB}} \Delta \mathrm{A} - \mathrm{T} \Delta \mathrm{S} \tag{61}$$

The term $\Delta \mathrm{S}$ can be approximated as

$$\Delta \mathrm{S} = -\mathrm{n_d} k_{\mathrm{B}} \left[\ln \phi + \left(\frac{1-\phi}{\phi} \right) \ln(1-\phi) \right] \tag{62}$$

where k_{B} is the Boltzmann constant and ϕ the dispersed phase volume fraction. If $\Delta \mathrm{G}_{\mathrm{Dispersion}}$ is negative meaning that γ_{AB} is sufficiently small and $\Delta \mathrm{S}$ is positive, the emulsion will be created spontaneously. Often $\Delta \mathrm{G}_{\mathrm{Dispersion}}$ is positive, and a mechanical treatment is necessary to create the emulsion. As seen in equation 62 an increase in the number of droplets (n_d) will increase the numerical value of $\Delta \mathrm{S}$. Herby follows that

$$\underset{\rightarrow -\infty}{\Delta \mathrm{G}} \text{ for } \underset{\rightarrow \infty}{\mathrm{n_d}} \tag{63}$$

7.2 Chalk/water emulsion

To create emulsions a setup with a mixer of the type RE-16 from Janke & Kunkel Ika-Werk, see figure 72 on the following page, was used. The impeller diameter was 45 mm and the chosen RPM was ≈ 1000. The tip speed was calculated to 2,36 m/s which should give the conditions for an emulsion [I12].

300 mL of deionized water and APW was used for the experiment. 1,020 and 1,007 g $CaCO_3$ was added to APW and deionized water respectively and treated for 30 sec. with ultrasonic dispersion. 4 mL crude oil was added to the beaker and the oil/water solution was stirred vigorously for 10 min, see figure 73 on the next page.

Table 33: *Settings for the emulsion experiment.*

Impeller D [mm]	RPM	Tip speed [m/s]
45	1000	2,36

Figure 72: *Mixer used for the experiment.*

The two beakers were placed in a fume hood for 72 hours to allow the sedimentation of the dispersed $CaCO_3$ particles.

Table 34: *Composition of the two solutions of deionized water and APW for the first emulsion experiment.*

Matrix	Volume [mL]	Added $CaCO_3$ [g]	pH	Added crude oil [mL]
APW	300	1,020	9,04	4
Deionized water	300	1,007	9,59	4

Result

As seen on figure 74 on the facing page remains of crude were dragged with the sediment of $CaCO_3$ particles into the water phase. Inspection of samples from the crude containing sediment under the microscope, see figure 75 to 77 on page 84, showed that particles of $CaCO_3$ can act as a carrier for the crude oil and drag the crude in the water phase. This observation makes it plausible that $CaCO_3$ particles can contribute to more discharge of oil via the produced water stream, by acting as a transport mechanism in the HP and LP-separator of the water/oil separation.

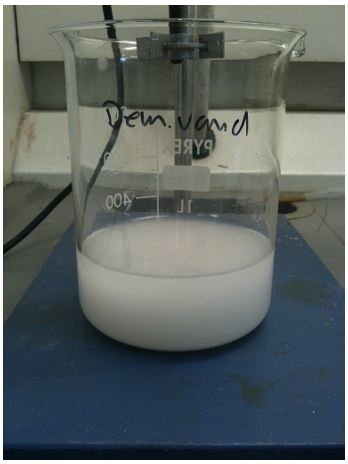

(a) Deionizes water with dispersed $CaCO_3$.

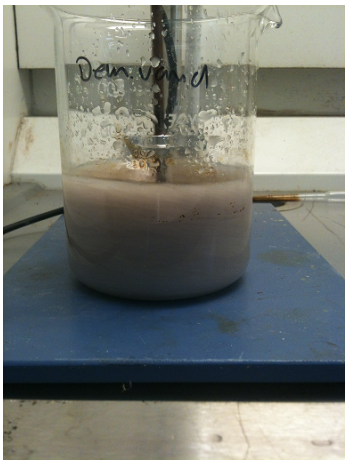

(b) Deionized water during mixing.

(c) Deionized water after 10 min. mixing.

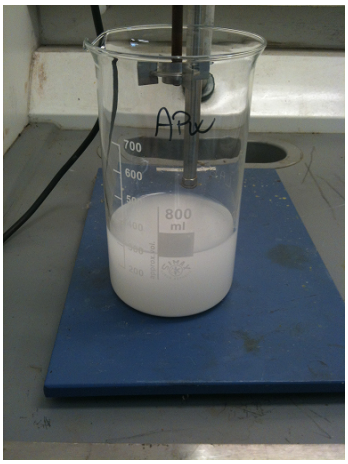

(d) APW with dispersed $CaCO_3$.

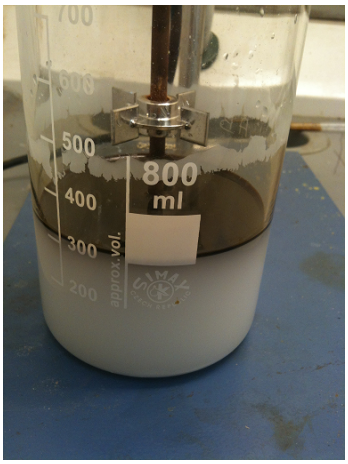

(e) APW with crude before mixing

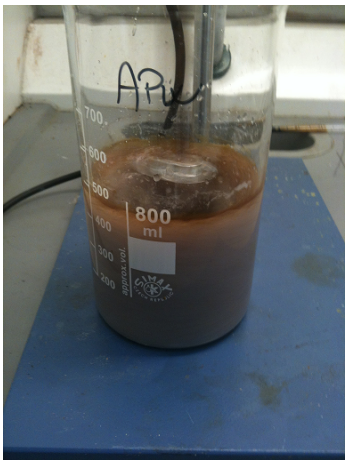

(f) APW during mixing.

Figure 73: *First experiment with emulsion of crude in deionized water and APW at 21 ℃.*

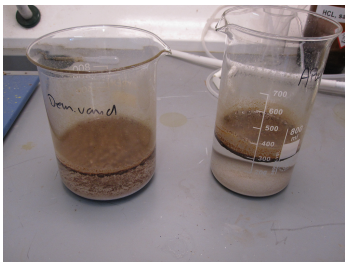

(a) $CaCO_3$ sediment after 72 hours with crude in the water phase.

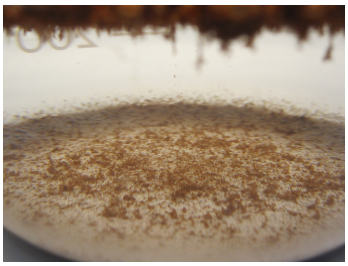

(b) $CaCO_3$ sediment in deionized water after 72 hours.

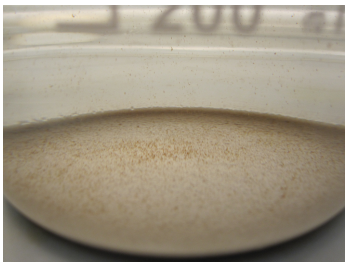

(c) $CaCO_3$ sediment in APW after 72 hours.

Figure 74: *$CaCO_3$ sediment containing remains of crude after 72 hours.*

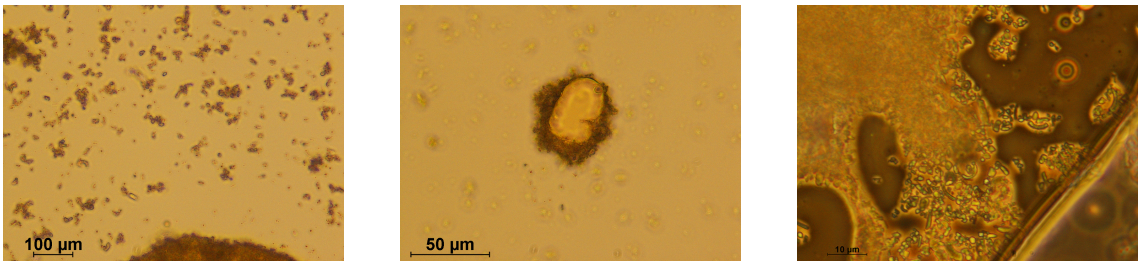

(a) 10X magnification. *(b) 40X magnification.* *(c) 100X magnification.*

Figure 75: *$CaCO_3$ sediment in deionized water containing remains of crude after 72 hours.*

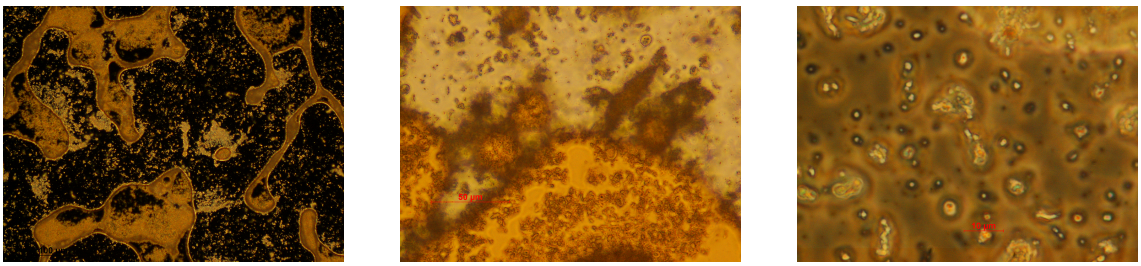

(a) 10X magnification. *(b) 40X magnification.* *(c) 100X magnification.*

Figure 76: *$CaCO_3$ sediment in APW containing remains of crude after 72 hours.*

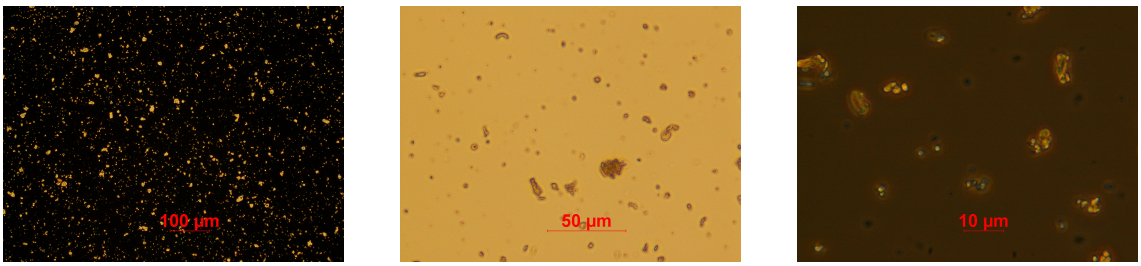

(a) 10X magnification. *(b) 40X magnification.* *(c) 100X magnification.*

Figure 77: *$CaCO_3$ dispersed in deionized water without addition of crude.*

7.3 Emulsion stability

To see the stability of an emulsion containing $CaCO_3$ an experiment has been processed with four alike beakers containing mixes of DW, APW and $CaCO_3$. The composition of the beakers can be seen in table 35.

Table 35: *The composition of the liquid and solid/liquid solutions for the emulsion stability experiment.*

	DW	DW w. $CaCO_3$	APW	APW w. $CaCO_3$
Volume	300 mL	300 mL	300 mL	300 mL
$CaCO_3$ added	0,0	1,0 g	0,0	1,0 g
pH	5,21	9,48	6,96	8,82

The beakers containing both liquid and solids where treated with ultrasonic dispersion prior to adding crude.

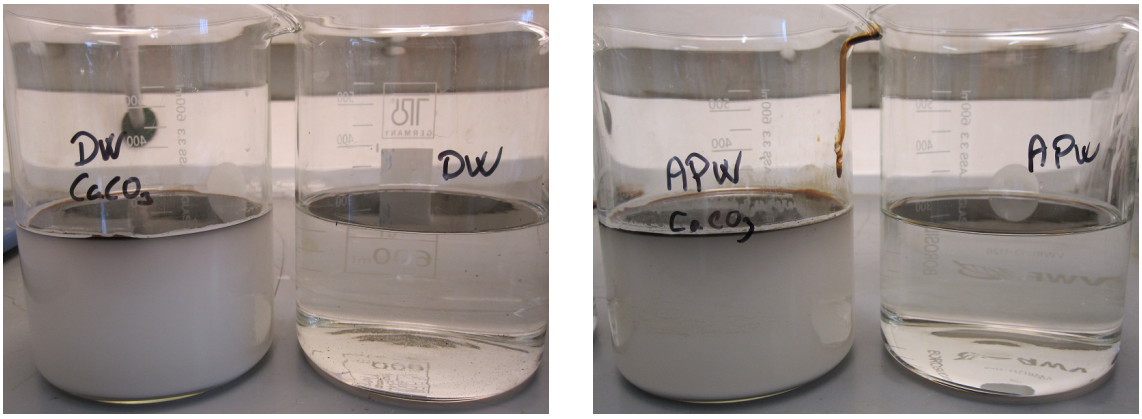

(a) DW with $CaCO_3$ and DW respectively with 4 mL crude.

(b) APW with $CaCO_3$ and APW respectively with 4 mL crude.

Figure 78: *2 beakers with deionized water and APW respectively where one beaker has been added 1 g $CaCO_3$ and one is with liquid alone.*

The same setup with the impeller as described in section 7.2 on page 81 was used. Figure 79 on the following page shows the emulsions of the liquid solutions without $CaCO_3$. It can be seen the the emulsion created in DW is more stable than the one created in APW. The reason for this behaviour is probably caused by the difference in ionic strength of the two solutions where APW has a ionic strength of 0,41 M and DW of 0 M. The higher ionic strength will decrease the thickness of the diffuse double layer around the oil droplets and thereby reduce the electrostatic repulsive forces. The oil droplets will tend to coalesce.

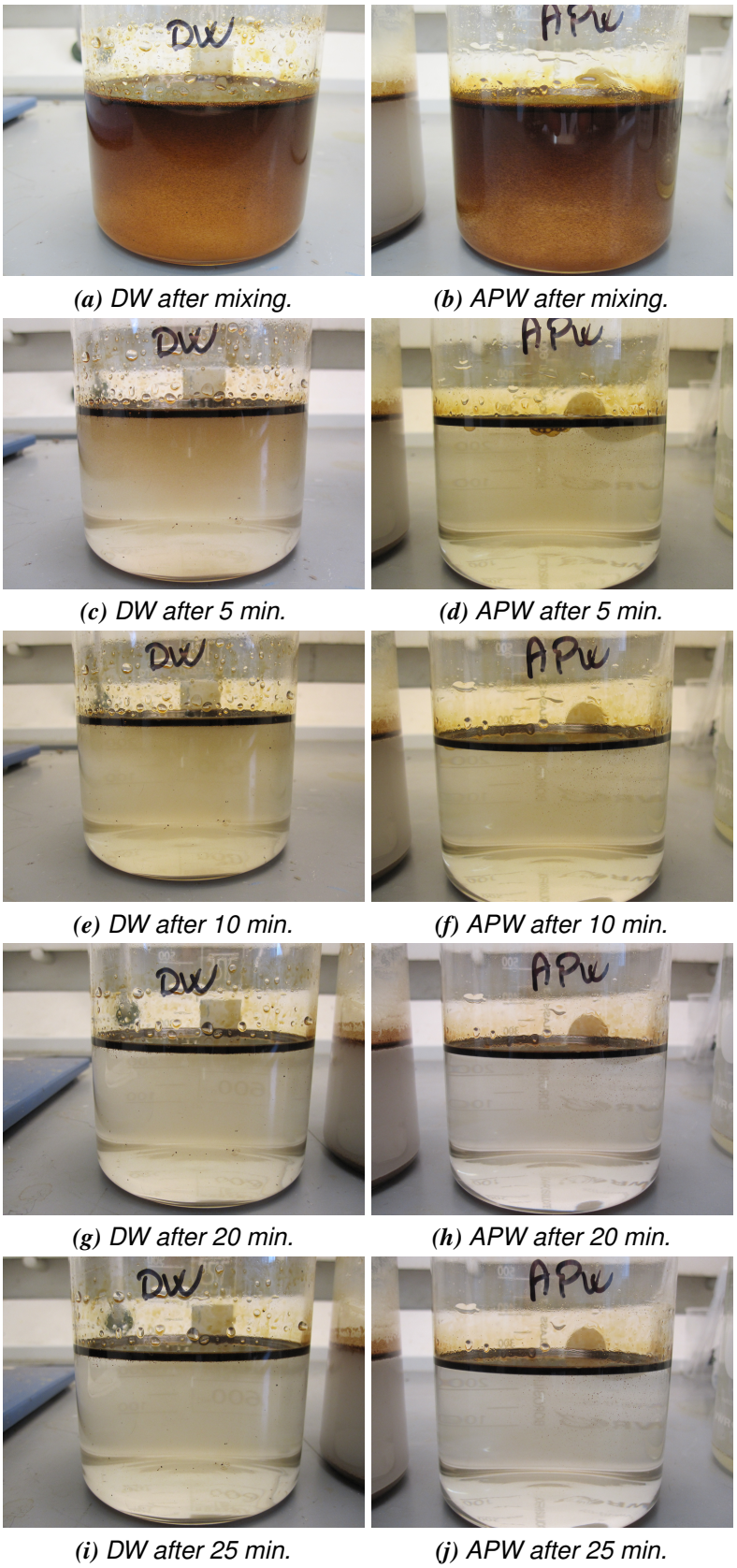

(a) DW after mixing. *(b) APW after mixing.*

(c) DW after 5 min. *(d) APW after 5 min.*

(e) DW after 10 min. *(f) APW after 10 min.*

(g) DW after 20 min. *(h) APW after 20 min.*

(i) DW after 25 min. *(j) APW after 25 min.*

Figure 79: *2 beakers with deionized water and APW respectively containing crude.*

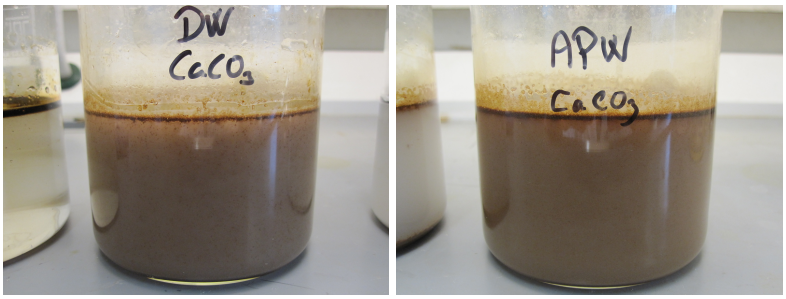

(a) DW/$CaCO_3$ after mixing. *(b)* APW/$CaCO_3$ after mixing.

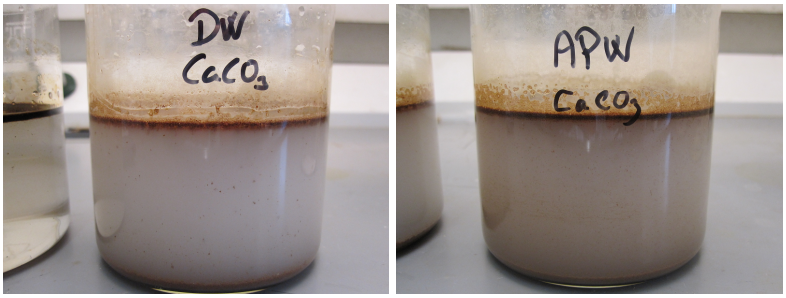

(c) DW/$CaCO_3$ after 5 min. *(d)* APW/$CaCO_3$ after 5 min.

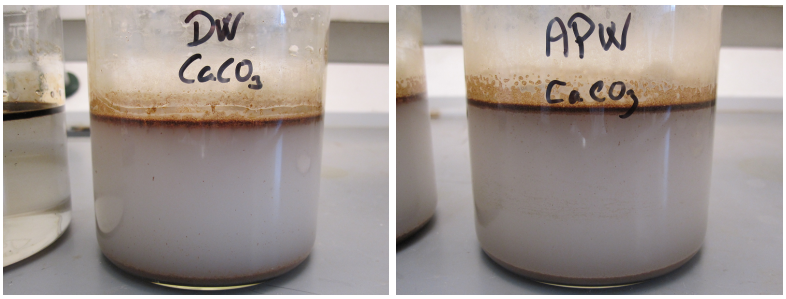

(e) DW/$CaCO_3$ after 10 min. *(f)* APW/$CaCO_3$ after 10 min.

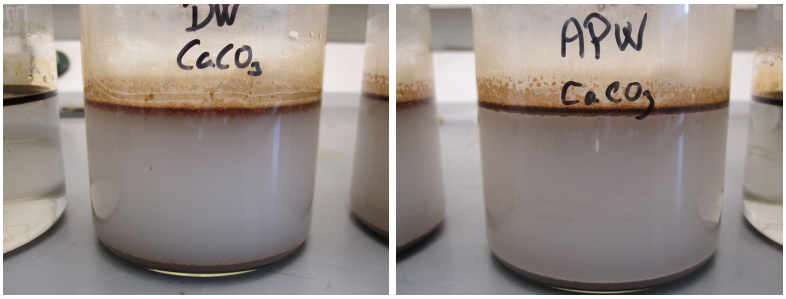

(g) DW/$CaCO_3$ after 20 min. *(h)* APW/$CaCO_3$ after 20 min.

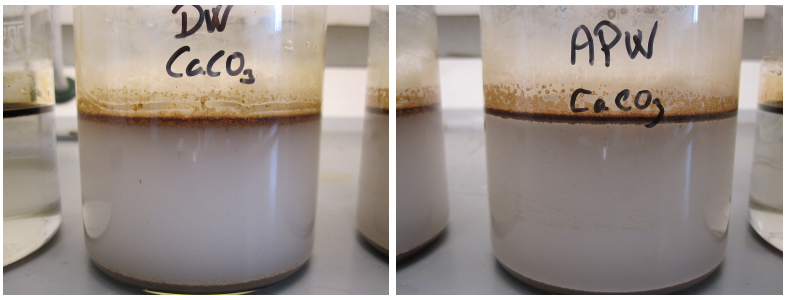

(i) DW/$CaCO_3$ after 25 min. *(j)* APW/$CaCO_3$ after 25 min.

Figure 80: *2 beakers with deionized water and APW respectively where 1 g $CaCO_3$ has been added to each beaker.*

In figure 80 on the previous page the same procedure is repeated but with the solutions containing $CaCO_3$. It can be sen that the emulsions created are more or less stable from a $CaCO_3$ point of view. On the beakers containing APW a slightly darker color is visible. Especially after 5 min the color difference is visible. The dark color can only originate from the crude which gives the impression that the APW containing $CaCO_3$ particle can in some way stabilize an emulsion. The extend of the stabilization is not clarified.

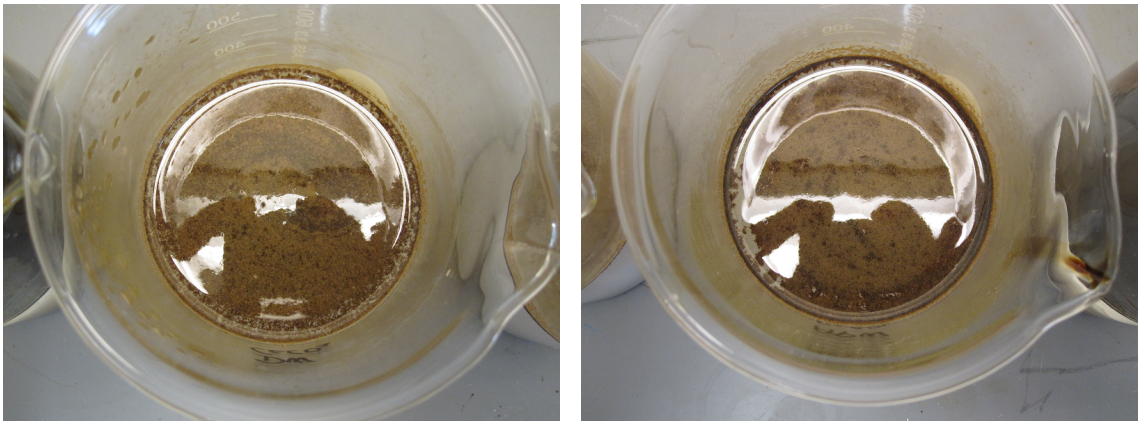

(a) DW/$CaCO_3$ after 45 min seen from the top. *(b) APW/$CaCO_3$ after 35 min seen from the top.*

Figure 81: *2 beakers with deionized water and APW respectively where 1 g $CaCO_3$ has been added to each beaker.*

Figure 81 shows the two liquid/solid solution from the top. It can be seen that the crude phase has turned brown instead of the dark brown / black colour which was the initial colour of the crude. Small $CaCO_3$ particles has been moved from the water phase to the crude phase. This indicates that $CaCO_3$ both can drag crude into the water phase, as seen in section 34 on page 82, and create a heterogenous mix of $CaCO_3$ particles and crude. This solid/crude mixture could create problems in a separation train if the solid particles migrates from the crude phase to the water phase with small oil droplets on the surface. The consequence of that is not clarified and will not be precessed further do to limited time.

8. PW Analysis

Samples of PW from six different platforms in the Noth Sea has been provided by Maersk Oil and Gas in Esbjerg. These samples have been analyzed in order to specify the constituents. The result of the analyses can be seen in table 37 on the following page.

The samples where taken from

1. Tyra West B-Sep
2. Harald
3. Gorm
4. Dan F
5. Tyra West A-sep
6. Tyra East

8.1 Quality of the analysis

To see whether the found constituents represent a good ionic description of the PW, some simple mathematical processing of the found concentrations (C) can be performed. The principle of electroneutrality is used. The amount of positive and negative ions in a solution should be the same as

$$\sum \text{cations} = \sum \text{anions} \tag{64}$$

in order to get a neutral solution. By rewriting C from mg/L to milliequivalent weight per liter (meqv/L) for both anions and cations as

$$\frac{\text{molecular weight, mg}}{\text{chargenumber, z}} = \text{equivalent weight(eqv, w)} \quad \Rightarrow \quad \frac{\text{C}}{\text{eqv, w}} = \frac{\text{meqv}}{\text{L}} \tag{65}$$

where z is the absolute ion charge number, the accuracy of the analysis can be calculated as

$$\text{Difference}[\%] = 100\% \times \left(\frac{\sum \text{cations} - \sum \text{anions}}{\sum \text{cations} + \sum \text{anions}} \right) \tag{66}$$

According to Tchobanoglous et al [B9], the criteria for a well representing analysis can be seen in table 36. The result of the rewriting from mg/L to meqv/L and the calculated

Table 36: *Approval criteria of the charge difference in an a analysis.*

$\sum$ Anions, meqv/L	Acceptable difference
0 - 3,0	±0,2 meqv/L
3,0 - 10,0	±2%
10 - 800	±5%

difference and quality of the analysis can be seen in table 38 on page 91.

Table 37: *Result of the analysis of PW from six different platforms in the North Sea with the result given as mg/L.*

Sample	1	2	3	4	5	6	Molar weight	Valency
pH	6,95	5,08	6,60	6,75	6,98	6,73	-	-
				[mV]				
ORP	−101,3	−53,2	−116,9	−43,4	−96,7	−235,1	-	-
				[meqv/L]				
Alkalinity	19,01	1,18	10,37	6,53	19,59	15,35	-	-
				[mg/L]			[g/mol]	[q]
Mg^{2+}	60,49	394,67	155,46	368,29	63,81	84,01	24,31	2
Ca^{2+}	140,88	4058,33	224,21	515,83	143,33	280,04	40,08	2
K^{+}	95,73	745,00	196,20	319,50	100,82	104,89	39,10	1
Ba^{2+}	18,40	259,75	1,96	0,60	20,75	22,19	137,33	2
Sr^{2+}	27,85	0,47	34,74	73,00	30,93	32,67	87,62	2
Cl^{-}	21 700,40	91 461,00	25 311,00	54 783,00	38 845,00	27 182,00	35,45	1
SO_4^{2-}	13,90	15,30	255,40	1712,00	12,30	22,60	96,06	2
Na^{+}	16 700,00	47 620,00	19 245,00	30 195,00	15 525,00	17 055,00	22,99	1
Mn^{2+}	0,00	2,98	0,00	0,00	0,00	0,00	54,94	2
Zn^{2+}	0,00	0,47	0,07	0,00	0,00	0,00	65,41	2
Ti^{4+}	0,00	0,00	0,21	0,00	0,00	0,00	47,87	4
Fe^{2+}	0,17	46,13	0,04	0,09	0,06	1,22	55,85	2
Cu^{2+}	0,01	0,02	0,01	0,00	0,00	0,00	63,55	2
Br^{-}	200,60	474,60	156,01	146,60	224,70	228,48	79,90	1

Table 38: *Result of the analysis of PW from six different platforms in the North Sea with the result given as meqv/L. It can be seen that the analysis results, besides the result from Tyra East, are incomplete.*

Sample	1	2	3	4	5	6	Cation	Anion
Species				[meqv/L]				
Alkalinity	19,01	1,18	10,37	6,53	19,59	15,35		+
Mg^{2+}	4,98	32,48	12,79	30,31	5,25	6,91	+	
Ca^{2+}	7,03	202,52	11,19	25,74	7,15	13,97	+	
K^{+}	2,45	19,05	5,02	8,17	2,58	2,68	+	
Ba^{2+}	0,27	3,78	0,03	0,01	0,30	0,32	+	
Sr^{2+}	0,64	0,01	0,79	1,67	0,71	0,75	+	
Cl^{-}	612,09	2579,80	713,94	1545,24	1095,69	766,71		+
SO_4^{2-}	0,29	0,32	5,32	35,64	0,26	0,47		+
Na^{+}	726,41	2071,36	837,11	1313,41	675,30	741,85	+	
Mn^{2+}	0,00	0,11	0,00	0,00	0,00	0,00	+	
Zn^{2+}	0,00	0,01	0,00	0,00	0,00	0,00	+	
Ti^{4+}	0,00	0,00	0,02	0,00	0,00	0,00	+	
Fe^{2+}	0,01	1,65	0,00	0,00	0,00	0,07	+	
Cu^{2+}	0,00	0,00	0,00	0,00	0,00	0,00	+	
Br^{-}	2,51	5,94	1,95	1,83	2,81	2,86		+
$\sum$cation	741,78	2330,98	866,95	1379,31	691,29	766,56		
$\sum$anion	633,91	2587,24	726,26	1589,25	1118,35	785,39		
Difference [%]	**7,84**	**-5,21**	**8,83**	**-7,07**	**-23,60**	**-1,21**		

The analysis quality shown in table 38 on the previous page shows a relative good coverage of ions in solution 1, 2, 3, 4 and 6. The difference in percent is between 1,21 and 8,83%. Sample 5 has a discrepancy of 23,60%, and a closer look on table 37 on page 90 shows a high concentration of Cl^- compared to the concentration of Na^+. This could be the result of a failure during analysis, or a not found species with a positive charge is a significant constituent of the Tyra West A-sep PW.

A conclusion of the PW analysis could be that even though the geographical area of the Danish part of the North Sea with the 6 fields is relative small, the concentrations and type of constituent varies from field to field. It is not possible to create a generally applicable PW sample to substitute for the actual PW sample when creating experiments as seen in chapter 6 on page 52.

9. Final conclusion

The litterature survey performed on the chalk extrusion problem has shown a reasonable explanation in the pressure variations during swing operations in the North Sea. The pressure limitations of the chalk formation should be investigated well by well and should be considered as the minimum pressure at the specific well. If the minimum limit is exceeded, chalk influxes should be expected and precautions should be made to obtain a a good quality in the water treatment facilities in use. A secondary solution could be a cautious procedure allowing the pressure in the well bore to reach equilibrium with the formation by changing the pressure in small steps to avoid chalk influxes. The secondary solution is probably the most economical attractive method but the use of it will not reveal the formation limits.

The use of ordinary solid removal methods like hydro cyclones is still the preferred method in many operations due to the simple and "non-mechanical" mode of operation. No moving parts makes the system more reliable but the limitations in cut size can be a disadvantage. Small chalk particles can cause problems in many parts of a production facility, and by removing a larger part of the solids, the influence of these particles will decrease. Methods like centrifugal solids removal can increase the efficiency of a solids removal proces. That said, an intensive fields study of e.g. disc stack centrifuges and their use on an offshore oil production platform should be done to see if the technique is applicable. The fear of moving parts and the risk of failure should not be a limitation in getting a better and more efficient solids removal and thereby a better quality of the process.

The ionic concentration of constituents in the water has to be taken into account. The experiments and analyses performed on chalk particles have shown the effect of normal constituents like Mg^{2+}, Ca^{2+} and CO_3^- on the ζ-potential of chalk particles. Since the ζ-potential can give an idea of the effect of e.g. membrane filtration by showing repulsive or attractive behavior of the solids towards the membrane due to their electrical potential, this parameter could be of interest. It is important though to make the measurements and analysis in electrolyte solutions similar to the original one to gain valid results. The analyses of PW from six different fields show significant differences of constituents and their concentration.

Emulsions can be created by mixing oil and water. The presence of solids can stabilize this emulsion as a Pickering emulsion. The experiments performed for this thesis could not reveal any stabilizing effect of the chalk particles added to the emulsion. The ability of chalk particles to drag oil from the oil phase to the water phase was documented. This ability could give rise to the idea that removal of chalk particles could improve the quality of the produced water with regards to the oil in water limitations given by the environmental authorities. That again gives rise to experiments with more sophisticated solid removal techniques than the hydro cyclone with its limitations.

Bibliography, Books

[B1] Mark A. Andersen. *Petroleum Research in North Sea Chalk*. Amoco Norway Oil Company and RF - Rogaland Research, 1995. ISBN 82-7220-725-7.

[B2] K.W. Glennie. *Petroleum Geology of the North Sea*. Blackwell Science, fourth edition, 1998.

[B3] Daniel C. Harris. *Quantitative Chemical Analysis*. W.H. Freeman and Company, New York, seventh edition, 2007.

[B4] David G Kinniburgh and David M Cooper. *PhreePlot Creating graphical output with PHREEQC*. Centre for Ecology and Hydrology, Deiniol Road, bangor, Gwynedd, LL57 2UW, UK, June 2011. http://www.phreeplot.org/.

[B5] Ladislav Svarovsky, Dipl Ing, Phd, CEeng, FIChem E. *Solid-Liquid Separation*. Butterworth.Heinemann, forth edition, October 2000. ISBN: 978-0-7506-4568-3.

[B6] R H Perry and D W Green. *Perry's Chemical Engineers' Handbook*. McGraw-Hill, 2008.

[B7] Erling Fjær, Rune M. Holt, Per Horsrud, Arne M. Raaen, and Rasmus Risnes†. *Petroleum Related Rock Mechanics*. Elsevier, Amsterdam, The Netherlands and Oxford, UK, second edition, 2008.

[B8] G. Rayner-Canham and T. Overton. *Descriptive inorganic chemistry*. W.H. Freeman, 2006.

[B9] G. Tchobanoglous, F.L. Burton, Metcalf & Eddy, and H.D. Stensel. *Wastewater Engineering: Treatment and Reuse*. McGraw-Hill Series in Civil and Environmental Engineering. McGraw-Hill, 2004.

Bibliography, Internet

[I10] Alfa-Laval Corporate AB. Aldec G3. Internet. http://www.alfalaval.com/solution-finder/products/aldec-g3/pages/howitworks.aspx.

[I11] Michael Kaszuba andJason Corbett, Fraser Mcneil Watson, and Andrew Jones. High-concentration zeta potential measurements using light-scattering techniques. *Philosophical Transaction of The Royal Society A*, 368(1927):4439–4451, September 2010.

[I12] ChemicalProcessing.com. How do you create an emulsion? Internet, - -. http://www.chemicalprocessing.com/experts/answers/2011/047.html. Date 30-04-2012.

[I13] Energi- og olieforum.dk. Eventyret i Nordsøen. Internet, - -. http://www.eof.dk/Viden/Temaer/Olien%20i%20Danmark/Artikler/Eventyret%20i%20Nordsoen.aspx.

[I14] Energistyrelsen. Yearly production 2010. Internet. http://www.ens.dk/da-DK/UndergrundOgForsyning/Olie_og_gas/Data/Produktionsoversigter/Documents/Yearly%20Production%202010.xls.

[I15] Flottweg Separation Technology. Flottweg Separatoren für innovative Fest-Flüssig-Trennung. Internet, October 2009. http://www.flottweg.de/cms/upload/downloads/old/Disc_Stack_Centrifuges_de.pdf.

[I16] Geologiportalen Olie og Gas. Bjergarters reservoiregenskaber. Internet. http://www.geologi.dk/oliegas/e4/e41/d411.htm. 08-05-2012.

[I17] Geoff Gough, Staven Talbot, and Hasse Moos. UBD unlocks pay in North Sea wells. Internet, March 2011. http://www.drillingcontractor.org/ubd-unlocks-pay-in-north-sea-wells-8787.

[I18] OK US) Montgomery, Carl T. (Bartlesville. Method for enhancing well productivity. Internet, May 2005. http://www.freepatentsonline.com/6874580-0-large.jpg.

[I19] Schlumberger Oilfield Glossary. Openhole Gravel Pack. Internet, - 2011. http://www.glossary.oilfield.slb.com/DisplayImage.cfm?ID=516.

[I20] U.S. Department of the Interior | U.S. Geological Survey. U.S. Geological Survey Open-File Report 2006-1195. Internet, april 2007. http://pubs.usgs.gov/of/2006/1195/htmldocs/images/chart.pdf.

[I21] Wikipedia. Stress (mechanics) — wikipedia, the free encyclopedia, 2012. [Online; accessed 30-May-2012].

Bibliography, Other

[A22] Tanni Abramovitz. Geophysical imaging of Porosity variations in the Danish North Sea chalk. *Geological Survey of Denmark and Greenland Bulletin*, 15:17–20, 2008. http://www.geus.dk/publications/bull/nr15/nr15_p17-20.pdf.

[A23] Kenichi Akamine and Isamu Kashiki. Corrosion Protection of Steel by Calcareous Electrodeposition in Seawater : Part 1 - Mechanism of Electrodeposition -. *IHI Engineering Review*, 36(3):141 – 147, October 2003.

[A24] Charles M. Ambler. The Theory of Scaling up Laboratory Data for the Sedimentation Type Centrifuge. *Journal of Biochemical and Microbiological Technology and Engineering*, 1(2):185–205, 1959.

[A25] Chalotte Christine Poulsen. Process engineer, Technical Facilities Process & Risk. Maersk Oil and Gas, Kanalen 1, 6700 Esbjerg.

[A26] T. Hassenkam, L.L. Skovbjerg, and S.L.S. Stipp. Probing the intrinsically oil-wet surfaces of pores in North Sea chalk at subpore resolution. *PNAS*, 106(15):6071–6076, April 2009. DOI:10.1073/pnas.0901051106.

[A27] L. Hermansson and J.S. Gudmundson. Influence of production on chalk failure in the valhall field. Number 20952-MS, page 9. European Petroleum Conference, October 1990.

[A28] Ib Larsen. Denmark's Oil and Gasproduction - and Subsoil Use '09. Technical report, Danish Energy Agency, June 2010. ISBN: 978-87-7844-838-5 http://www.ens.dk/Documents/Netboghandel%20-%20publikationer/2010/Denmarks_oil_and_gas_production.pdf.

[A29] Finn Jacobsen, Jon R. Ineson, Lars Kristiansen, and Lars Semmerik. Characterization and zonation of marly chalk reservoir: tho lower Cretaceous Valdemar Field of the Danish Central Graben. *Petroleum Geoscience*, 10(1):21–33, February 2004.

[A30] M.V Jeppsen. Geological steering of horizontal wells in chalk reservoirs - Examples from the Danish North Sea. *Bulletin of the Geological Society of Denmark*, 41:138–144, Copenhagen 1994-11-30.

[A31] Henrik Jepsen. Filtration of produced water. Eight semester project, Aalborg University Esbjerg, June 2011.

[A32] Reidar I. Korsnes, Merete V. Madland, Tor Austad, Stig Haver, and Geir Rœsland. The effects of temperature on the water weakening of chalk by seawater. In *International Symposium of the Society of Core Analysts*, Trondheim, Norway 12-16 September 2006.

[A33] P. A. Kralchevsky, I. B. Ivanov, K. P. Ananthapadmanabhan, and A. Lips. On the thermodynamics of particle-stabilized emulsions: Curvature effects and catastrophic phase inversion. *Langmuir*, 21(1):50–63, 2005. PMID: 15620284.

[A34] S.K. Mishra. The Electrokinetics of Apatite and Calcite in inorganic electrolyt environment. *International Journal of Mineral Processing*, 5:69–83, 1978.

[A35] Pierre Eschenmann Henriksen. Production Technologist. Maersk Oil and Gas, Esplanaden 50, 1098 København.

[A36] Production Development Department. Review of the "Chalk-Collapse-Constraint". Technical report, Mærsk Olie og Gas A/S.

[A37] Rasmus Risnes† and Per Horsrud. Well stability in a chalk reservoir. In *North Sea chalk symposium May 1985 Amoco Oljedirektoratet mfl 20 mai 1985 b2 70s ill*. Paper presented at the (Second) North Sea Chalk Symposium, Stavanger, 1985.

[A38] Professor Rasmus Risnes†. A laboratory study of chalk extrusion. In *Chalk Research Program - Phase II, Project 2 - Chalk Instabilty,*. Paper presented at the Third North Sea Chalk Symposium, Copenhagen, 1990.

[A39] Skule Strand, Eli J. Høgensen, and Tor Austad. Wettability alteriation of carbonates: Effects of potential determining ions (Ca^{2+} and SO_4^{2-}. *Colloids and Surfaces A: Physicochem. Eng. Aspects*, 275:1–10, 2006.

[A40] Komkrit Suttiponparnit, Jingkun Jiang, Manoranjan Sahu, Sirikalaya Suvachittanont, Tawatchai Charinpanitkul, and Pratim Biswas. Role of Surface Area, Primary Particle Size, and Crystal Phase on Titanium Dioxide Nanoparticle Dispersion Properties. *Nanoscale Research Letters*, 6:27, 2011.

[A41] The State of Queensland (Department of Natural Resources and Water) . Measuring salinity. Internet, - 2007. `http://www.derm.qld.gov.au/factsheets/pdf/land/l137.pdf`.

[A42] Phillip Wodka. Justification of clean-up of chalk producing swing producers on Tyra and update of the operation procedure. Internal MEMO, Mærsk Olie & Gas, October 2008. -.

[A43] Peimao Zhang and Tor Austad. Wettability and oil recovery from carbonates: Effects of temperature and potential determining ions. *Colloids and Surfaces A: Physicochem. Eng. Aspects*, 279:179–187, 2006.

[A44] Peimao Zhang, Medad T. Tweheyo, and Tor Austad. Wettability alteriation and improved oil recovery by spontaneous imbibition of seawater into chalk: Impact of the potential determining ions Ca^{2+}, Mg^{2+} and SO_4^{2-}. *Colloids and Surfaces A: Physicochem. Eng. Aspects*, 301:199–208, 2007.

[A45] P.A. Ziegler. North Sea rift system. In: P.A. Ziegler (Editor), Geodynamics of Rifting, Volume I. Case History Studies on Rifts: Europe and Asia. *Tectonophysis*, 208:55–75, 1992.

Appendices

PHREEQC and PHREE-PLOT code

To produce the figures showing the concentration and % species in APW Phree-Plot is used. The program is downloaded from http://www.phreeplot.org/ and is a freeware program based on the the geochemical modeling program PHREEQC. Two input files are shown for the % species plot, see section 9, and the concentration plot, see section 9 on the next page. The two shown examples generate the plots containing information on the Carbon-species distribution. By changing the input in line 5 "main species" from C to either K, Mg, Ca or Na the plot will contain their possible ion pairs as a function of the pH. Line 38 - 39 describes the constituents in APW and there measured concentration for the modeling foundation.

PHREE-PLOT

Carbon

```
1  SPECIATION
2    jobTitle            "Speciation vs pH using 'species' plot type"
3    calculationType     species
4    calculationMethod   1
5    mainSpecies         C
6    xmin                -13.0          # logH range
7    xmax                -6.0
8    resolution          400
9
10 PLOT
11   plotTitle           "Carbon speciation<br>(in APW)"
12   customXcolumn       2              # x-axis value is the second column -
13                                      # the first column is 'pH' (see out file)
14   pxmax               13             # default is 14
15   minimumYValueForPlotting 5.0       # eliminates minor species
16   legendTitle         "Carbon species"
17   extraText           "extratextCdspeciation.dat"
18
19 CHEMISTRY
20
21 include 'speciesvsph.inc' # contains the logic for outputting the expected
22                         # x-axis, y-axis (%distr) pairs expected by 'species'
                               plot type
23
24 PHASES
25 Fix_H+
26   H+ = H+
27   log_k 0.0
28 SOLUTION 1
29   temp    21
30   pH      7
31   units   mol/kgw
32   density 1
33   K       5.02e-3
34   Mg      3.43e-3
35   Ca      3.66e-3
36   Na      3.78e-1 charge
37   Cl      4.15e-1
38   Alkalinity 1.3701e-3
```

```
END

USE solution 1
EQUILIBRIUM_PHASES
  O2(g)   -0.677 0.1
  Fix_H+ <x_axis> NaOH 10
    -force_equality true
END
```

Carbon

```
SPECIATION
  #jobTitle     "Speciation vs pH using 'species' plot type"
  calculationType species
  calculationMethod 1
  mainSpecies    C
  xmin           -13.0          # logH range
  xmax           -6.0
  resolution     200

PLOT
  plotTitle      "log species concentration vs pH<br>(APW)"
  ytitle         "log concentration (mol/kgw)"
  labelSize      1.7  # controls the size of the key text
  pxmax          13   # sets upper limit on x-axis
  customXcolumn  2    # x-column is second column
  legendTextSize 1.3  # reduce the size of the legend (key) text
  extraText      "extratextlogCdspeciation.dat" # places the
                                    # legend inside the plot

CHEMISTRY

include 'logspeciesvsph.inc' # contains the logic for outputting the expected
                      # x-axis, y-axis (log c) pairs expected by
                      # 'species' plot type
PHASES
Fix_H+
  H+ = H+
  log_k 0.0
SOLUTION 1
  temp    21
  pH      8.5
  units   mol/kgw
  density 1
  K      5.02e-3
  Mg     3.43e-3
  Ca     3.66e-3
  Na     3.78e-1 charge
  Cl     4.15e-1
  Alkalinity 1.3701e-3
END

USE solution 1
EQUILIBRIUM_PHASES
  O2(g)   -0.677 0.1
  Fix_H+ <x_axis> NaOH 10
    -force_equality true
END
```

PHREEQC

To see the calculated concentrations and calculated values for the ionic strength, conductivity and the electrical balance the program PHREEQC is used. PHREEQC is the foundation of PHREE-PLOT used for the plots described in section 9 on page 99, and is containing different thermodynamic databases used for modeling equilibrium reactions.

To produce the values of the previous mentioned plots, the code for PHREEQC is

```
1  Solution 1
2  pH 8.5
3  Temp 21
4
5  Units mol/L
6
7  K       5.02e-3
8  Mg      3.43e-3
9  Ca      3.66e-3
10 Na      3.78e-1
11 Cl      4.15e-1
12 Alkalinity 1.3701e-3
13 End
```

The pH used in the simulation is entered in line 2 and the temperature in line 3. The concentrations of the constituents is entered in line 7 - 12.

The result of that calculation is given as

```
1    Input file: C:\Users\Henrik\AppData\Local\Temp\phrq0000.tmp
2   Output file: C:\Users\Henrik\Dropbox\Phreeqc\APW_2.out
3  Database file: C:\Program Files (x86)\Phreeqc\Databases\Phreeqc.dat
4
5  ------------------
6  Reading data base.
7  ------------------
8
9        SOLUTION_MASTER_SPECIES
10       SOLUTION_SPECIES
11       PHASES
12       EXCHANGE_MASTER_SPECIES
13       EXCHANGE_SPECIES
14       SURFACE_MASTER_SPECIES
15       SURFACE_SPECIES
16       RATES
17       END
18 -----------------------------------
19 Reading input data for simulation 1.
20 -----------------------------------
21
22       Solution 1
23       pH 8.5
24       Temp 21
25       Units mol/L
26       K 5.02e-3
27       Mg 3.43e-3
28       Ca 3.66e-3
29       Na 3.78e-1
30       Cl 4.15e-1
31       Alkalinity 1.3701e-3
32       End
33 ----------------------------------------
34 Beginning of initial solution calculations.
35 ----------------------------------------
```

```
Initial solution 1.

-----------------------------Solution composition------------------------------

      Elements      Molality   Moles

      Alkalinity   1.404e-03 1.404e-03
      Ca           3.750e-03 3.750e-03
      Cl           4.252e-01 4.252e-01
      K            5.143e-03 5.143e-03
      Mg           3.514e-03 3.514e-03
      Na           3.873e-01 3.873e-01

----------------------------Description of solution----------------------------

                                pH =  8.500
                                pe =  4.000
     Specific Conductance (uS/cm, 21 oC) = 37341
                     Density (g/cm3) = 1.01496 (Millero)
                  Activity of water = 0.986
                    Ionic strength = 4.238e-01
                 Mass of water (kg) = 1.000e+00
               Total carbon (mol/kg) = 1.284e-03
                  Total CO2 (mol/kg) = 1.284e-03
                Temperature (deg C) = 21.000
              Electrical balance (eq) = -1.964e-02
 Percent error, 100*(Cat-|An|)/(Cat+|An|) = -2.36
                         Iterations = 5
                           Total H = 1.110136e+02
                           Total O = 5.551007e+01

----------------------------Distribution of species----------------------------

                                      Log    Log      Log
   Species           Molality Activity Molality Activity Gamma

   OH-              3.537e-06 2.292e-06 -5.451 -5.640 -0.189
   H+               4.100e-09 3.162e-09 -8.387 -8.500 -0.113
   H2O              5.551e+01 9.860e-01 1.744 -0.006  0.000
C(4)         1.284e-03
   HCO3-            1.032e-03 7.257e-04 -2.986 -3.139 -0.153
   NaHCO3           1.024e-04 1.129e-04 -3.990 -3.947  0.042
   NaCO3-           5.665e-05 4.150e-05 -4.247 -4.382 -0.135
   CO3-2            4.047e-05 9.885e-06 -4.393 -5.005 -0.612
   CaCO3            1.409e-05 1.553e-05 -4.851 -4.809  0.042
   CaHCO3+          1.242e-05 8.730e-06 -4.906 -5.059 -0.153
   MgHCO3+          1.199e-05 8.783e-06 -4.921 -5.056 -0.135
   MgCO3            8.458e-06 9.325e-06 -5.073 -5.030  0.042
   CO2              5.010e-06 5.523e-06 -5.300 -5.258  0.042
Ca           3.750e-03
   Ca+2             3.723e-03 1.008e-03 -2.429 -2.997 -0.568
   CaCO3            1.409e-05 1.553e-05 -4.851 -4.809  0.042
   CaHCO3+          1.242e-05 8.730e-06 -4.906 -5.059 -0.153
   CaOH+            7.118e-08 5.214e-08 -7.148 -7.283 -0.135
Cl           4.252e-01
   Cl-              4.252e-01 2.795e-01 -0.371 -0.554 -0.182
H(0)         1.297e-28
   H2               6.484e-29 7.148e-29 -28.188 -28.146 0.042
K            5.143e-03
   K+               5.143e-03 3.381e-03 -2.289 -2.471 -0.182
   KOH              3.315e-09 3.655e-09 -8.480 -8.437  0.042
Mg           3.514e-03
   Mg+2             3.492e-03 1.051e-03 -2.457 -2.978 -0.521
```

```
100    MgHCO3+           1.199e-05 8.783e-06 -4.921 -5.056 -0.135
101    MgCO3             8.458e-06 9.325e-06 -5.073 -5.030  0.042
102    MgOH+             1.126e-06 8.252e-07 -5.948 -6.083 -0.135
103 Na            3.873e-01
104    Na+               3.871e-01 2.766e-01 -0.412 -0.558 -0.146
105    NaHCO3            1.024e-04 1.129e-04 -3.990 -3.947  0.042
106    NaCO3-            5.665e-05 4.150e-05 -4.247 -4.382 -0.135
107    NaOH              5.169e-07 5.698e-07 -6.287 -6.244  0.042
108 O(0)          6.650e-38
109    O2                3.325e-38 3.666e-38 -37.478 -37.436 0.042
110
111 ------------------------------Saturation indices-------------------------------
112
113        Phase           SI log IAP log KT
114
115        Aragonite     0.31  -8.00 -8.31 CaCO3
116        Calcite       0.46  -8.00 -8.46 CaCO3
117        CO2(g)       -3.84  -5.26 -1.42 CO2
118        Dolomite      1.01 -15.98 -17.00 CaMg(CO3)2
119        H2(g)       -25.01 -28.15 -3.13 H2
120        H2O(g)       -1.62  -0.01  1.61 H2O
121        Halite       -2.68  -1.11  1.57 NaCl
122        O2(g)       -34.57 -37.44 -2.86 O2
123
124 ------------------
125 End of simulation.
126 ------------------
127
128 ------------------------------------
129 Reading input data for simulation 2.
130 ------------------------------------
131
132 -----------
133 End of run.
134 -----------
```

In line 3 the database used is seen. For this calculation the phreeqc.dat is used. It is possible to choose between eight different thermodynamic databases. The choice of the right database is important since not all species are present in each database.

The description of the calculated solution is shown on line 50 - 68. The possible species distribution are shown on line 68 - 109 as Molality, Activity, Log Molality, log Activity and Log Gamma (the logarithmic activity coefficient) respectively.

Saturation indices is shown on line 111 - 123. The Saturation Index (SI), the logarithmic ion activity product (IAP) and the log of the equilibrium constant for the water temperature (KT) are given.

Calibration data

To follow the condition of the Zeta-CAD IV, a log of the measured ζ-potentials of milk is recorded, see table 39. It is seen that the control measurements from the 19th - 25th of February are clearly lower than the rest of the measurements. This is due to the fact, that a different label of milk was used. The normal milk used was Skummetmælk from DanMælk®, and the milk used in the before mentioned period was Økologisk Letmælk from Naturmælk.

Table 39: *History of control measurements on milk.*

Calibration on milk				
Date		ζ-potential		Average
30. jan 2012	−33,12	−34,13	−33,71	−33,65
31. jan 2012	−25,83	−26,55	−30,68	−27,69
01. feb 2012	−23,10	−24,27	−26,77	−24,71
06. feb 2012	−30,30	−24,78	−27,29	−27,46
19. feb 2012	−20,13	−20,81	−19,17	−20,04
22. feb 2012	−19,30	−18,35	−17,23	−18,29
25. feb 2012	−17,71	−17,86	−18,88	−18,15
05. mar 2012	−31,46	−30,42	−31,25	−31,04
06. mar 2012	−31,96	−32,13	−31,49	−31,86
07. mar 2012	−28,21	−27,58	−28,49	−28,09
14. mar 2012	−27,27	−27,92	−29,60	−28,26
15. mar 2012	−38,42	−37,69	−38,57	−38,23
16. mar 2012	−35,10	−36,56	−37,43	−36,36

Supplement

Well log

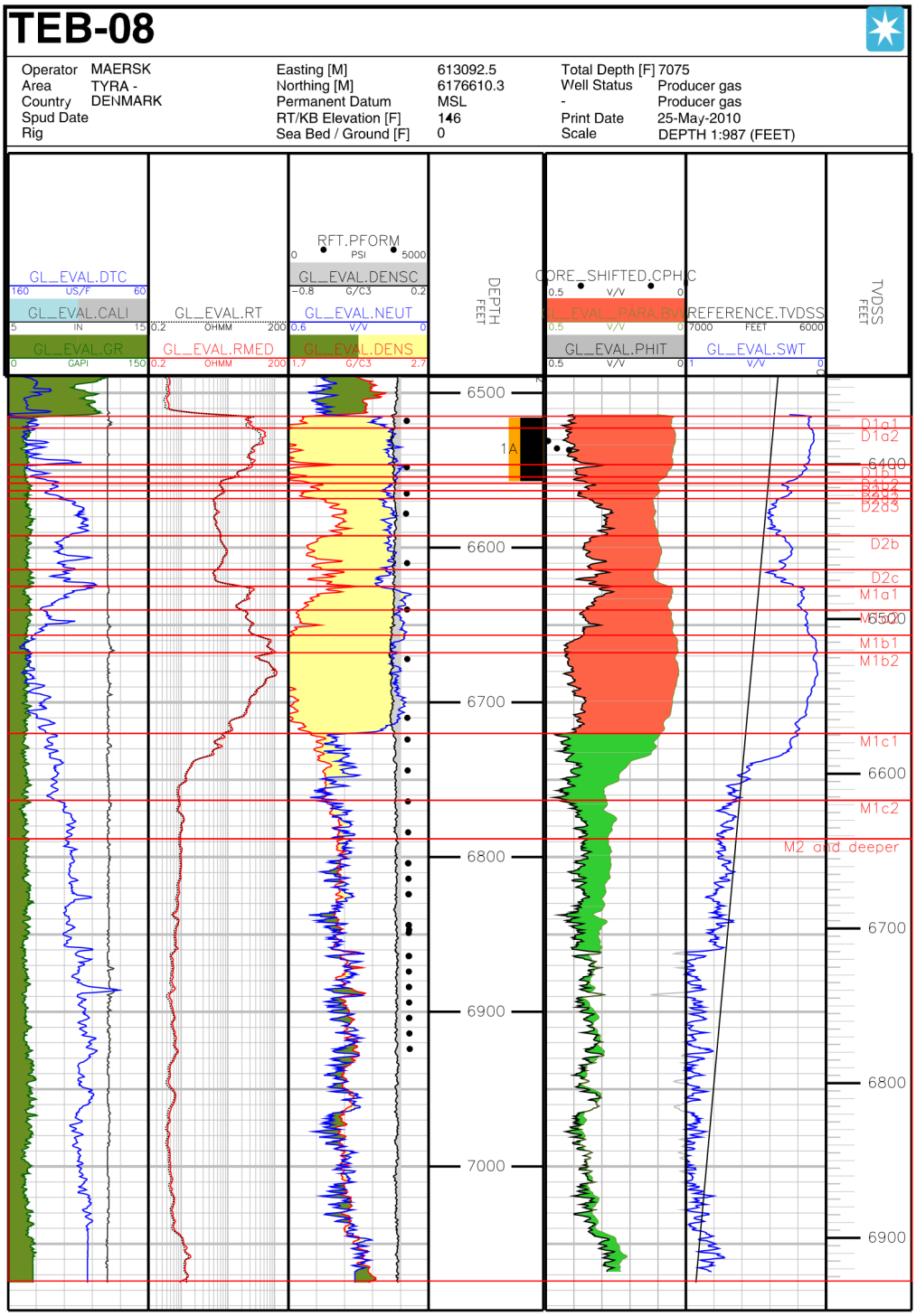

Figure 82: *Well log from Tyra East.*

Grain size chart

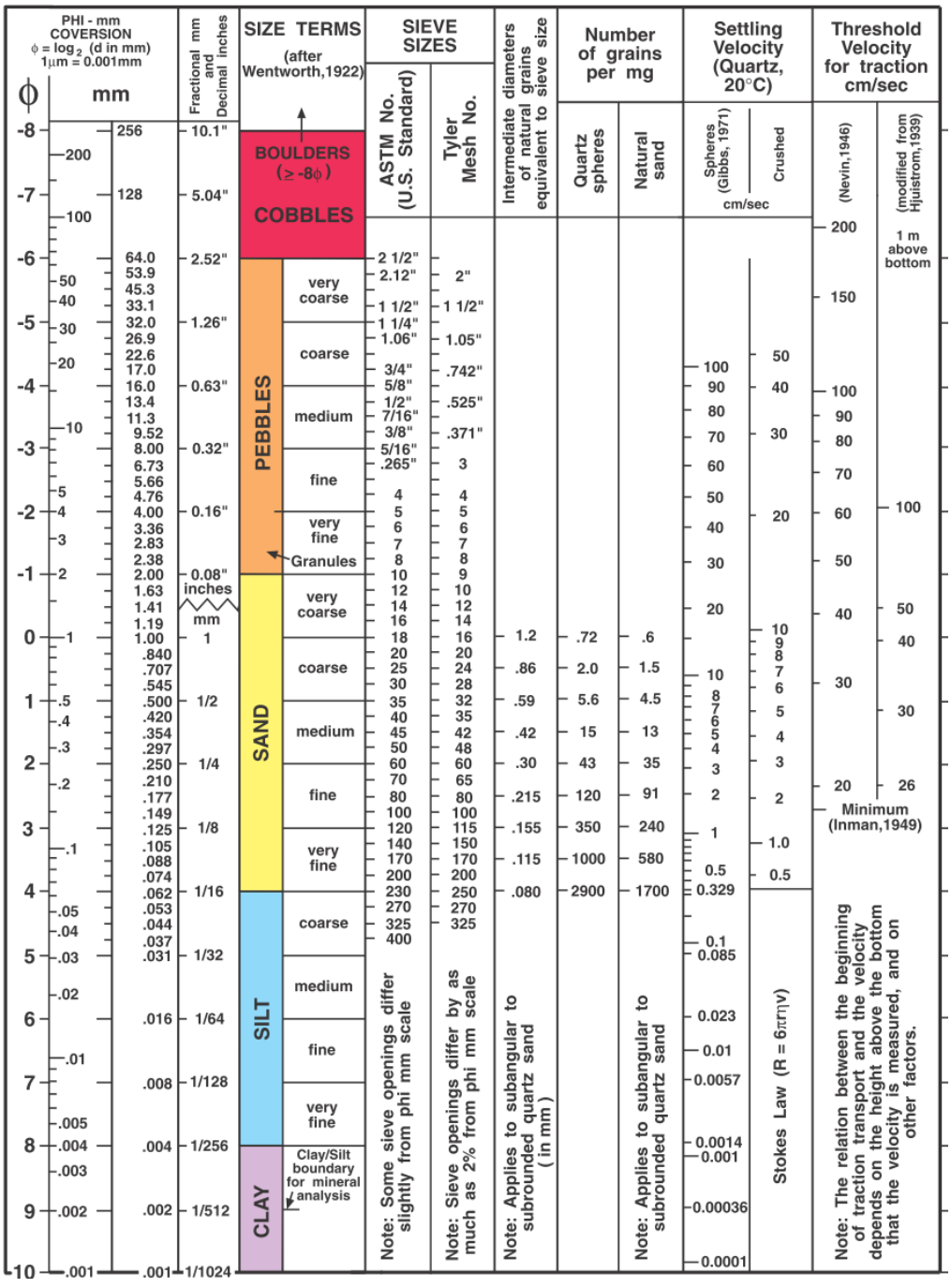

Figure 83: *Grain size chart. [I20]*

GEUS Size distribution

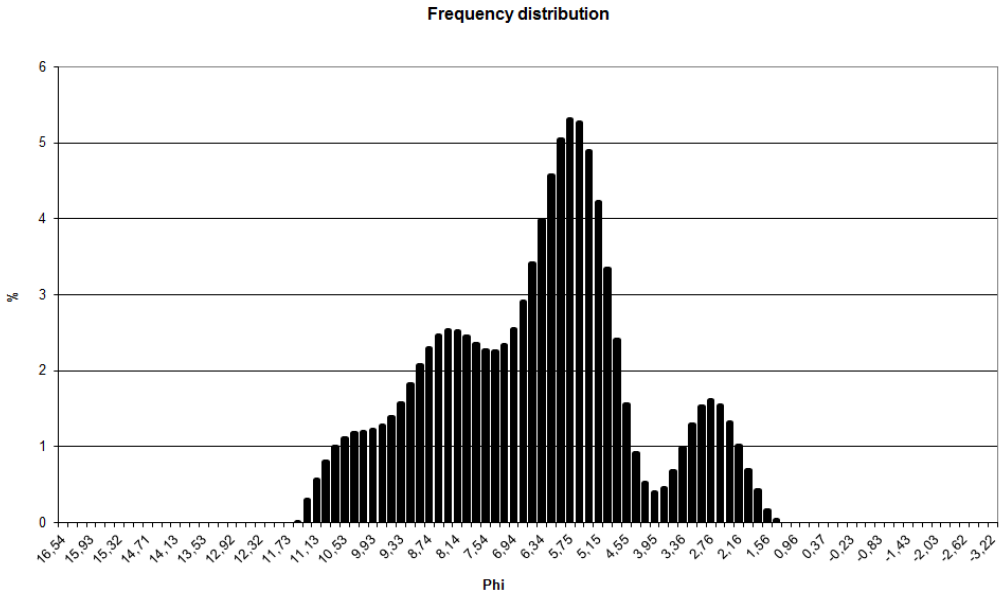

Figure 84: *Sample 28398 - 1, delivered by GEUS*

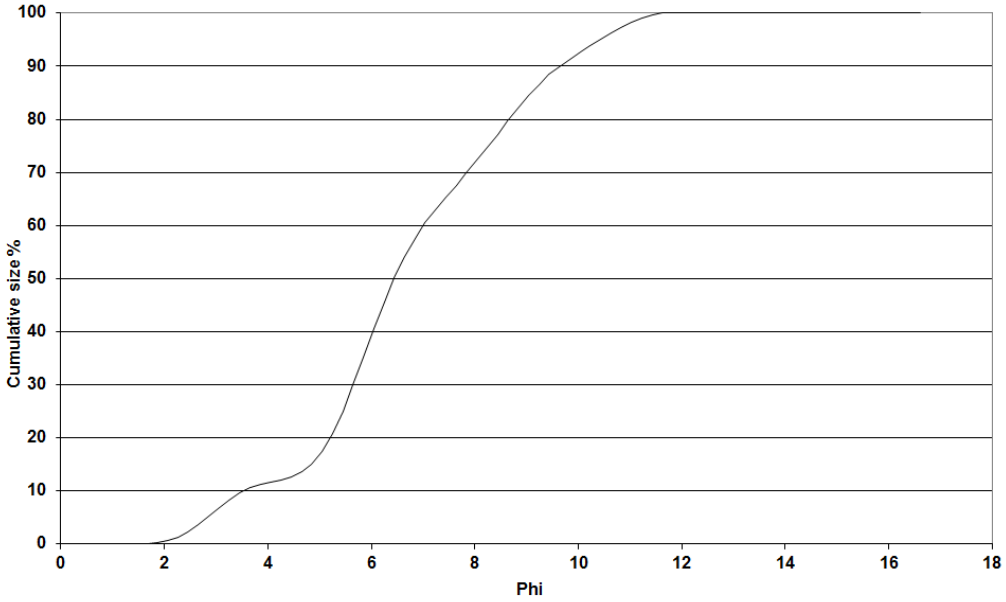

Figure 85: *Sample 28398 - 1, delivered by GEUS*

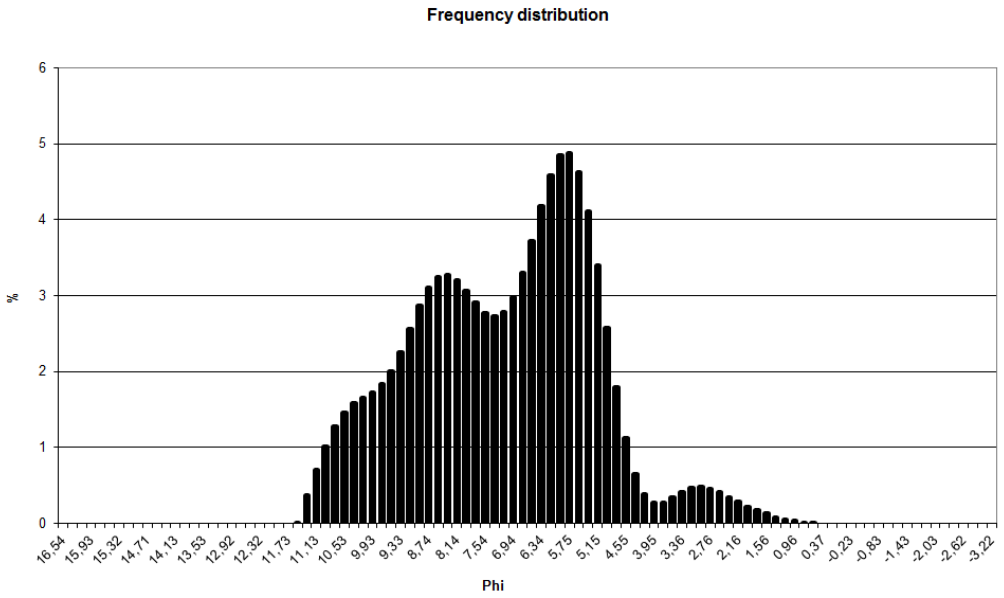

Figure 86: *Sample 28398 - 2, delivered by GEUS*

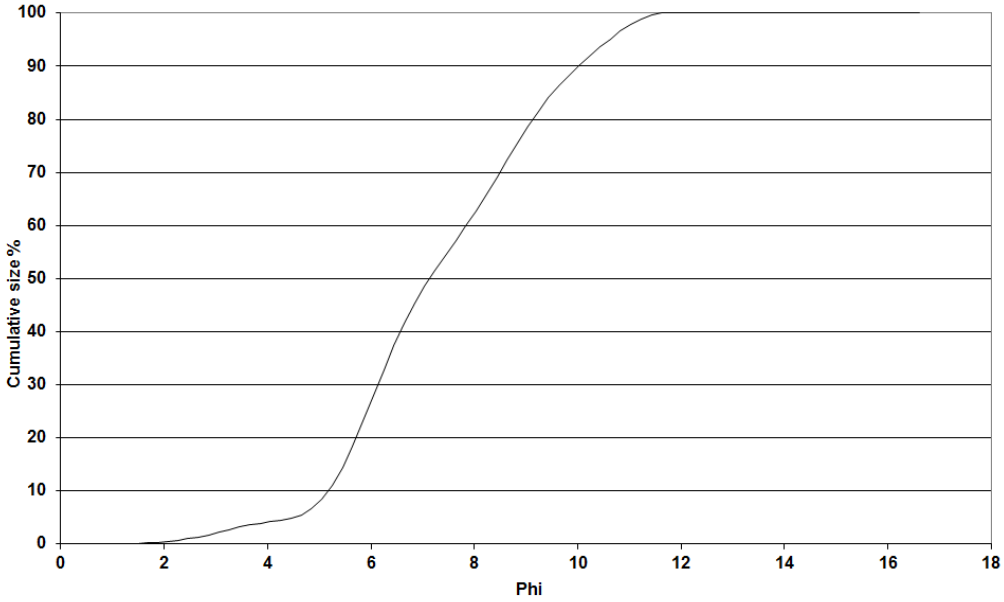

Figure 87: *Sample 28398 - 2, delivered by GEUS*

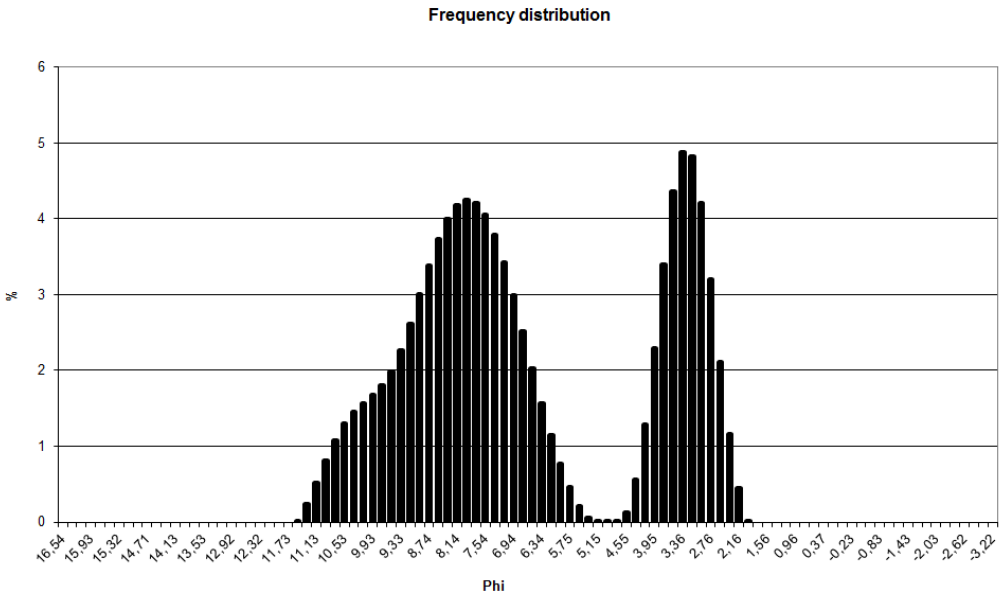

Figure 88: *Sample 28399 - 1, delivered by GEUS*

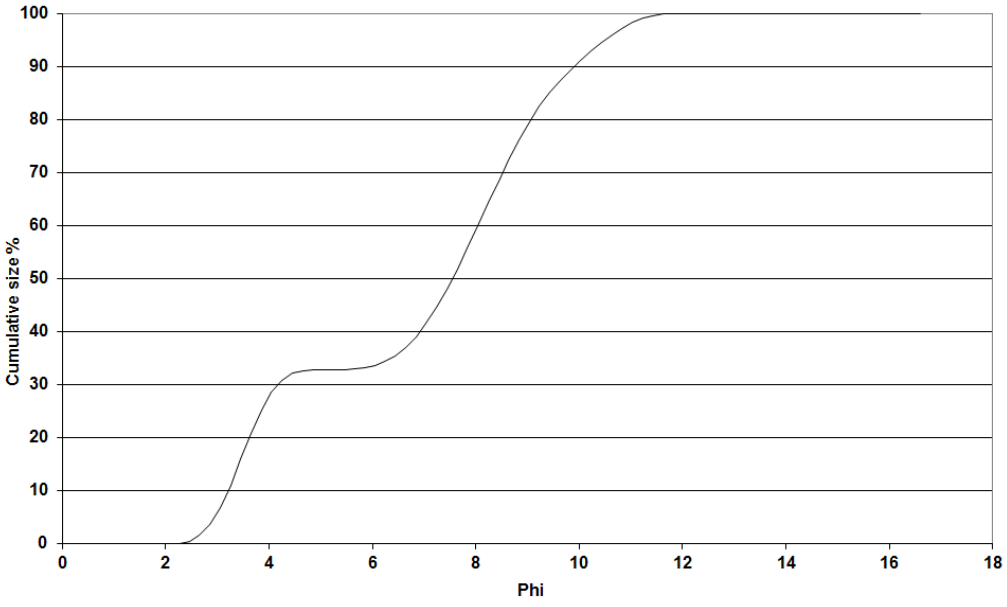

Figure 89: *Sample 28399 - 1, delivered by GEUS*

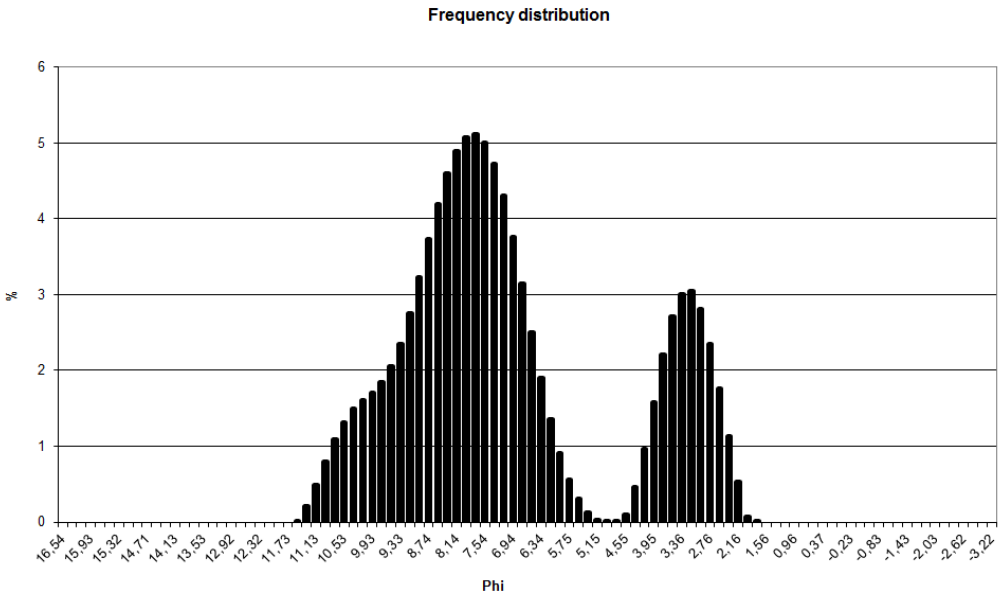

Figure 90: *Sample 28399 - 2, delivered by GEUS*

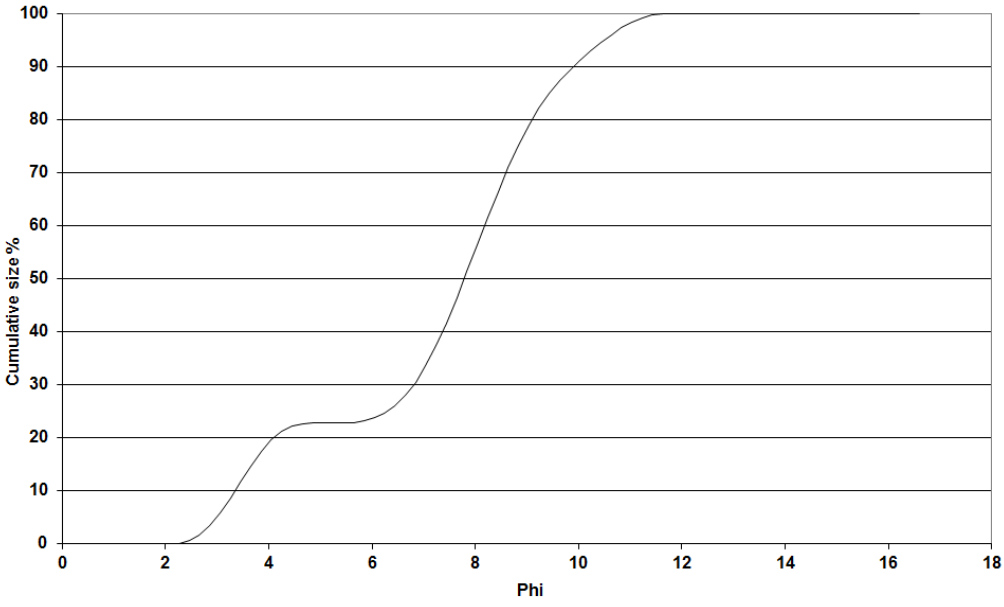

Figure 91: *Sample 28399 - 2, delivered by GEUS*

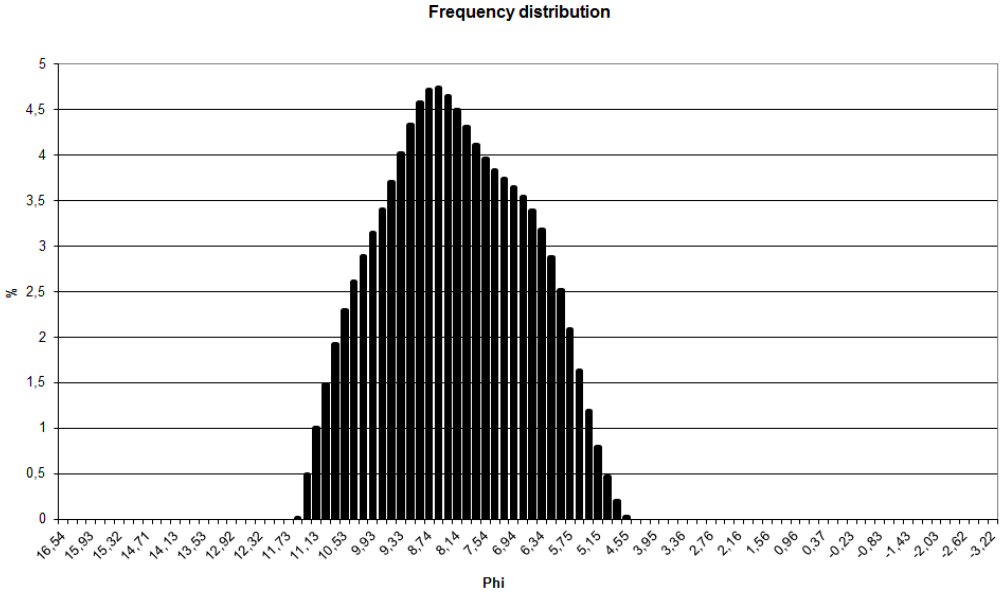

Figure 92: *Sample 28457 - 1, delivered by GEUS*

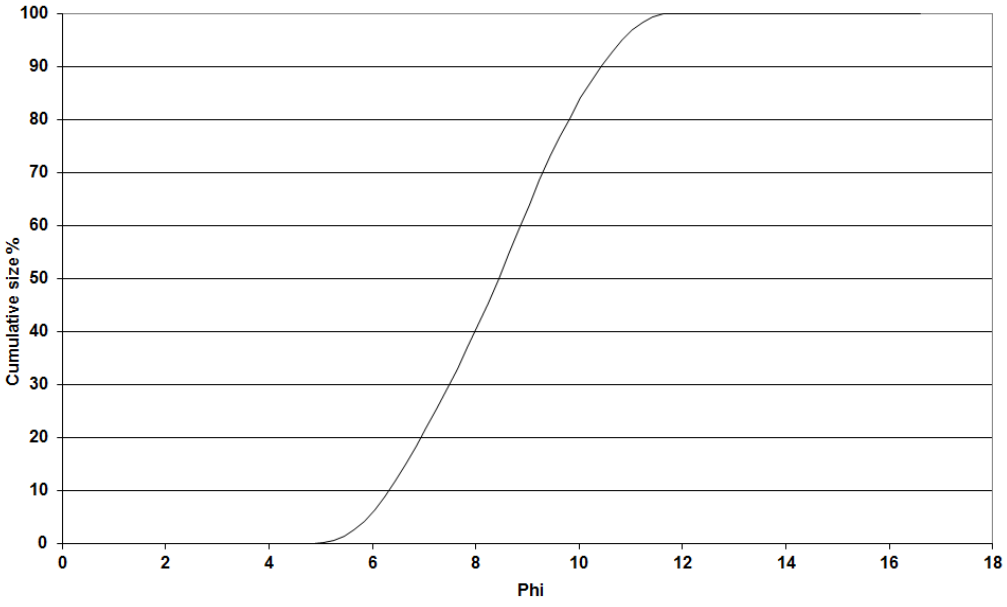

Figure 93: *Sample 28457 - 1, delivered by GEUS*

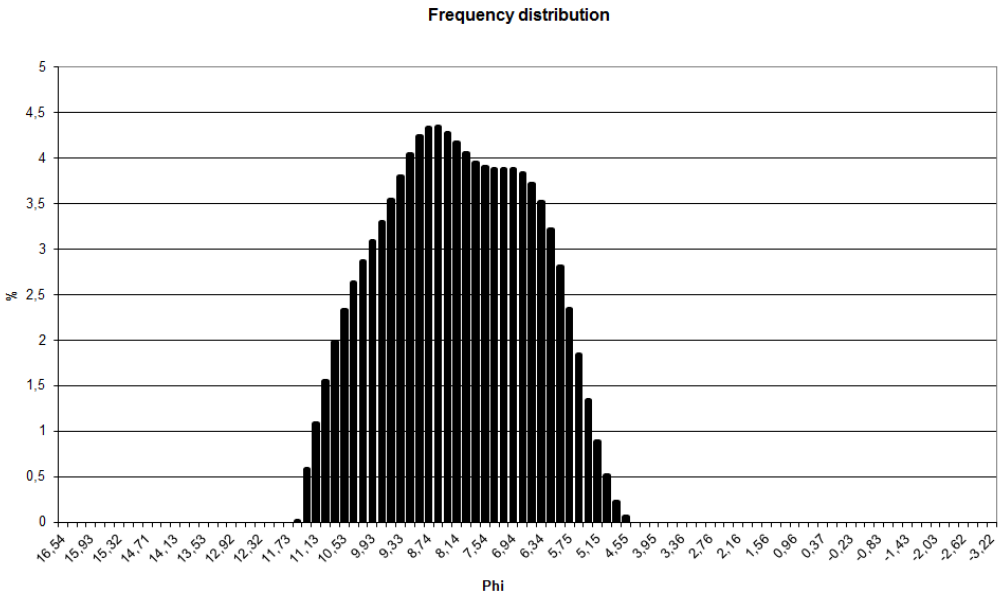

Figure 94: *Sample 28457 - 2, delivered by GEUS*

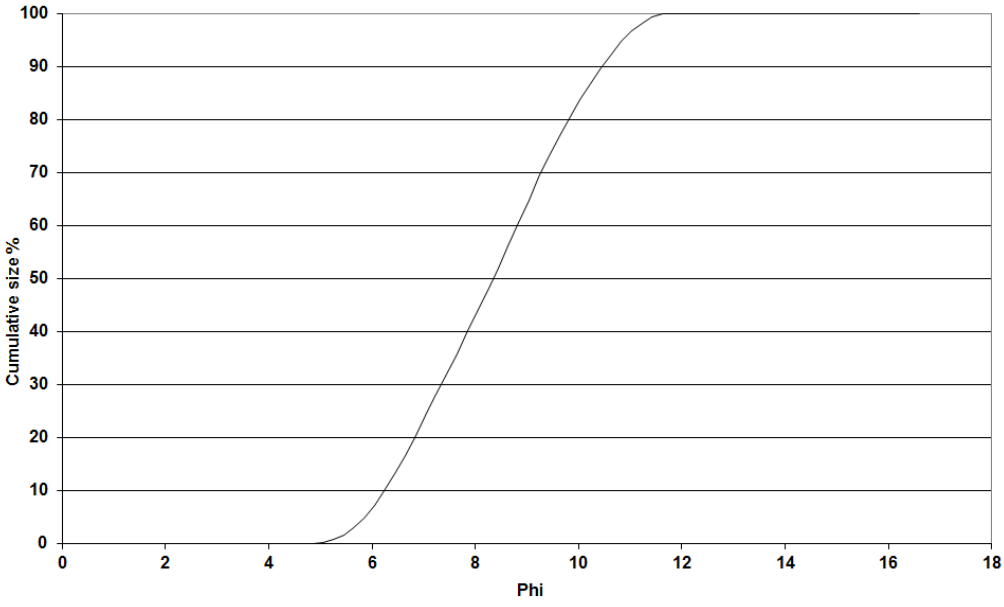

Figure 95: *Sample 28457 - 2, delivered by GEUS*